D 1

PNE-1107
PART I

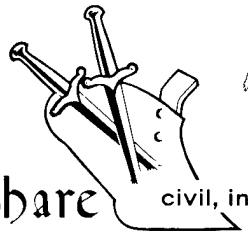

Plowshare

civil, industrial and scientific uses for nuclear explosives

UNITED STATES ARMY CORPS OF ENGINEERS

FORT PECK RESERVOIR
MONTANA

PROJECT
PRE-GONDOLA I

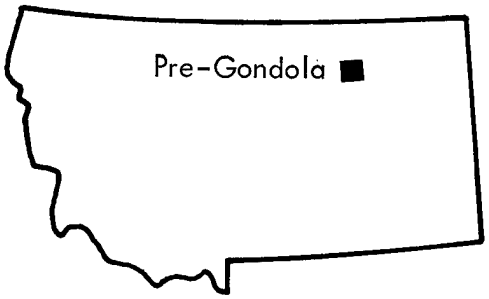

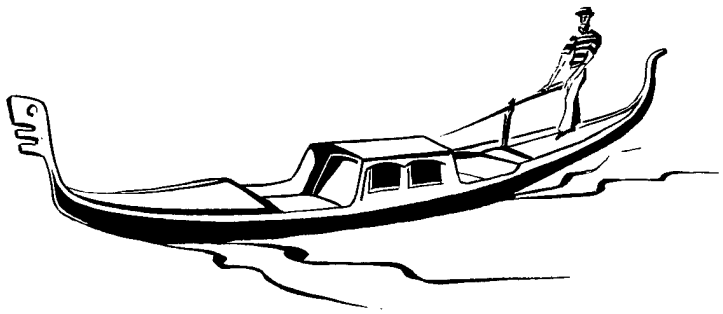

CRATER STUDIES: CRATER MEASUREMENTS

CAPTAIN R. W. HARLAN
U. S. Army Engineer Nuclear Cratering Group
Livermore, California

U. S. Army Engineer Nuclear Cratering Group
Livermore, California

ISSUED: DECEMBER 1967

Printed in USA. Available from the Clearinghouse for Federal
Scientific and Technical Information, National Bureau of Standards,
U. S. Department of Commerce, Springfield, Virginia 22151
Price: Printed Copy $3.00; Microfiche $0.65.

PNE-1107 PART I
FINAL REPORT

PROJECT PRE-GONDOLA I

CRATER STUDIES: CRATER MEASUREMENTS

Captain Ronald W. Harlan

U. S. Army Engineer
Nuclear Cratering Group
Livermore, California

May 1967

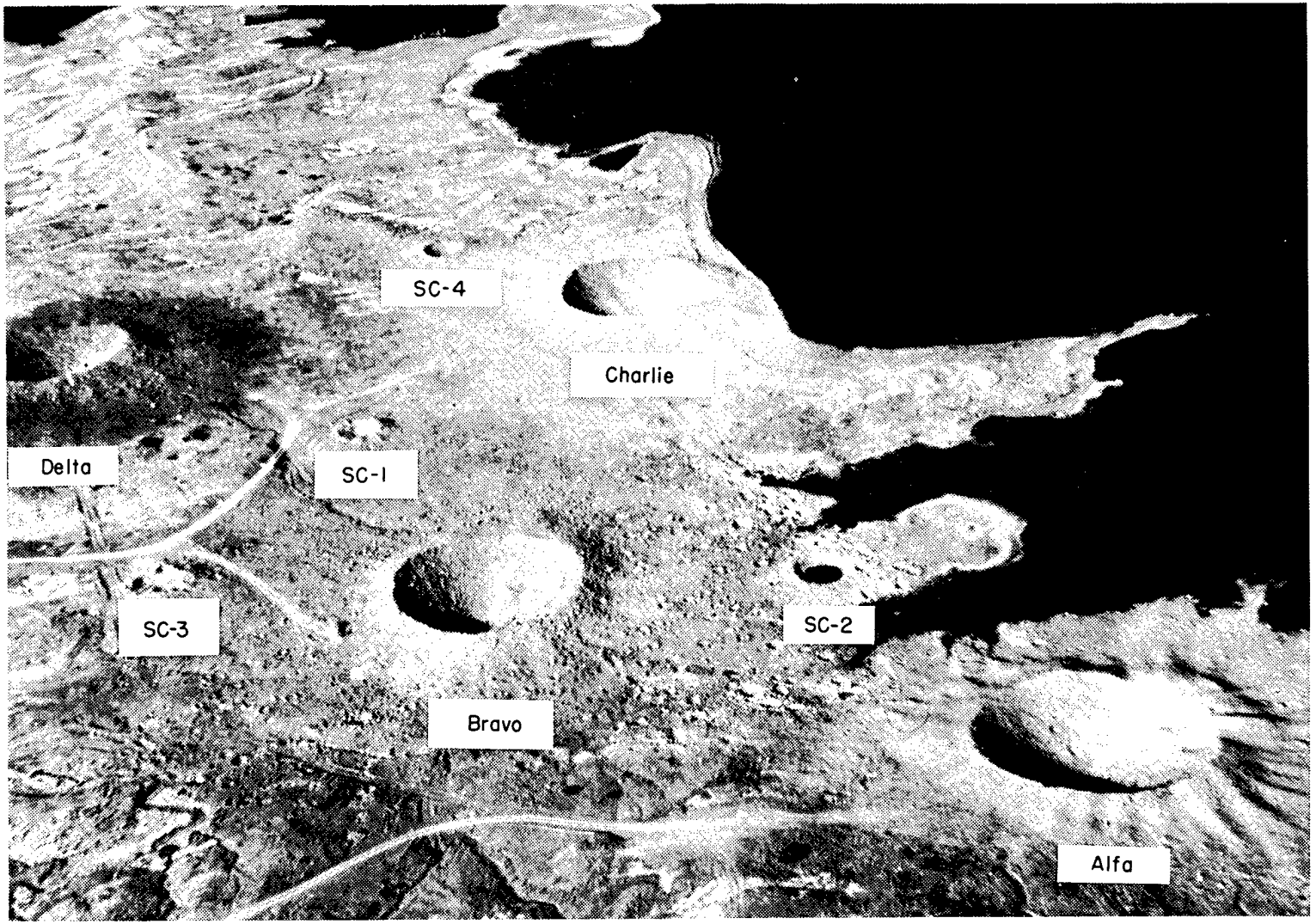

Frontispiece. Pre-Gondola Craters (November 4, 1966).

ABSTRACT

Project Pre-Gondola I, a series of four 20-ton high explosive cratering detonations, was conducted by the U. S. Army Engineer Nuclear Cratering Group during October and November 1966 in order to determine the cratering characteristics of the Pre-Gondola project site located about 18 miles south of the town of Glasgow, Valley County, Montana. The essentially flat site medium consisted of uncemented, highly compacted, moderately jointed shale of the Late Cretaceous age, Bearpaw shale formation. The craters produced were both deeper and wider than those previously observed in either alluvium or basalt, but had flatter slopes. For single-charge craters in Bearpaw shale the optimum depth of burst for both apparent crater depth and radius is about 130 $ft/kt^{1/3.4}$. Pertinent data for the four events are summarized below.

Event	Energy Equivalent Yield	Depth of Burst		Apparent Crater Radius		Apparent Crater Depth	
	tons	feet	$ft/kt^{1/3.4}$	feet	$ft/kt^{1/3.4}$	feet	$ft/kt^{1/3.4}$
Charlie	21.58	42.49	131.2	80.4	248.0	32.6	100.7
Bravo	21.30	46.25	143.4	78.5	243.4	29.5	91.5
Alfa	22.39	52.71	161.1	76.1	232.5	32.1	98.1
Delta	22.26	56.87	174.0	65.1	199.3	25.2	77.1

PREFACE

This report, Part I of PNE-1107, is the final report of the crater measurement and ejecta study programs for the Pre-Gondola I cratering calibration series. Part II covers the surface motion program. PNE-1107 updates preliminary results reported earlier, and also contains cratering data obtained from the 1000-pound Seismic Site Calibration Series.

The efforts of Major Richard H. Benfer and Specialists Frederick H. Foster and Michael A. Novak in the preparation of this report are gratefully acknowledged.

CONTENTS

CONTENTS (Continued)

CONTENTS (Continued)

CONTENTS (Continued)

CHAPTER 1
INTRODUCTION

1.1 DESCRIPTION AND PURPOSE

Project Pre-Gondola I was a series of chemical explosive single-charge cratering experiments in weak, wet clay-shale conducted by the U. S. Army Engineer Nuclear Cratering Group (NCG) as a part of the joint Atomic Energy Commission-Corps of Engineers nuclear excavation research program. The purpose of Pre-Gondola I was to calibrate the project site with respect to its cratering characteristics and to provide a basis for design of the proposed 140-ton Pre-Gondola II and the Pre-Gondola III row-charge cratering detonations in the same medium.

The Pre-Gondola I detonations were executed in Valley County, near the edge of the Fort Peck Reservoir approximately 18 miles south of Glasgow, Montana, on the following schedule:

Event	Date	Time (MST)	Longitude	Latitude
Bravo	25 October 1966	1000:00.760	W 106°38'24.894"	N 47° 55'46.154"
Charlie	28 October 1966	1200:00.654	W 106°38'29.974"	N 47° 55'53.294"
Alfa	1 November 1966	1000:00.275	W 106°38'15.325"	N 47° 55'46.570"
Delta	4 November 1966	1000: 00.032	W 106°38'38.134"	N 47° 55'48.077"

The four 20-ton (nominal) spherical charges of liquid explosive nitromethane (CH_3NO_2) resulted in the following craters:

Event	Tons	Depth of Burst		Apparent Crater Radius		Apparent Crater Depth	
		feet	meters	feet	meters	feet	meters
Charlie	19.62	42.49	12.95	80.4	24.50	32.6	9.94
Bravo	19.36	46.25	14.10	78.5	23.93	29.5	8.99
Alfa	20.35	52.71	16.07	76.1	23.19	32.1	9.78
Delta	20.24	56.87	17.34	65.1	19.84	25.2	7.68

To assist in seismic site calibration and to provide preliminary information for the design of the Pre-Gondola I experiment, NCG had earlier conducted the following Pre-Gondola Seismic Site Calibration Series at the Pre-Gondola I site:

Event	Date	Time (MST)	Longitude	Latitude
SC-1	20 June 1966	0845	W 106°38'30.573"	N 47°55'48.383"
SC-4	21 June 1966	0811	W 106°38'35.059"	N 47°55'53.380"
SC-2	22 June 1966	0805	W 106°38'20.792"	N 47°55'48.181"
SC-3	23 June 1966	0837	W 106°38'29.495"	N 47°55'44.579"

The four 1000-pound spherical charges of nitromethane resulted in the following craters:

Event	Tons	Depth of Burst		Apparent Crater Radius		Apparent Crater Depth	
		feet	meters	feet	meters	feet	meters
SC-4	0.5	12.2	3.72	24.5	7.48	13.0	3.96
SC-2	0.5	15.8	4.81	27.3	8.32	12.5	3.81
SC-1	0.5	19.1	5.82	7.1*	2.16	2.8*	0.85
SC-3	0.5	23.3	7.10	14.6*	4.45	3.4*	1.04

Figure 1.1, an index map of the Fort Peck Reservoir area, shows the location of the Pre-Gondola project site.

1.2 SCOPE OF REPORT

This report, Part I of PNE-1107, is the final report of the crater measurement and ejecta study programs for the Pre-Gondola I cratering calibration series. Part II covers the surface motion program. PNE-1107 updates preliminary results reported in Reference 1, and also contains cratering data obtained from the 1,000-pound Seismic Site Calibration Series.

1.3 PROGRAM OBJECTIVES

1.3.1 Purposes of Crater Studies Technical Program. There follows a list of the purposes of the crater studies:

1. To extend single-charge explosive cratering experience to a weak, wet, clay-shale medium.

2. To calibrate the Pre-Gondola project site with respect to its cratering characteristics and to provide design input to Pre-Gondola II and III row-charge cratering detonations at this site.

3. To provide experimental data for use in theoretical studies of crater formation and for the design of future single- and row-charge cratering detonations in wet media.

*Anomalous and very asymmetrical; may have produced a mound on level terrain.

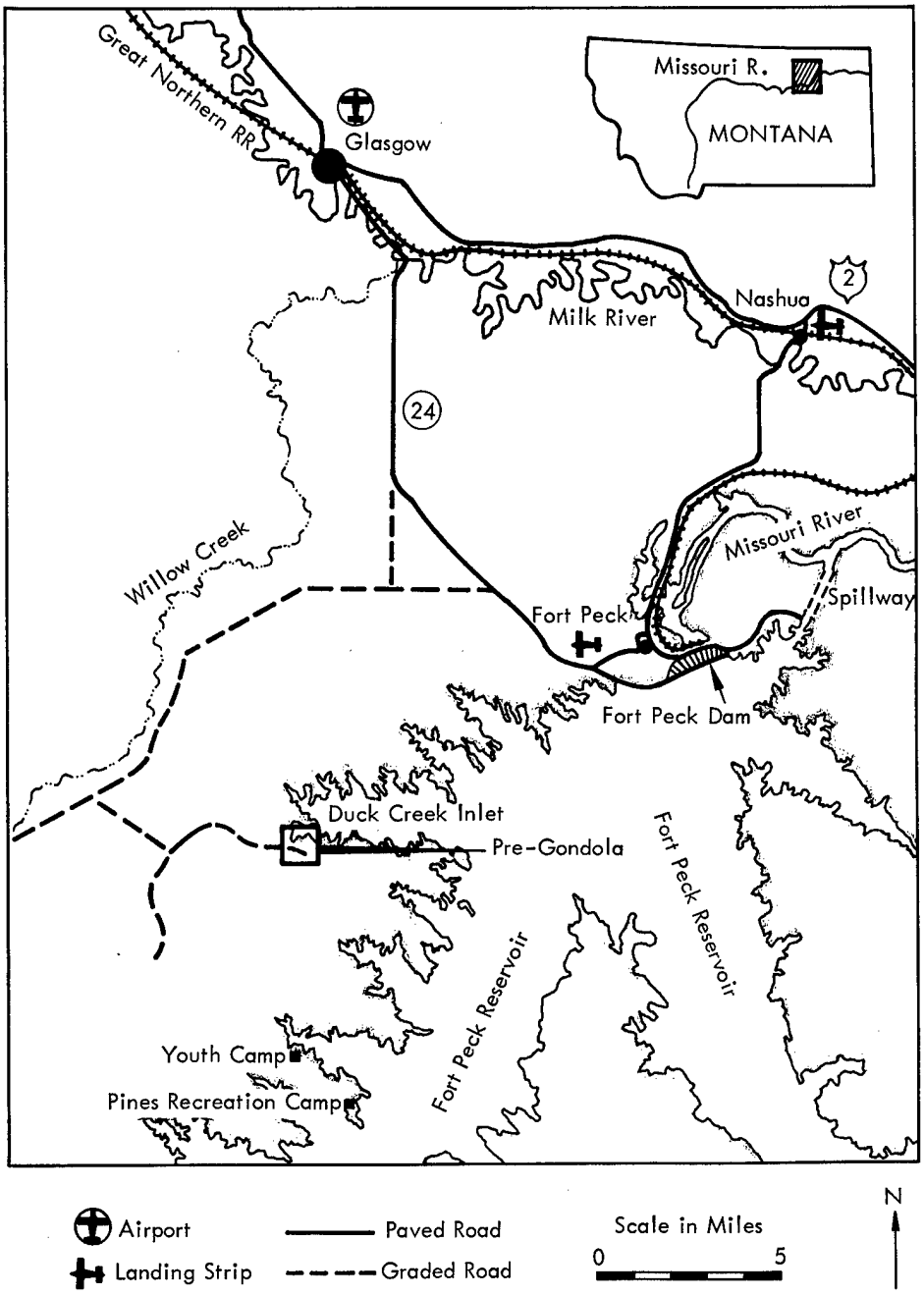

Figure 1.1 Index map of Ft. Peck Reservoir area showing location of Pre-Gondola project site.

1.3.2 Crater Measurements. The technical objectives of the crater measurement program were (1) to determine the size and shape of the apparent craters and crater lips produced by detonations at varying depths of burial, (2) to determine the maximum range of missiles resulting from each of the detonations, (3) to evaluate the shape and size of the apparent craters and lips with respect to the medium, varying geologic conditions, and varying depths of burial, and (4) to analyze and to present the collected data in a manner for efficient use in the design of future cratering events.

1.3.3 Ejecta Studies. The technical objectives of the ejecta study program were (1) to determine the origin, displacement, and deposition of material ejected from the crater, and (2) to present the collected data in a manner for efficient use in the analysis of the cratering phenomena of these detonations as well as the design of future cratering events.

1.4 BACKGROUND

Prior to the Pre-Gondola project no significant cratering experiments had been conducted in a weak, wet, clay-shale medium. Because of the lack of meaningful cratering experience in this type of medium, a row-charge excavation could not be designed until the cratering characteristics of the project site were determined. Thus, the Pre-Gondola I project was designed to calibrate the site for the Pre-Gondola II and III row-charge cratering events.

The Pre-Gondola project site was selected based upon a number of site selection requirements (Reference 2). The Pre-Gondola I surface ground zero (SGZ) locations were selected on the basis of suitable topography and suitable though minimal distances between the SGZ locations. The 1,000-pound spherical, liquid explosive nitromethane (CH_3NO_2) Seismic Site Calibration Events were then located to provide a seismic source near each of the Pre-Gondola I sites. The frontispiece shows the relative position of each of the craters produced by the Seismic Site Calibration and Pre-Gondola I Events.

Appendix A lists the crater measurements of each event of the previous 1,000-pound series. Appendix A also includes drawings which show in plan view the outline of the apparent crater, the outer boundary of continuous ejecta, and the range of the most distant missile in each quadrant of the section about the SGZ. Preshot and postshot orthogonal, topographic profiles of each crater accompany the plan view drawings.

A wide range of depths of burst was employed for the 1,000-pound shots so that the general shape and position of the cratering curves for Bearpaw shale could be approximated. The resulting curves were utilized to select the depths of charge emplacement for the Pre-Gondola I series.

CHAPTER 2
PRESHOT SITE DESCRIPTION

2.1 TOPOGRAPHY

The topography of the experimental area consisted of a slightly undulating surface adjacent to the Fort Peck Reservoir on one side and gently rolling hills on the other. The maximum slope of the ground surface at the site of any of the detonations was only about 1:20 (Delta). Figure 2.1 shows the general nature of the preshot ground surface. Figures 2.2 through 2.5, show the preshot topography of the ground surface for each event.

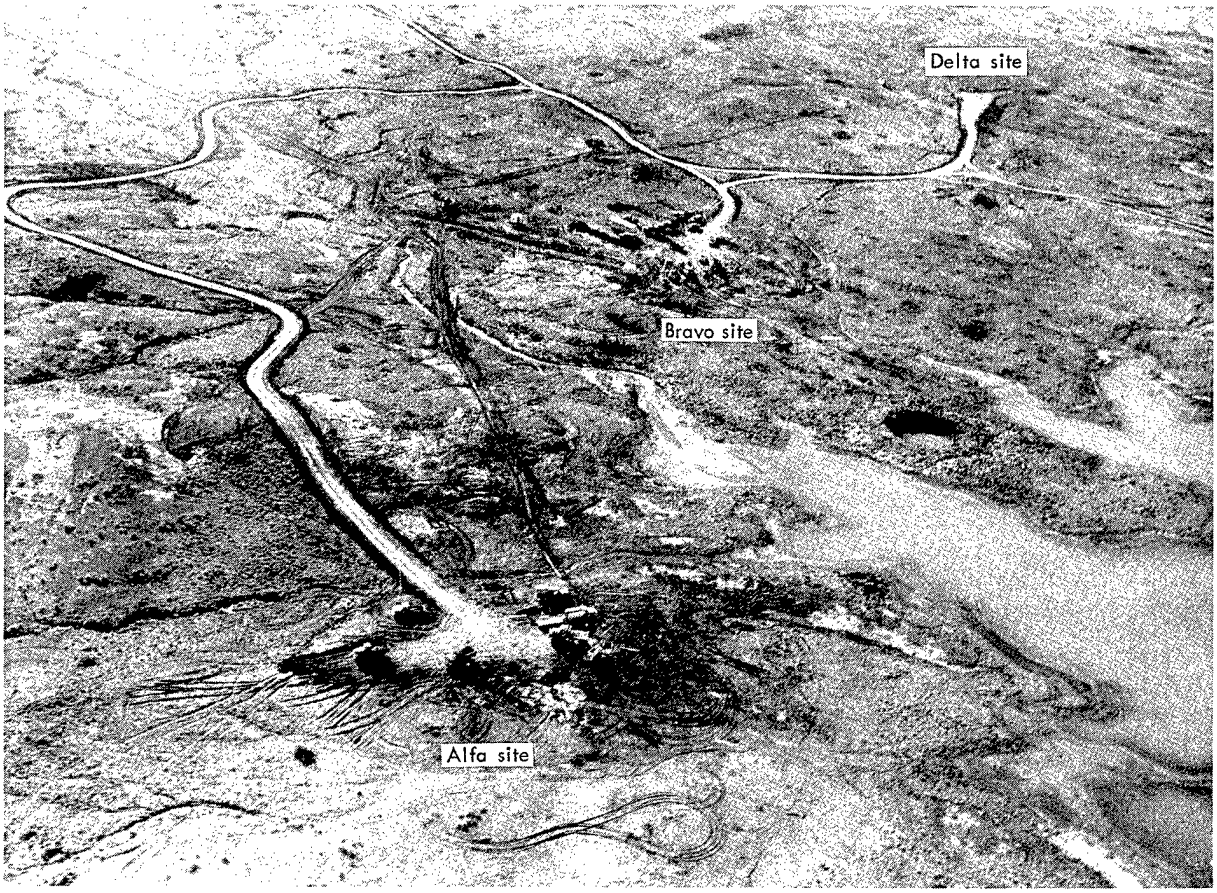

Figure 2.1 Alfa, Bravo, and Delta sites.

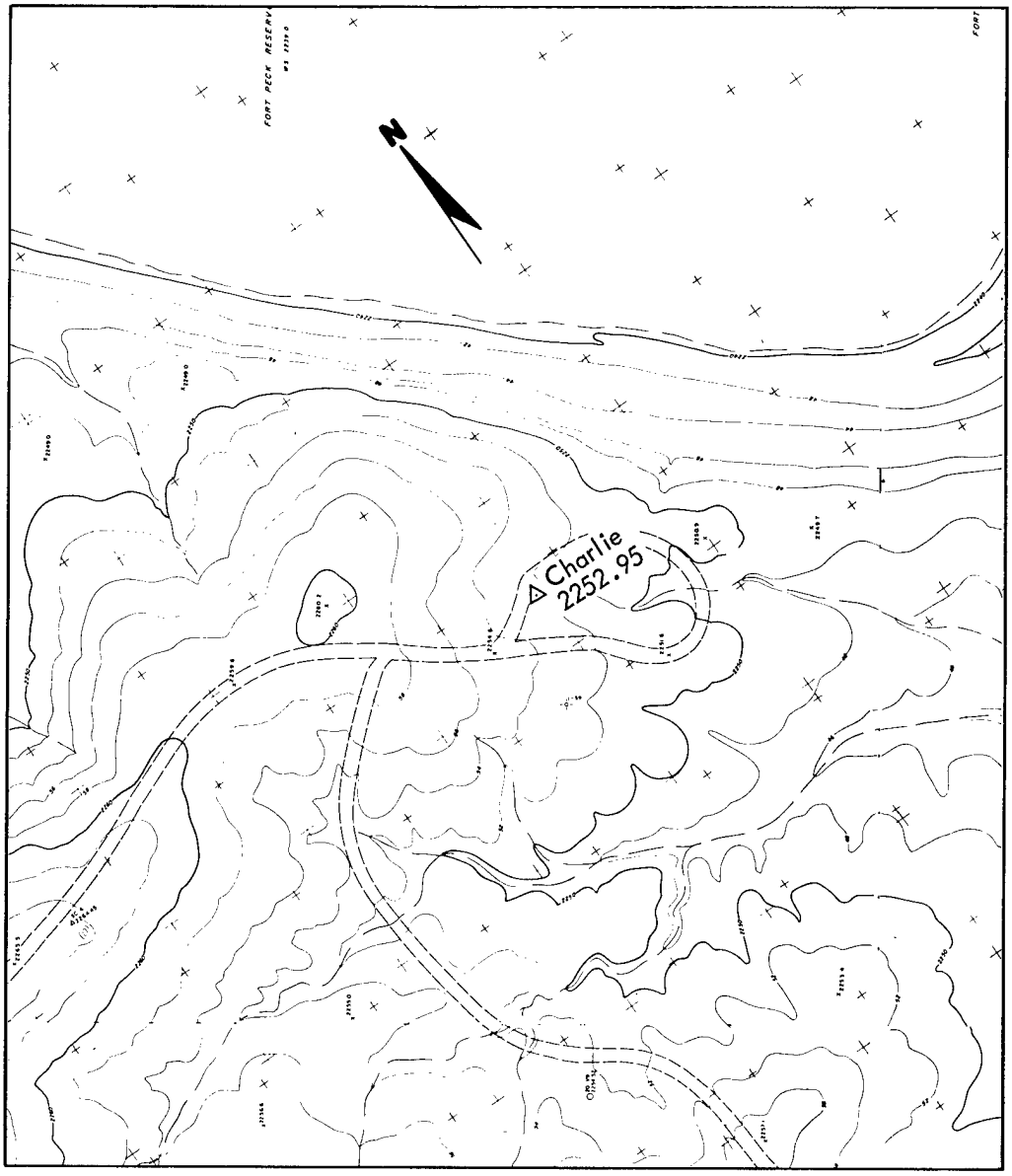

Figure 2.2 Preshot topography, Charlie site.

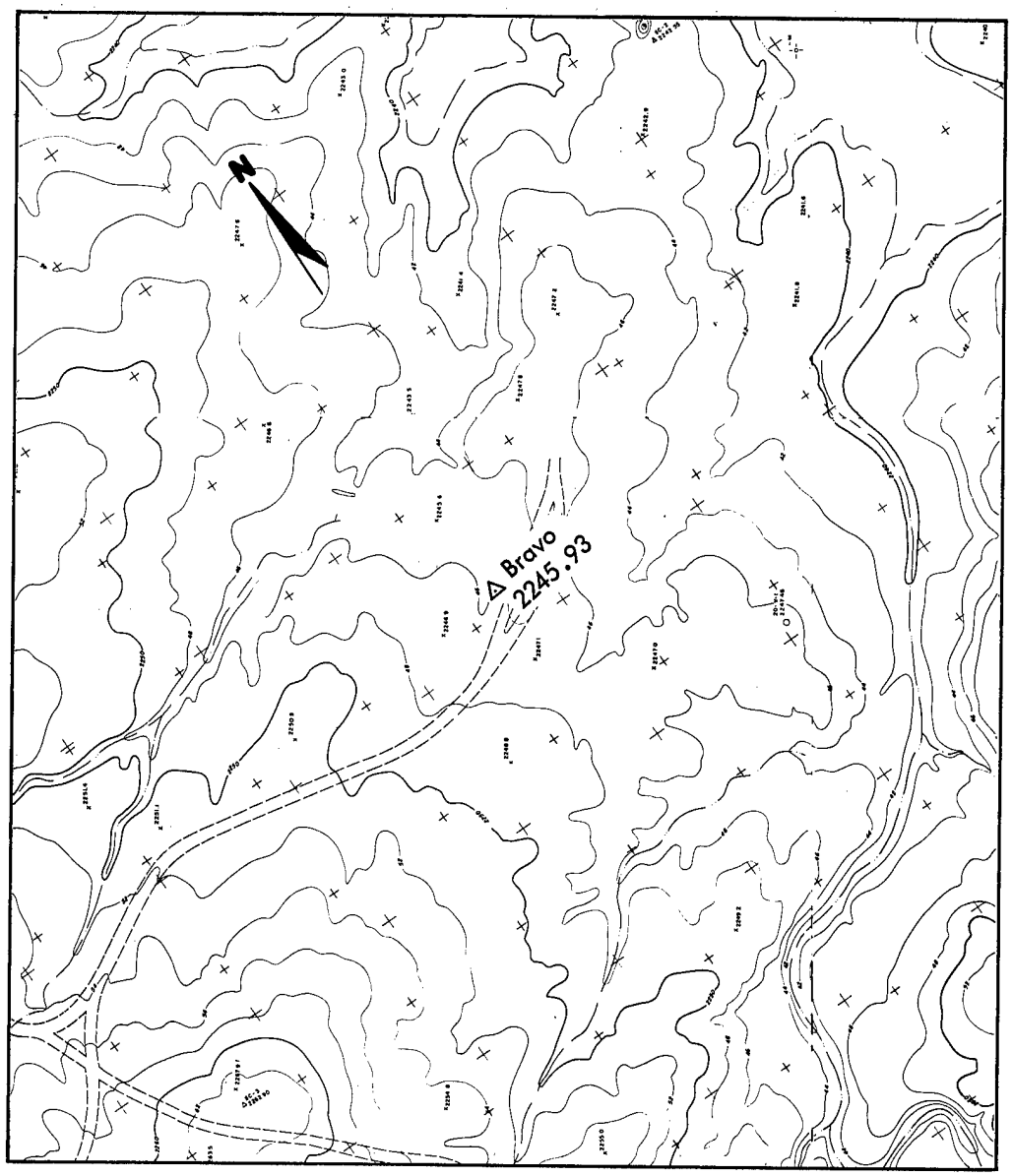

Figure 2.3 Preshot topography, Bravo site.

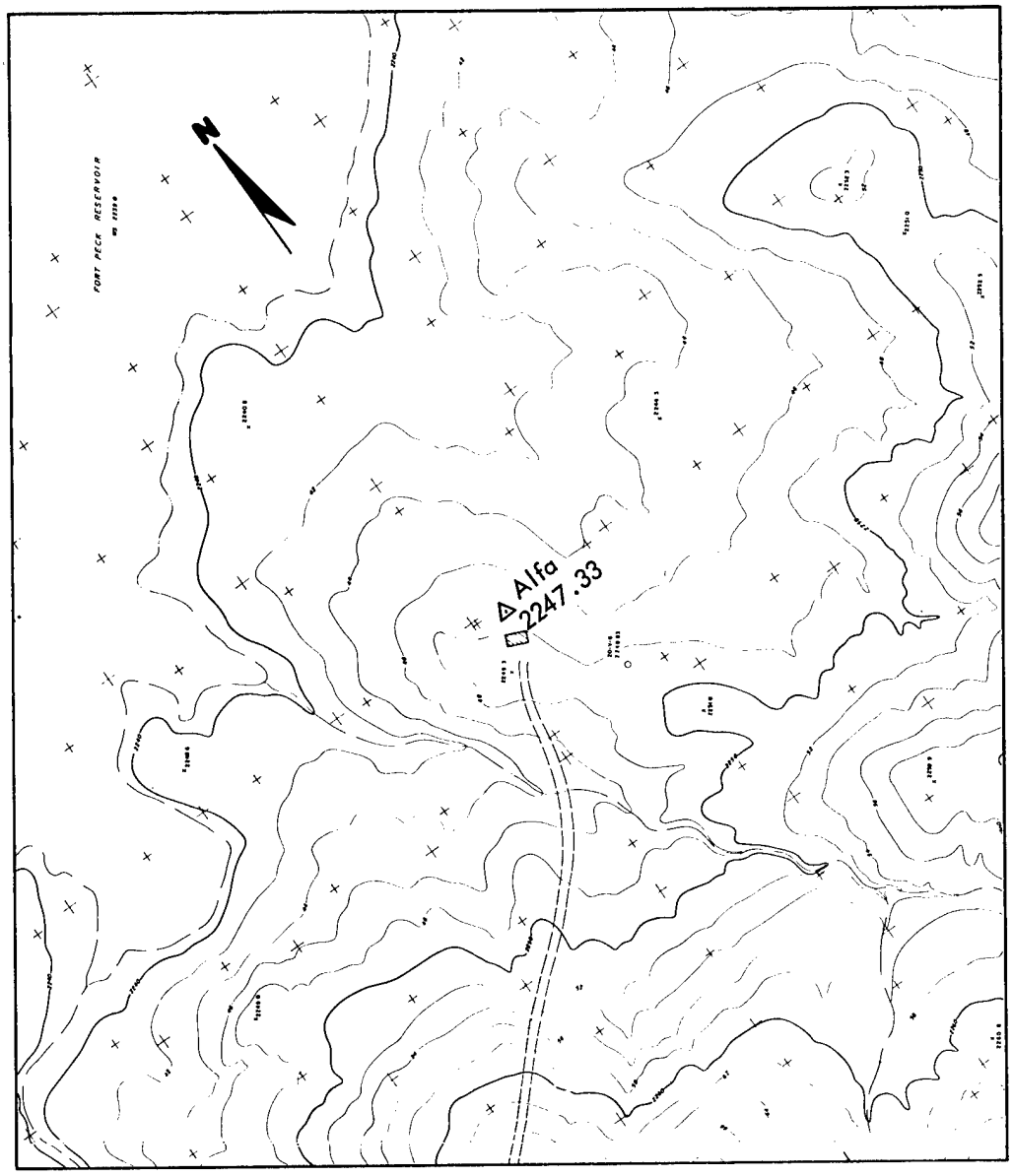

Figure 2.4 Preshot topography, Alfa site.

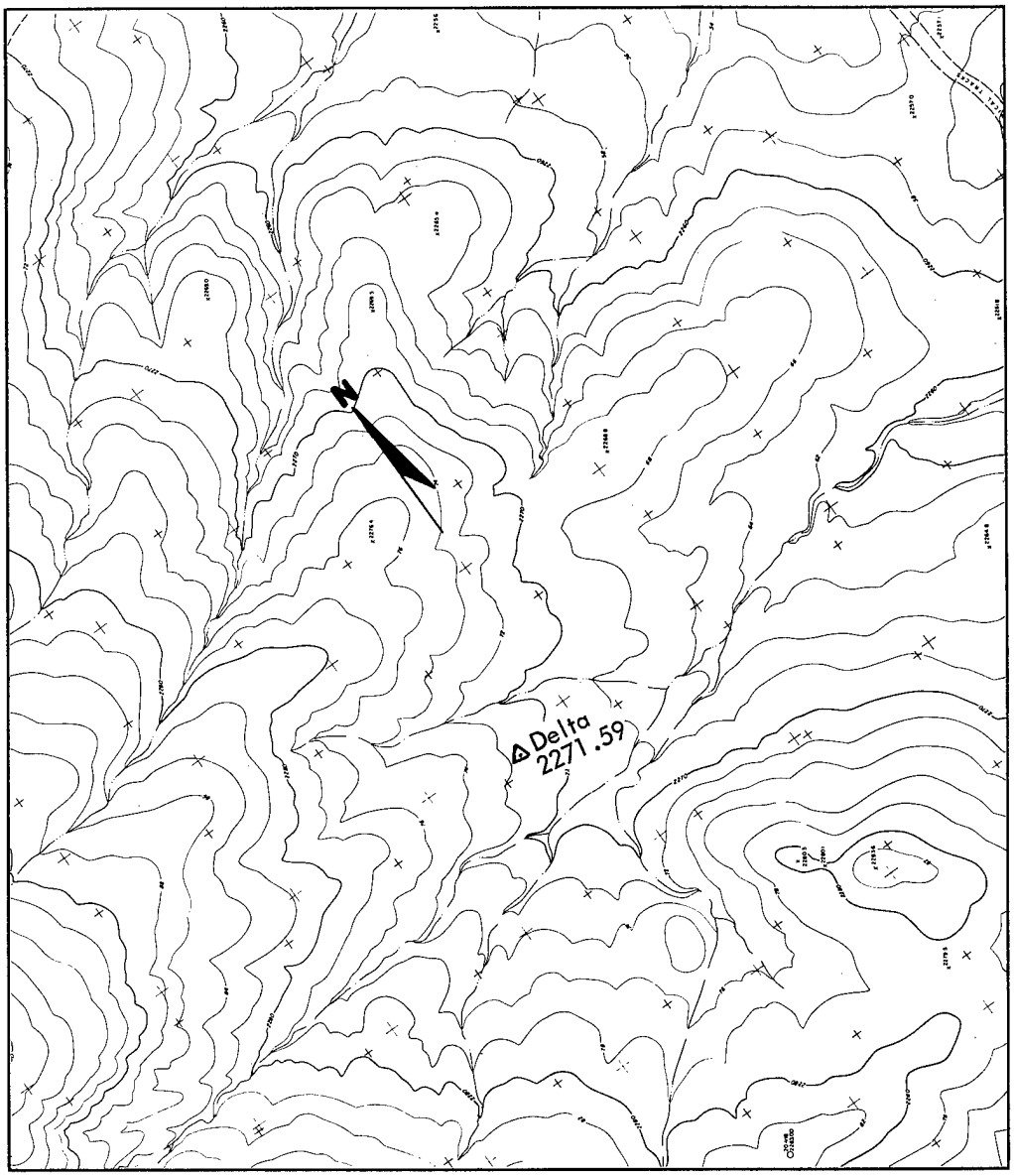

Figure 2.5 Preshot topography, Delta site.

2.2 GEOLOGY

The ground surface at each of the sites was underlain by the Late Cretaceous age, Bearpaw shale formation. At the Bravo site the shale was covered by a mantle of 5 to 6 feet of glacial till and alluvium, and at the Delta site the shale was covered by an insignificant amount of overburden. The Bearpaw formation has been described as a dark gray, uncemented but highly compacted, moderately jointed shale (Reference 2). Weathering effects were observed to depths of about 5 feet at the Alfa and Bravo sites, while at the Charlie and Delta sites the effects of weathering extended to depths of about 14 feet.

Below the weathered zone, the Bearpaw shale was essentially homogeneous, except for thin but persistent bentonite layers and occasional disk-shaped calcareous concretions which ranged up to about 1 foot in diameter. The stratigraphic section revealed by boreholes at the four sites may be divided into two distinct parts. The upper member is, for the most part, devoid of bentonite layers except for a pair of bentonite layers whose thicknesses range up to 4 inches and which always occur about 30 feet above the base of the member. Underlying this upper member, the stratigraphic section contains numerous thin bentonite layers. The top of the member is distinctively marked by a 6-inch bentonite layer. Figure 2.6 is a topographic map which shows the location of a geologic cross section drawn through the SGZ boreholes, and Figure 2.7 shows the geologic cross section (Reference 1).

A shear plane cut the Alfa SGZ boring at a depth of about 58 feet. About 60 feet of the stratigraphic section was absent from the borehole core because of faulting (Figure 2.7). Several joint sets with inconsistent orientations occurred at spacings of 1/2 to 3 feet, and numerous hairline cracks were visible between the major joints. The average moisture content of the core samples which were analyzed was 20 percent by weight, while the average percentage of saturation was 98 percent (Reference 1).

2.3 CHARGE AND EMPLACEMENT

2.3.1 General. Each chemical explosive charge for Pre-Gondola I consisted of approximately 40,000 pounds (20 tons) of liquid explosive nitromethane, contained in a mined spherical cavity approximately 10 feet in diameter and center-detonated with a booster charge. Figure 2.8 shows the charge design.

2.3.2 Cavity Construction. To construct the cavity, an access hole 38-inches in diameter was first drilled 8 feet, 6 inches deeper than the desired depth of burst (DOB). Near the bottom of the access hole, a spherical cavity, roughly 11 feet in diameter, was then excavated using standard mining methods with pneumatic and hand tools. Blasting was not permitted. During construction a sump, 3 feet deep, was maintained at the bottom of the access hole to collect and to control the ground water and facilitate mucking operations. Rock anchors and long shale pins were installed radially on a

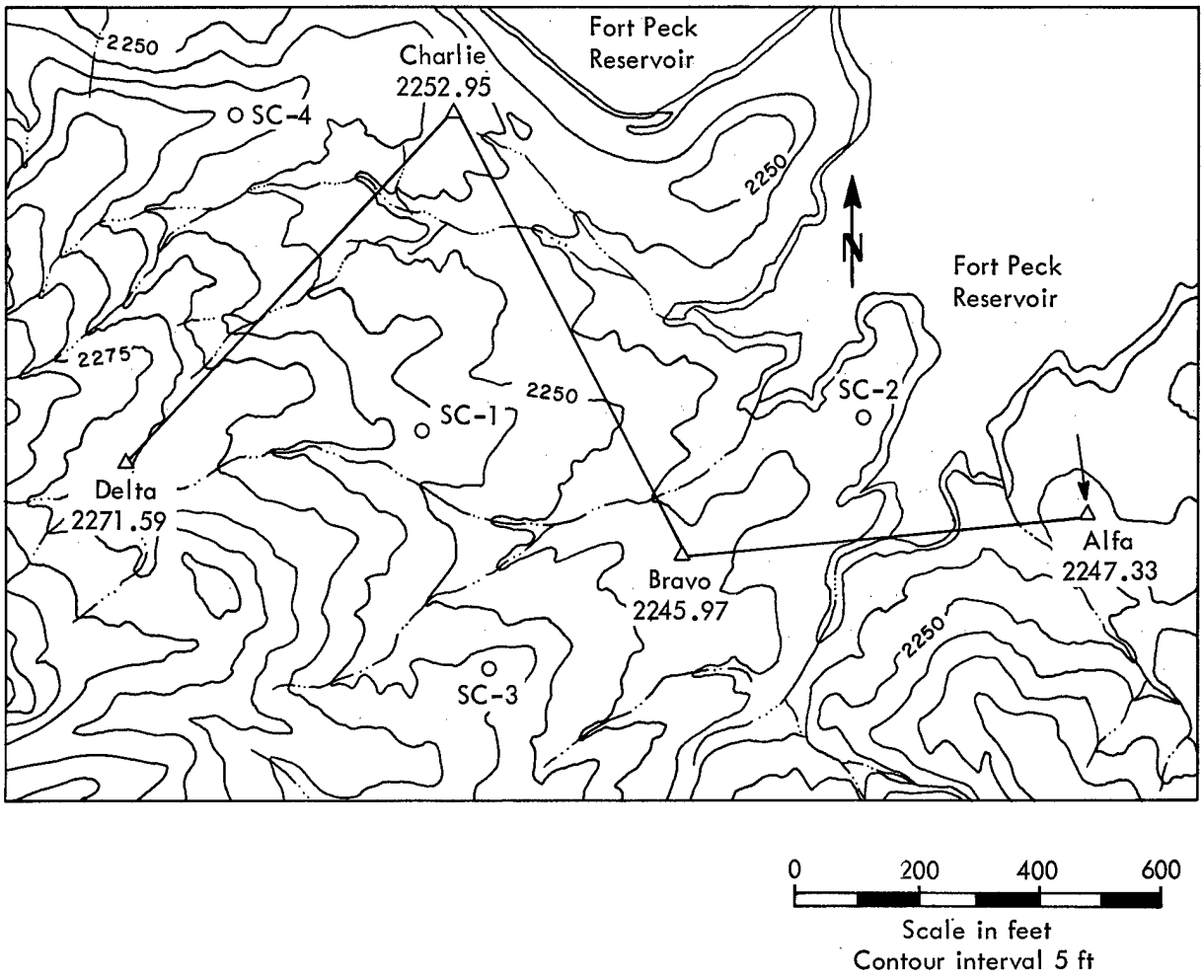

Figure 2.6 Topographic map showing location of geologic profile.

concentric ring pattern to insure personnel safety, cavity integrity, and support of the shotcrete wire fabric reinforcing. The cavity was brought into spherical tolerance, 10 feet 3-1/4 inches ± 1-1/4 inches in diameter, with pneumatically applied mortar (shotcrete) and made liquid tight with an elastomer seal coat reinformed with glass fabric. After completion the cavities were filled with water to determine whether any leaks were present. The water was removed shortly before the loading of the nitromethane by lowering a submersible pump down the vent line.

2.3.3 Booster Charge and Down-Hole Hardware Emplacement. Upon completion of the liquid-tight test, the down-hole loading assembly consisting of mounting ring, aluminum fill, and vent lines was installed. The mounting ring was suspended from steel channels set in the access hole keyway by three 3/4-inch coil-proof chains and grouted in place. The booster charge, 6 pounds of composition C-4 explosive in an aluminum canister detonated by two SE-1 high-energy detonators, was lowered down the

vent line by hand and suspended at the cavity center after the emplacement of the nitromethane charge. Fill and vent lines were sand-stemmed.

2.3.4 Access Hole Stemming. The access hole stemming material was designed to react to the cratering mechanisms of the explosion in the same manner as the surrounding in situ material. Stemming material consisted of colored concrete, the properties of which matched as closely as possible the pertinent strength characteristics (compression, tension, shear) of the clay-shale medium. The concrete was color-layered to assist in the postshot identification of the material and the evaluation of the stemming effectiveness. The stemming configuration was designed so that the total bond-shear resistance of the concrete-shale interface was at least equal to the total unconfined dynamic shear resistance of the in situ rock mass. Final stemming designs, as developed by the Waterways Experiment Station (WES), are shown in Figure 2.9.

2.3.5 Nitromethane Emplacement. The explosive nitromethane was transported to the project site in factory-sealed 55-gallon drums. On the day preceding the scheduled detonation, the nitromethane was transferred from the drums to the cavity by gravity flow through plastic hoses connected to an aluminum manifold, and finally to the 1-1/2-inch fill line which extended down the access hole into the cavity.

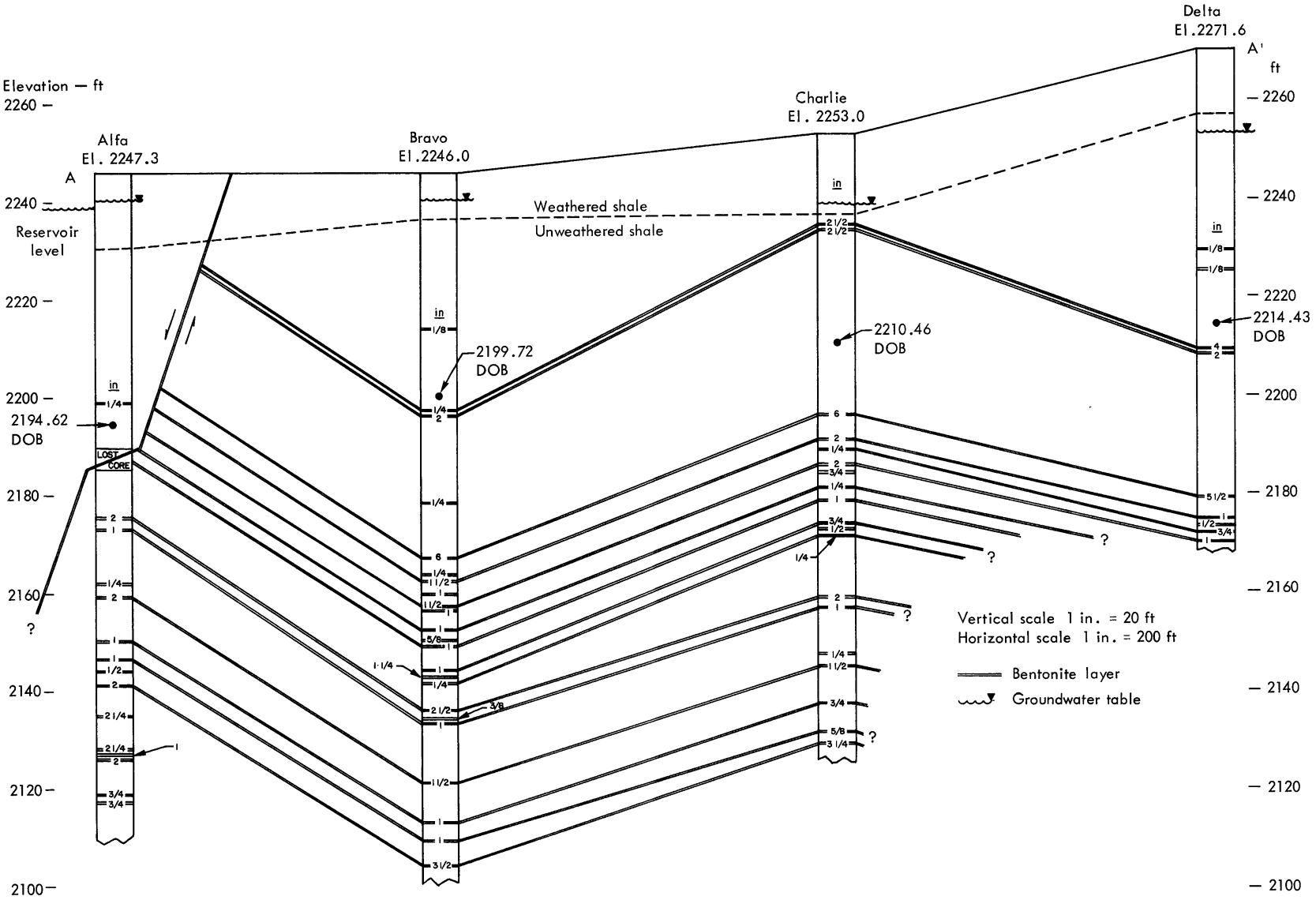

Figure 2.7 Geologic cross section drawn through Alfa, Bravo, Charlie, and Delta surface ground zeros.

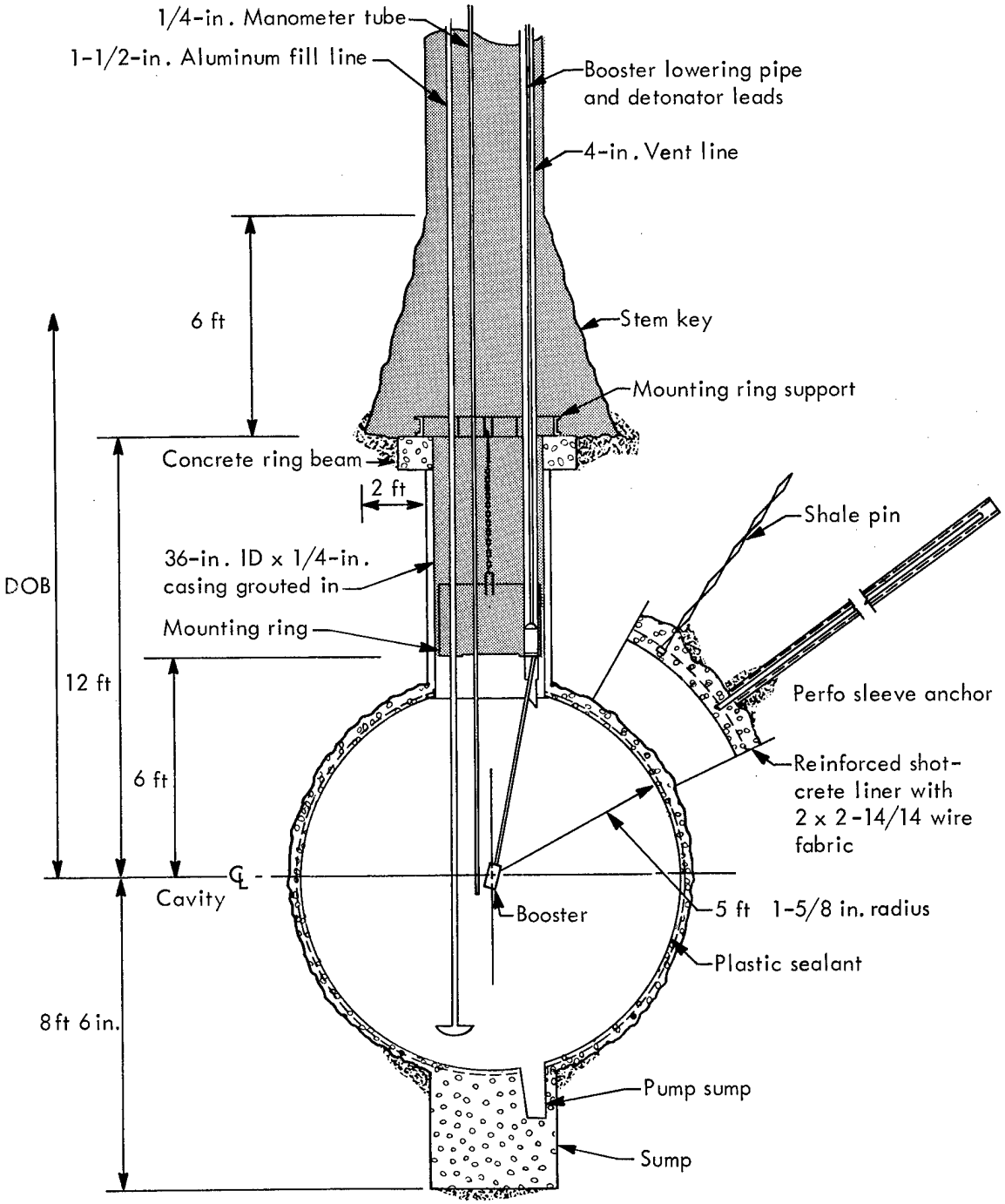

Figure 2.8 Cross section of chemical explosive charge.

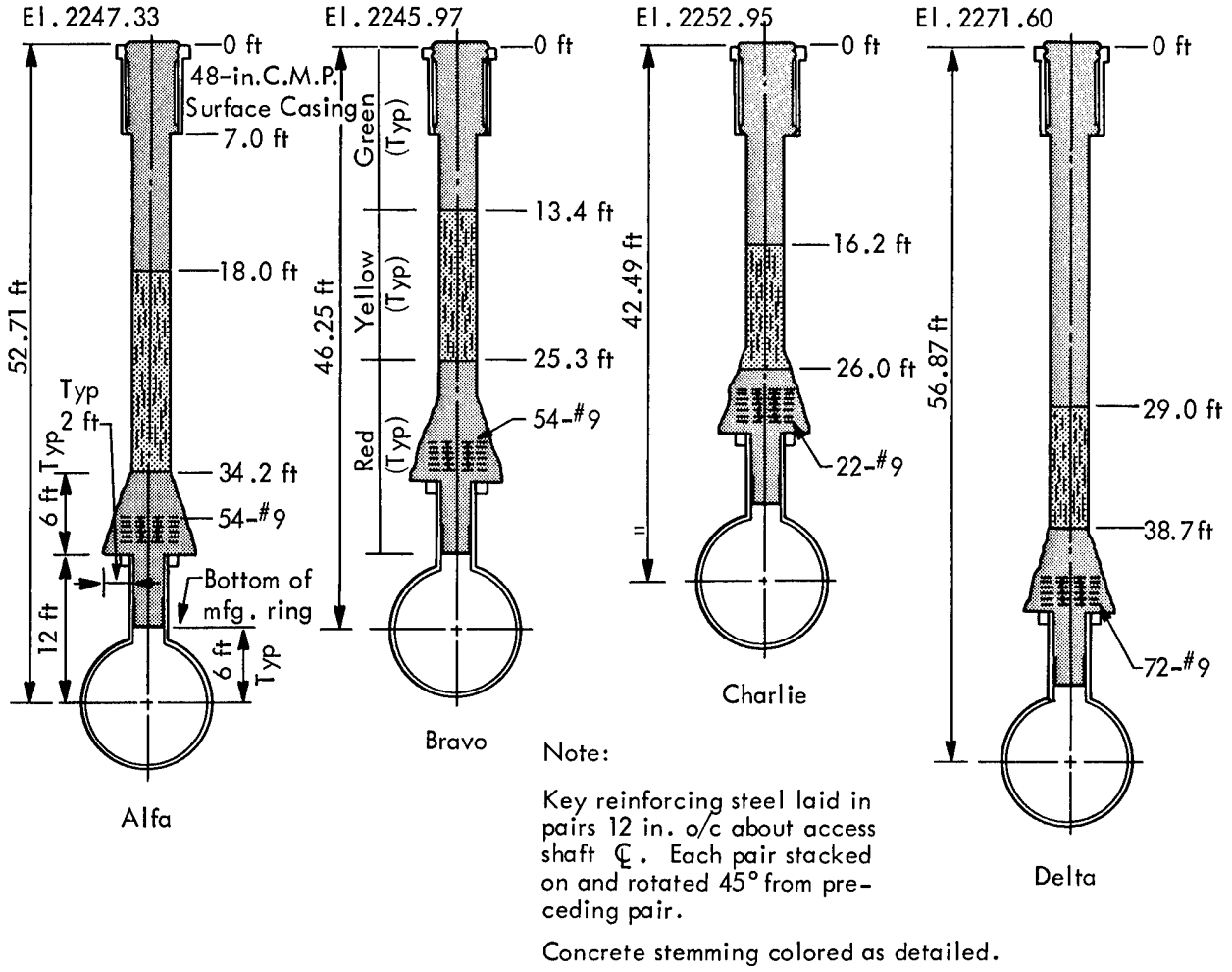

Figure 2.9 Access hole stemming designs.

CHAPTER 3
EXPERIMENTAL PROCEDURES

3.1 CRATER NOMENCLATURE

The system of crater nomenclature and notation shown in Figure 3.1 has been followed in this report.

3.2 PRESENTATION OF POSTSHOT CRATER TOPOGRAPHY

The apparent crater dimensions as given in this report were determined by comparing the preshot and postshot topographic surfaces of each crater area. In order to facilitate these measurements and better illustrate the changes in the ground surface caused by the detonation, a map very similar to an isopach map has been used in this report. This map consists of contours of the interval between the preshot and postshot ground surfaces. The zero contour lines follow the trace of the intersection of the preshot and postshot ground surfaces. The inner zero contour line delineates the outline of the apparent crater, and the outer zero contour line delineates the outer edge of the apparent lip. Negative contour lines show the configuration of the apparent crater. Positive contour lines show the configuration of the apparent crater lip. This map may be used, therefore, to determine directly all apparent crater measurements of interest.

3.3 CARTOGRAPHY

The scale of the maps from which the measurements were taken was 1 inch = 20 feet. The preshot topographic maps had a contour interval of 2 feet, and the postshot topographic maps had a contour interval of 1 foot. Each of the maps was made from aerial photographs by stereophotogrammetric techniques. The isopach-type maps were prepared by superimposing the preshot and postshot topographic maps, by plotting the value of the positive or negative difference between the preshot and postshot contour lines at their points of intersection, and, finally, by contouring the plotted points.

3.4 CRATER MEASUREMENT PROCEDURES

The following procedures were followed to determine the apparent crater and lip measurements.

3.4.1 Average, Maximum, and Minimum Apparent Crater Radii. The area inside the inner zero contour line on the isopach-type map was measured with a

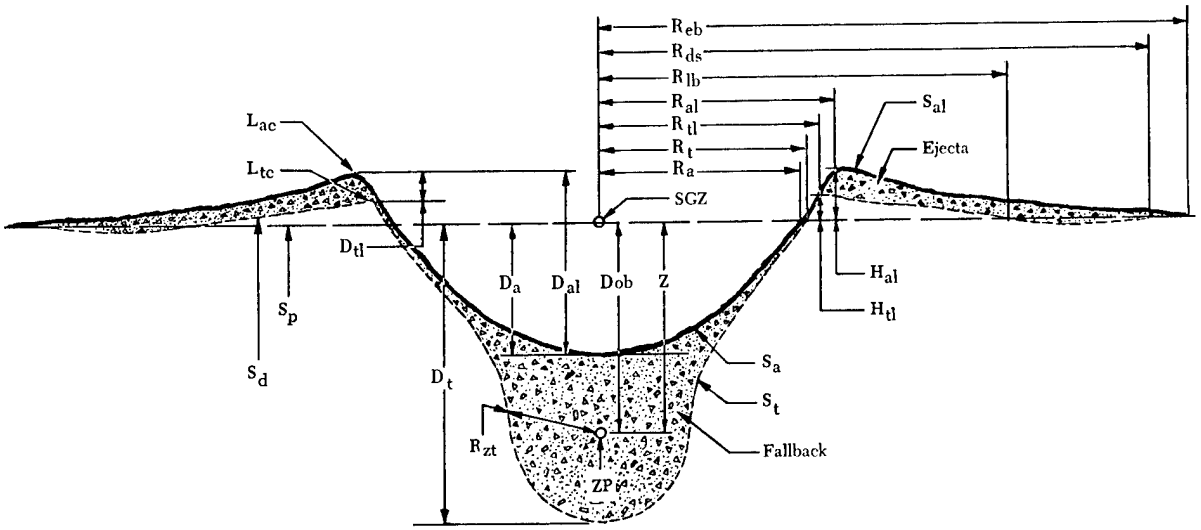

D_a . . . Maximum depth of apparent crater below preshot ground surface measured normal to the preshot ground surface.*

D_{al} . . . Depth of apparent crater below average apparent crater lip crest elevation.

Dob . . Normal depth of burst (measured normal to preshot ground surface).

Dt . . . Maximum depth of true crater below preshot ground surface.

D_{tl} . . . Depth of true crater lip crest below apparent crater lip crest.

Ejecta . Material above and or beyond the true crater and includes: (1) foldback; (2) breccia—ballastic trajectory; (3) dust—aerosol transport; etc.

Fallback. Material fallen inside the true crater and includes: (1) slide blocks; (2) breccia and stratified fallback —ballastic trajectory; (3) dust—aerosol transport; (4) talus; etc.

H_{al} . . . Apparent crater lip crest height above preshot ground surface.

H_{tl} . . . True crater lip crest height above preshot ground surface.

L_{ac} . . . Apparent crater lip crest.

L_{tc} . . . True crater lip crest.

R_a . . . Radius of apparent crater measured on the preshot ground surface.

Note: The radius measurements pertain only to single charge craters and represent average dimensions. If crater shape deviates substantially from circular, the direction of measurement must be specified. An average radius value can also be determined by dividing the plan area by π and taking the square root.

R_{al} . . . Radius of apparent lip crest to center.

R_{ds} . . . Outer radius of displaced surface.

R_{eb} . . . Radius of outer boundary of continuous ejecta.

R_{lb} . . . Outer radius of true lip boundary.

R_t . . . Radius of true crater measured on the preshot ground surface.

R_{tl} . . . Radius of true lip crest to center.

R_{zt} . . . Distance between the zero point and the true crater surface measured in any specified direction. When measured in a direction below the zero point is equivalent to lower cavity radius.

S_a . . . Apparent crater surface, e.g. rock-air or rubble-air interface.

S_{al} . . . Apparent lip surface.

SGZ . . Surface ground zero.

S_d . . . Displaced ground surface.

S_p . . . Preshot ground surface.

S_t . . . . True crater surface, e.g. rock-air or rock rubble interface.

V_a . . . Volume of apparent crater below preshot ground surface.

V_{al} . . . Volume of apparent crater below apparent lip crest.

V_t . . . Volume of true crater below preshot ground surface.

V_{tl} . . . Volume of true crater below true crater lip crest.

Z . . . . Vertical depth of burst (equivalent to Dob when crater is formed on a horizontal surface).

ZP . . . Zero Point—effective center of explosion energy.

Note: The following definitions apply to linear craters only. Linear crater refers to the excavation formed by overlapping crater effects resulting from a row of charges. All above terms applicable to single craters apply also to linear craters with the exception of the radius terms which are replaced by the width terms below.

W_a . . . Width of apparent linear crater measured on the preshot ground surface.

W_{al} . . Width of apparent lip crest measured across linear crater.

W_{ds} . . Width of displaced surface measured across linear crater.

W_{eb} . . Width of outer boundary of continuous ejecta measured across linear crater.

W_{lb} . . Width of true crater outer lip boundary measured across linear crater.

W_t . . . Width of true linear crater measured on the preshot ground surface.

W_{tl} . . . Width of true linear crater lip crest measured across crater.

*All distances, unless specified otherwise, are measured parallel or perpendicular to preshot ground surface.

Figure 3.1 Crater nomenclature.

planimeter, and the average apparent crater radius, R_a, was calculated as the radius of a circle having the same area. The center of the apparent crater was estimated visually as the location of the center of a circle of radius, R_a, in the position which most closely approximated the apparent crater outline or the inner zero contour line. Maximum and minimum radii were measured from the apparent crater center.

3.4.2 Apparent Crater Depth. The apparent crater depth, D_a, is defined as the distance between the deepest point in the crater and the preshot ground surface measured perpendicular to the preshot ground surface. Because all of the Pre-Gondola I sites were essentially level, the depths of the apparent craters were measured as the difference in elevation between the deepest point in each crater and the elevation of the preshot ground surface vertically above that point. The apparent depths of each crater may be read directly from the isopach-type map.

3.4.3 Average, Maximum, and Minimum Apparent Lip Radii. The trace of a line drawn along the crest of the apparent lip on either the postshot topographic map or the isopach-type map corresponds to the outline of the lip crest radius. The average lip crest radius, R_{al}, and the maximum and minimum lip crest radii were determined in the same manner as the average, maximum, and minimum apparent crater radii.

3.4.4 Average, Maximum, and Minimum Apparent Lip Height. The average apparent lip height, H_{al}, was determined by (1) plotting from the isopach-type map a profile of the relief along the apparent lip crest, (2) using a planimeter to determine the area between the lip crest profile and the zero level on the profile, and (3) dividing the measured area by the length of the lip crest profile. The maximum and minimum apparent lip heights may be read directly from the isopach-type maps as the maximum and minimum values which occur along the apparent lip crests.

3.4.5 Average Radius of Outer Boundary of Continuous Ejecta. The area inside the outer zero contour line on the isopach-type map was measured with a planimeter, and the average radius of the outer boundary of continuous ejecta, R_{eb}, was calculated as the radius of a circle having the same area.

3.4.6 Apparent Crater Volume. The apparent crater volume, V_a, was determined by (1) measuring with a planimeter the area inside each negative contour line on the isopach-type map, and (2) calculating, by use of an average end-area method applied to horizontal sections taken at 1-foot intervals (the contour interval of the large scale isopach-type map), the total volume of the apparent crater.

3.4.7 Apparent Lip Volume. The apparent lip volume, V_{al}, was determined in a manner similar to that of the apparent crater volume. The average end-area method was applied to the areas of the positive contour lines on the isopach-type map.

3.4.8 Maximum Range of Missiles. The maximum range of missiles was determined by (1) locating and marking the most distant missiles found around the perimeter

of each crater, and (2) measuring on aerial photographs the most distant missile marked. The markers consisted of white plastic panels, 1 foot by 6 feet, fastened to wooden stakes which had been driven into the ground.

3.5 EMPLACEMENT AND CHARACTERISTICS OF EJECTA PELLETS

Prior to each of the events, individually coded ejecta pellets were placed in an array of five vertical holes which extended from a point near the SGZ to a point slightly beyond the predicted apparent crater radius. At the Bravo site two arrays of emplacement holes were constructed. In this report, the two arrays are distinguished from one another by the designation "A" for the array which extended toward the Control Point and the designation "B" for the other array. The only difference in the construction of the two arrays is that each of the emplacement holes in the "A" array extended to a depth of 35 feet, except the one nearest the SGZ which extended to a depth of only 20 feet.

The ejecta pellets consisted of cylinders (3 inches in diameter by 12 inches in length) of colored concrete grout which contained three quarters of a pound of colored glass fragments. The cylinders had a 7-day compressive strength of 3,000 psi. A separate color of concrete grout was used for each emplacement hole in any one array. Within each hole the position of each pellet was coded by the color or the combination of colors of its glass fragments. The elevation of the tops of each pellet was recorded to the nearest one-tenth of a foot after which concrete grout was used to fill the space between the ejecta pellets and the walls of the emplacement holes. Figure 3.2 schematically shows the spacings used between each of the ejecta emplacement holes for each event, lists the color of the concrete grout used to make the ejecta pellets, and lists the color scheme utilized to code individually each of the ejecta pellets.

3.6 POSTSHOT COLLECTION AND REDUCTION OF EJECTA STUDY DATA

After each detonation the location, approximate size, and individual code of each pellet which could be found was determined and recorded (Figure 3.3). The distance and bearing from existing reference points to the postshot position of each pellet was provided by a field survey team. These field data were converted by a computer to the actual postshot locations and distances relative to the SGZ of the particular event. The reduced data are tabulated in Appendix B.

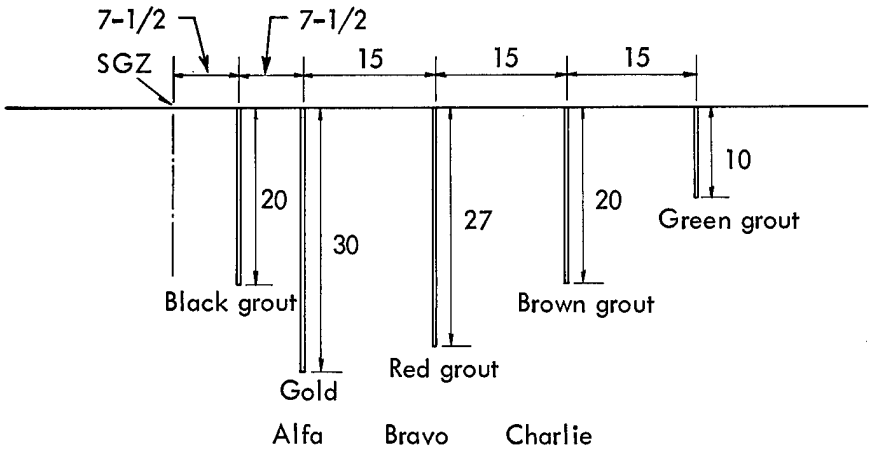

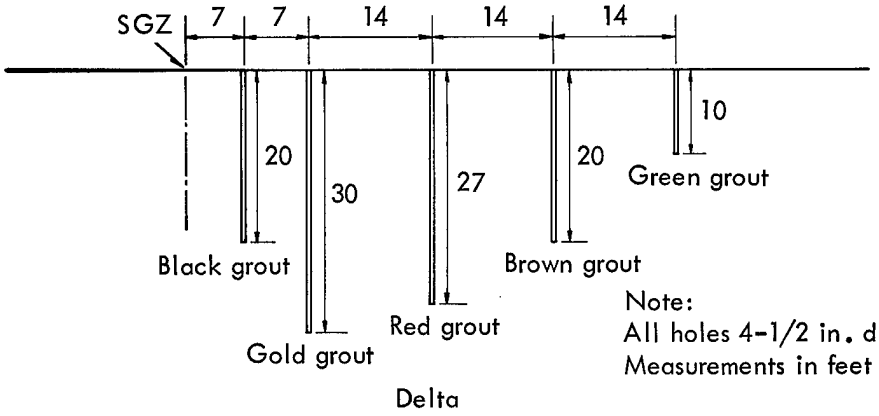

STANDARD COLOR CODE

1	2	3	4	5	6	7
Red	Green	Blue	Black	White	Yellow	Brown
8	9	10	11	12	13	14
Pink	Clear	Red Green	Red Blue	Red Black	Red White	Red Yellow
15	16	17	18	19	20	21
Red Brown	Red Pink	Red Clear	Green Blue	Green Black	Green White	Green Yellow
22	23	24	25	26	27	28
Green Brown	Green Pink	Green Clear	Blue Black	Blue White	Blue Yellow	Blue Brown
29	30	31	32	33	34	35
Blue Pink	Blue Clear	Black White	Black Yellow	Black Brown	Black Pink	Black Clear

Note: Pellet emplacement from top to bottom always in increasing numerical order

Figure 3.2 Ejecta pellet emplacement.

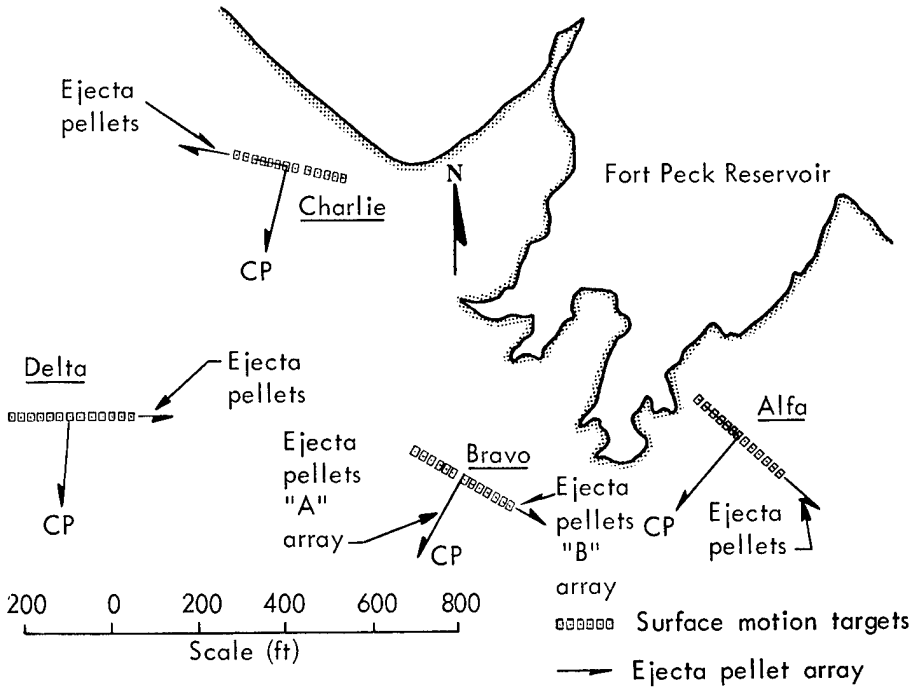

Figure 3.3 Location of ejecta pellet arrays and surface motion targets.

CHAPTER 4
SCALING AND PREDICTIONS OF CRATER PARAMETERS

4.1 SCALING OF CRATER DIMENSIONS

Because of the need for a consistent basis for comparison of crater dimensions produced by different charge weights and different charge compositions, both amongst shots within a specific medium and between shots of different media, each of the crater dimensions was scaled to a common yield of 1 kt assuming $W^{1/3.4}$ scaling.

The basis of the scaling calculations assumes the energy equivalent yield of 1 kt (2,000,000 pounds) to be the same as the release of 10^9 kcal of energy. Thus, an energy equivalent yield of 1 gram is:

$$1 \text{ gm} = \frac{10^9 \text{ kcal of energy}}{(2{,}000{,}000 \text{ lb})\ (453.5924 \text{ gm/lb})} = 1.1023 \text{ kcal}$$

The experimental heat of detonation of nitromethane is 1.227 ± 5 kcal per gram (Reference 3). Therefore, the actual weights of nitromethane were converted to energy equivalent yields by multiplying the acual weight of nitromethane by the ratio:

$$\frac{1.227 \text{ kcal}}{1.1023 \text{ kcal}} = 1.113 \approx 1 \qquad (1 \text{ ton} = 0.0011 \text{ kt})$$

where the ratio value of 1.113 was rounded to a working value of 1.1.

Table 4.1 gives the actual weights, energy equivalent yields, and scaling factors for each of the Pre-Gondola I Events.

TABLE 4.1 CHARGE YIELDS AND SCALING FACTORS

Event	Charge Weight	Energy Equivalent Yield	Scaling Factor ($kt^{1/3.4}$)
	ton	kt	
Charlie	19.62	0.021582	0.3238
Bravo	19.36	0.021296	0.3225
Alfa	20.35	0.022385	0.3273
Delta	20.24	0.022264	0.3267

4.2 PREDICTED CRATER PARAMETERS

4.2.1 Tabulated Crater Dimension Predictions. The predicted crater measurements and the maximum missile range of the four Pre-Gondola I Events are given in Table 4.2.

TABLE 4.2 PREDICTED CRATER DIMENSIONS FOR PRE-GONDOLA I

Event	Depth of Burst		Apparent Crater Radius		Apparent Crater Depth		Maximum Range of Missiles	
	1 kt	20 tons NM	1 kt	20 tons NM	1 kt	20 tons NM	1 kt	20 tons NM
Charlie	130	42.4	240	78.3	115	37.5	4200	1370
Bravo	142	46.3	240	78.3	113	36.8	3550	1160
Alfa	160	52.2	237	77.3	105	34.2	2750	900
Delta	174	56.7	227	74.0	93	30.3	2250	730

Notes: 1. Scaling factor $= \left[\frac{20 \times 1.1}{1000}\right]^{1/3.4} = 0.3261$

2. NM = nitromethane
3. All dimensions in feet

4.2.2 Prediction Procedure. The crater dimension predictions were based on data from the four 1000-pound Seismic Site Calibration shots, scaling experience in hard rock and alluvium, and limited small-charge cratering data in other clay-shale formations (Reference 4). The maximum missile range predictions were based on previous experience in hard rock and alluvial media and the observed ranges of the 1000-pound shots.

CHAPTER 5
RESULTS

5.1 GENERAL

The actual and scaled apparent crater dimensions and the results of the ejecta study measurements are tabulated in Table 5.1 using nomenclature and notations presented in Chapter 3.

Table 5.1 PRE-GONDOLA I CRATER RESULTS

Dimension[a]	Units	Event			
		Charlie	Bravo	Alfa	Delta
Charge Weight, W	(tons)	19.62	19.36	20.35	20.24
Energy Equivalent Scaling Factor	$(kt^{1/3.4})$	0.3238	0.3225	0.3273	0.3267
Depth of Burst, DOB	(ft)	42.49	46.25	52.71	56.87
Scaled dob	$(ft/kt^{1/3.4})$	131.2	143.4	161.1	174.0
Average Radius, R_a	(ft)	80.4	78.5	76.1	65.1
Scaled r_a	$(ft/kt^{1/3.4})$	248.0	243.4	232.5	199.3
Maximum Radius	(ft)	84.0	80.9	80.8	70.5
Minimum Radius	(ft)	74.3	75.0	60.0	52.0
Depth, D_a	(ft)	32.6	29.5	32.1	25.2
Scaled d_a	$(ft/kt^{1/3.4})$	100.7	91.5	98.1	77.1
Average Lip Crest Radius, R_{al}	(ft)	101.8	102.1	100.4	94.5
Scaled r_{al}	$(ft/kt^{1/3.4})$	314.4	316.6	306.8	287.4
Maximum Radius	(ft)	106.9	107.9	107.6	99.7
Minimum Radius	(ft)	95.9	96.9	92.4	89.0
Average Lip Height, H_{al}	(ft)	14.5	13.7	13.9	13.0
Scaled h_{al}	$(ft/kt^{1/3.4})$	44.8	42.5	42.5	39.8
Maximum Height	(ft)	17.2	16.1	18.4	20.0
Minimum Height	(ft)	12.4	10.8	9.9	6.2
Average Radius of Lip Boundary, R_{eb}	(ft)	294	265	227	221
Scaled r_{eb}	(ft)	908	822	694	676
Apparent Crater Volume, V_a	(ft^3)	277,550	241,260	235,300	133,880
Scaled v_a	$(ft^3/kt^{3/3.4})$	857,150	748,090	718,906	409,800
Apparent Lip Volume, V_l	(ft^3)	694,452	533,620	483,057	427,033
Scaled v_l	$(ft^3/kt^{3/3.4})$	2,144,694	1,654,635	1,475,884	1,307,110
Maximum Missile Range, R_{me}	(ft)	800	905	545	453
Scaled r_{me}	$(ft/kt^{1/3.4})$	2,471	2,806	1,665	1,387
Ejecta Pellet Recovery	(%)	28.3	10.6[b] 16.8[c]	14.9	31.2
Maximum Ejecta Pellet Range	(ft)	327	325[b] 404[c]	277	294
Scaled	$(ft/kt^{1/3.4})$	1,010	1,008[b] 1,253[c]	846	900

[a]Scaled dimensions are indicated by lower case letters.

[b]Referred to as "A" array in text.

[c]Referred to as "B" array in text.

The depth, volume, and average radius of the four apparent craters compared to their DOB show that, except for the depth of the Bravo crater, the progressively shallower DOB produced craters with progressively greater dimensions. It is interesting to note that while the difference of the average lip radius of the largest crater (Charlie) and the smallest crater (Delta) is only 6.3 feet, the difference between the average apparent crater radii of the same two craters is 15.3 feet. The small difference in the average lip radii causes the craters to appear to be about the same size (see Figure 5.1). However, the actual apparent crater volume of the largest crater is more than twice that of the smallest crater.

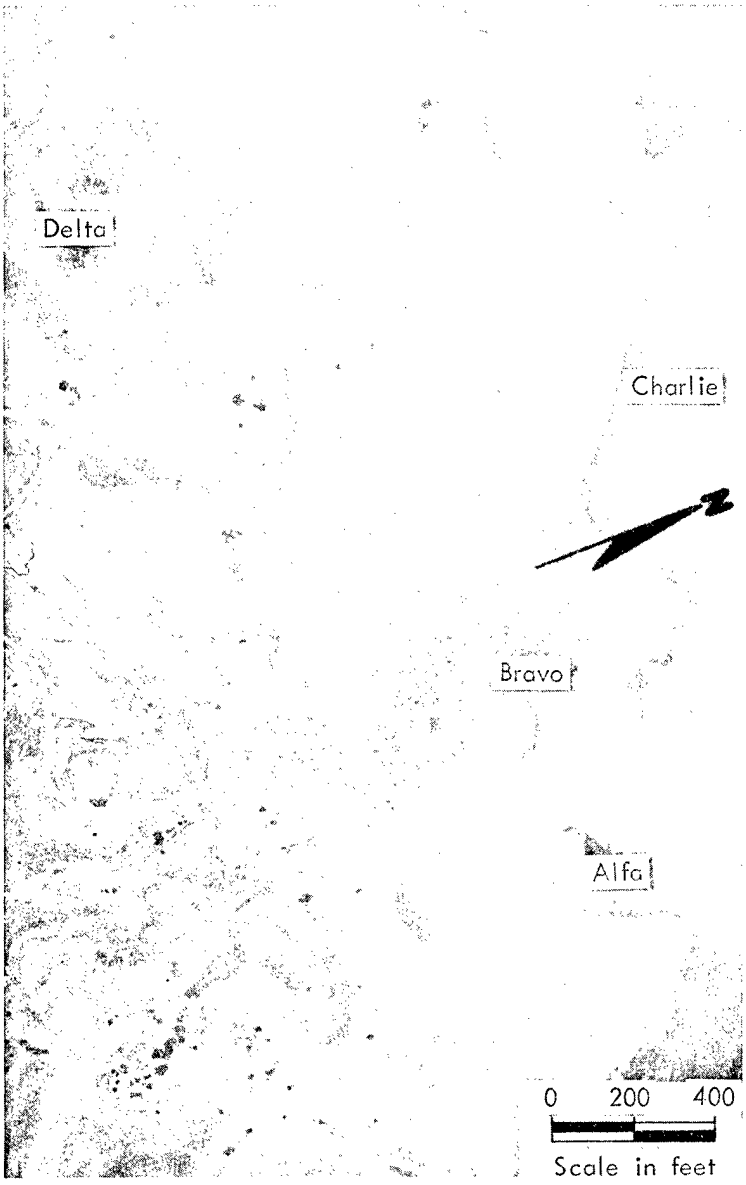

Figure 5.1 Vertical aerial photograph of Pre-Gondola I craters.

Included in Appendix B of this report are schematic drawings of each of the ejecta pellet arrays. These drawings show in cross section the ejecta pellet emplacement holes, the number of pellets installed in each hole, and adjacent to each of the recovered pellets its measured distance from SGZ.

5.2 CHARLIE EVENT

The shape of the Charlie crater was the most symmetrical of the four craters, although its deep point was displaced about 10.5 feet in a northeast direction from SGZ and the relatively flat bottom of the crater was rectangular in shape. Figure 5.2, a postshot topographic map of the Charlie crater, shows the shape and size of the apparent crater and lip. Figure 5.3 shows orthogonal profiles drawn through the apparent crater and lip, and Figure 5.4 is a contour map of the interval between the preshot and postshot ground surfaces, in which respect it is a type of isopach map. The inner zero contour line of this map corresponds to the outline of the apparent crater and the outer zero contour line corresponds to the outline of the outer boundary of continuous ejecta. This type of map is especially useful for showing the actual shape and height of the apparent lip.

The block-size of the ejecta produced by the Charlie crater was generally less than 1.5 feet in diameter, except within the crater and along the lip crest where many blocks 2.0 feet or more in diameter were found. In general, the block size was comparable to that produced by the Alfa and Delta detonations, but was considerably less than that produced by the Bravo Event. A large amount of relatively small fragments (<2 inches) occurred on the south-southeast outer part of the apparent lip (see Figure 5.5). Figure 5.6 is a high-angle oblique photograph of the Charlie crater, and Figure 5.7 is a photograph of the western part of the apparent lip. Both figures show the relative block-size produced by the detonation. A number of impact craters can be seen along the shoreline in the aerial photograph. In the photograph of the apparent lip, wooden laths mark the locations of recovered ejecta pellets.

Two cracks developed in the inside upper slope of the Charlie apparent lip. The longest crack was more than 100 feet in length and its position ranged between 3 and 9 feet below the south-southeast segment of the lip crest. Figure 5.8 is a photograph of a part of the crack. The other crack, which occurred on the west side of the crater, was less than 40 feet long and was located between 10 and 14 feet below the lip crest. The longest crack was first observed about 10 minutes after the detonation at which time its width was about 1 inch. It gradually widened during the next one-half hour after which its growth stopped. No further growth of the crack was observed during the following week. The final average width of the crack was about 2 inches and the vertical displacement was about 3 inches.

Twenty-eight percent of 106 ejecta pellets installed at the Charlie site were recovered. This recovery percentage was second only to the Delta Event. The average

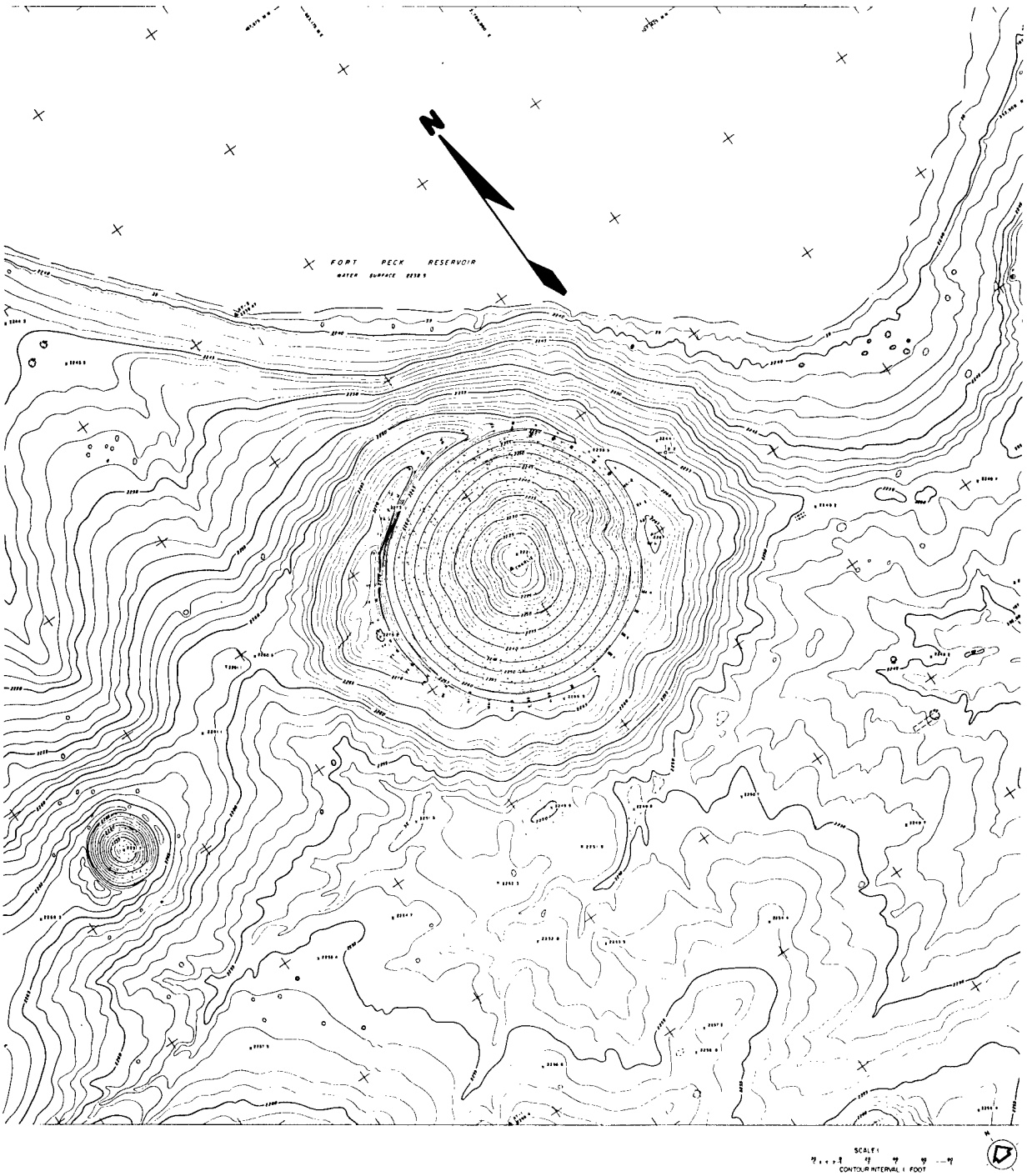

Figure 5.2 Postshot topography, Charlie crater.

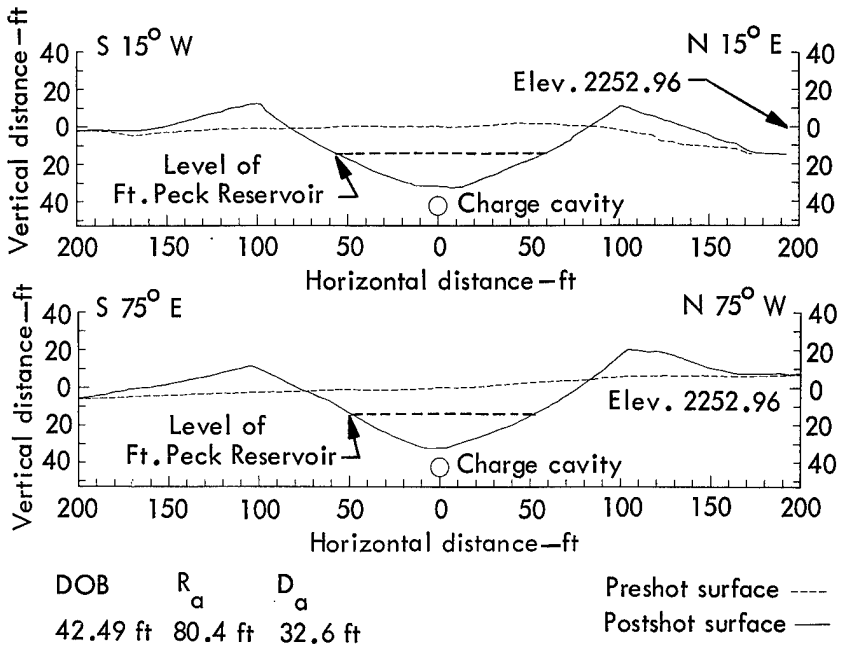

Figure 5.3 Charlie crater profiles.

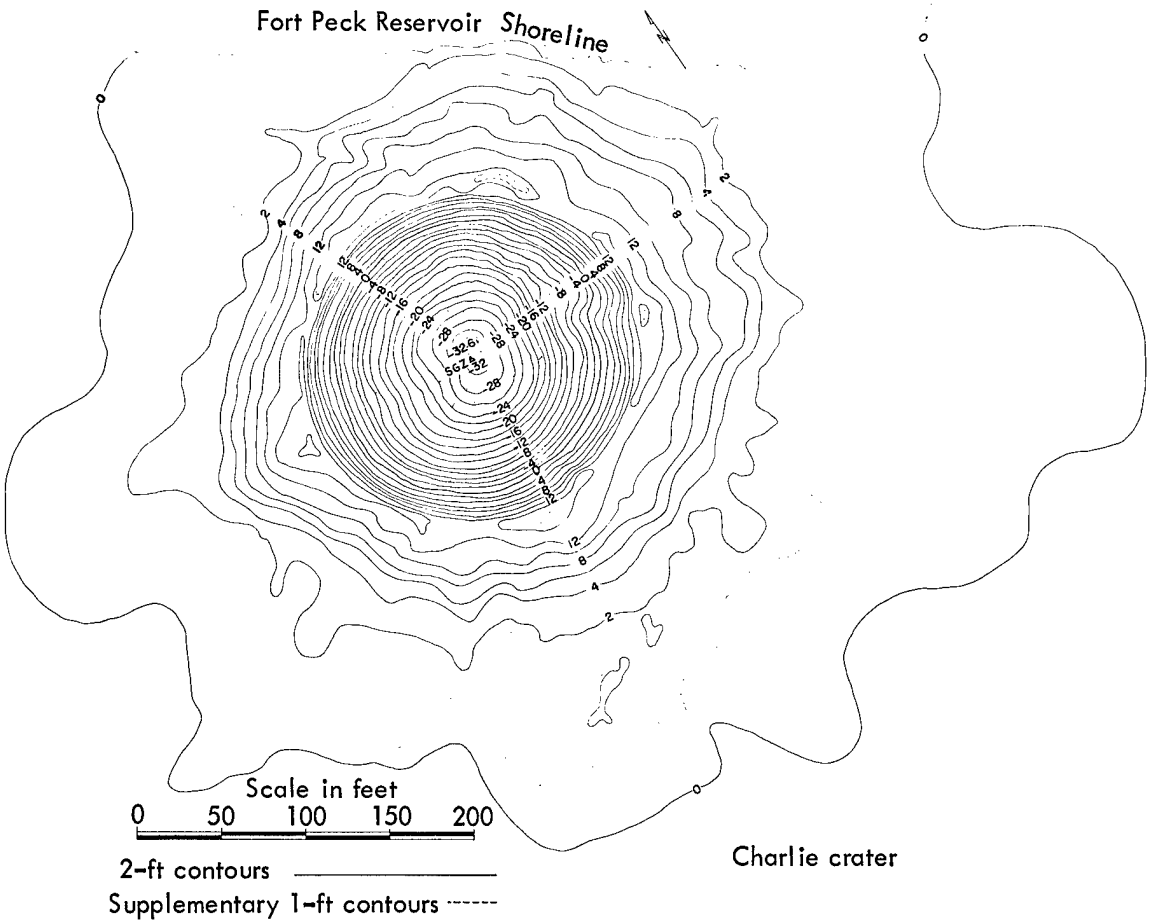

Figure 5.4 Contour map of interval between preshot and postshot ground surfaces, Charlie crater.

Figure 5.5 South part of Charlie apparent crater lip.

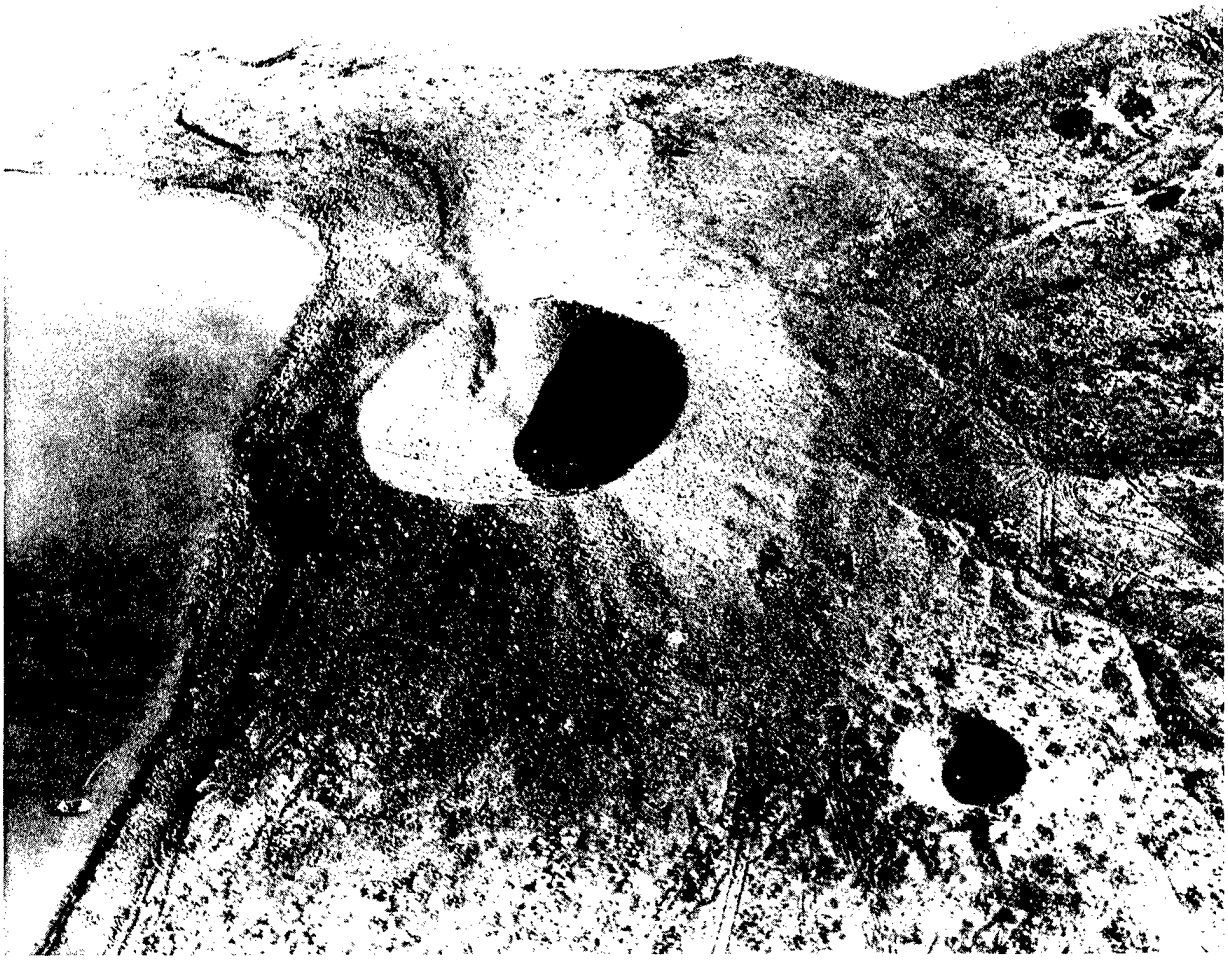

Figure 5.6 High-angle oblique photograph of Charlie crater.

Figure 5.7 Western part of Charlie apparent lip (wooden laths mark position of ejecta pellets).

Figure 5.8 Crack in inside upper slope of South-Southeast part of Charlie apparent lip.

recovery percentage was 20.4 percent. Figure 5.9 shows the locations of the postshot positions of the ejecta pellets found after the Charlie Event. The ejecta pellet numbers correlate the pellets with tabulated preshot and postshot ejecta data included in Appendix B of this report.

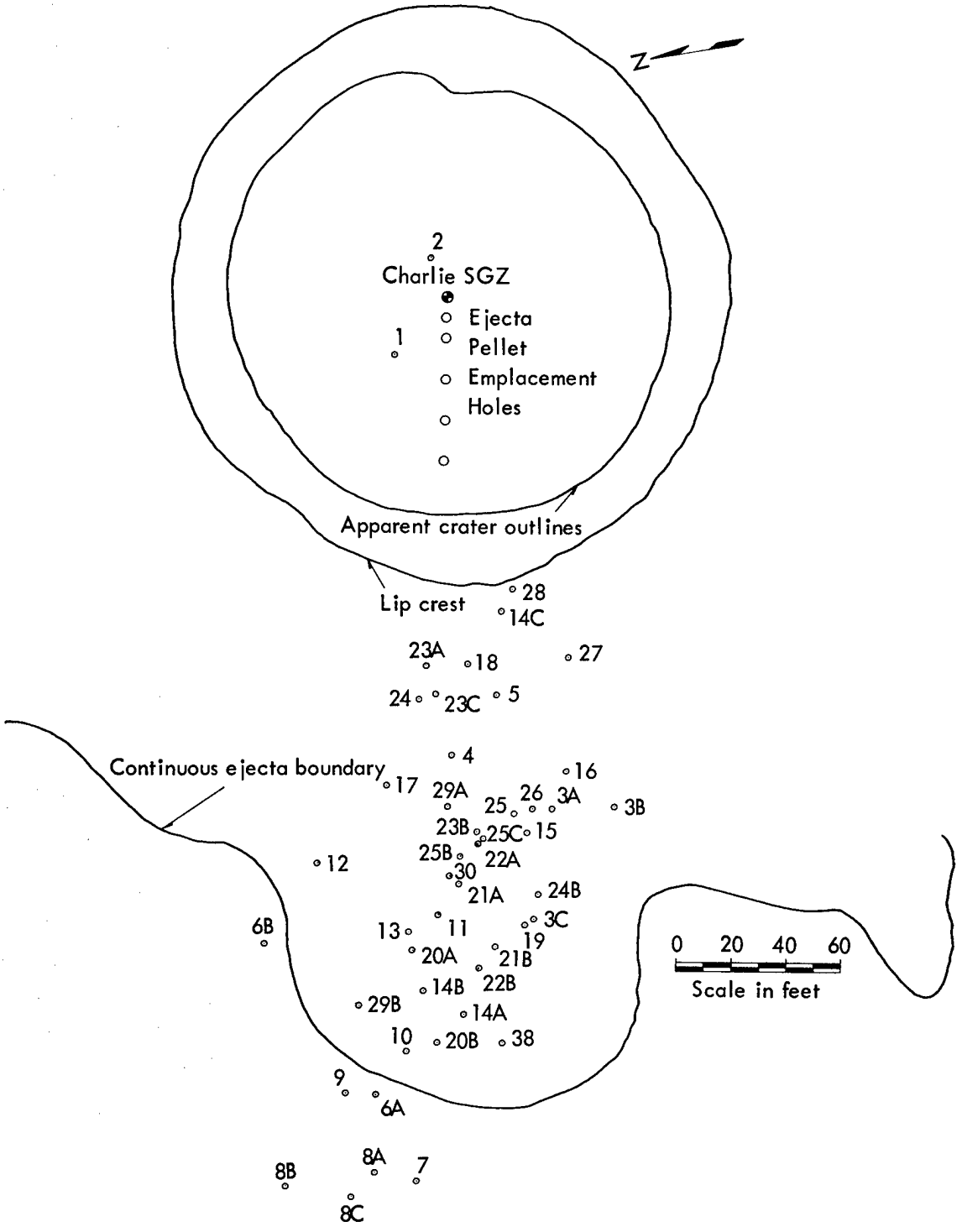

Figure 5.9 Postshot locations of Charlie ejecta pellets. Numbers adjacent to pellets correlate them with tabulated preshot and postshot ejecta data included in Appendix B.

5.3 BRAVO EVENT

The shape of the Bravo crater was nearly symmetrical, except for a mound or shoulder on the north slope of the crater and a 9-foot displacement of the deepest point of the crater in a southeast direction from the SGZ. The volume of the Bravo apparent crater was second only to that of the Charlie crater. Figure 5.10 is a topographic map of the Bravo crater, Figure 5.11 shows preshot and postshot orthogonal profiles drawn through the crater, and Figure 5.12 is a contour map of the interval between the preshot and postshot ground surfaces. Figure 5.13, a high-angle oblique photograph of the Bravo crater, shows the mound in the crater, the occurrence of large impact craters around the crater, the relatively large block-size of the fragments that make up the apparent lip, and a number of the T-shaped markers that designate the most distant missiles around the outer perimeter of the crater. Figure 5.14, a photograph of the east side of the Bravo apparent lip, and Figure 5.15, a photograph taken inside the crater, show the general block-size of the ejecta that comprise the lip and fallback material within the crater.

Although a systematic analysis of the ejecta block-size resulting from the various detonations has not yet been made, an on-site visual comparison of the apparent lips of each of the craters indicated that the maximum and average block-size produced by the Bravo Event was significantly greater than the block-size produced by the other events. Even more apparent was the greater number and size of impact craters produced by the Bravo Event. Some of the observed blocks were as large as 4 feet in diameter and some of the impact craters were as much as 15 feet in diameter. The large magnitude of the block-size appears to be directly related to the large magnitude of the impact crater size.

Other than abundance and size, the impact craters of the Bravo site varied from those at the other sites in that many of the largest ones occurred at relatively great distances from the Bravo SGZ; i. e., well beyond the limit of continuous ejecta material. In addition, the missiles that produced the distant impact craters consisted of both weathered and unweathered shale fragments, although a visual inspection indicated that the most distant large craters were predominantly produced by missiles of weathered shale which unlike missiles of unweathered shale tended to lose their identity upon impact.

Even though the DOB of the Bravo Event was intermediate between the shallowest DOB (Charlie Event) and the two greatest DOB (Alfa and Delta Events), the maximum missile range of the Bravo event was significantly greater than that recorded for the Charlie Event and was twice that of the Delta Event. The most distant missiles located around the crater consisted of one-half to one-pound fragments of shale which in every case appeared to be highly weathered and can be assumed to have come from relatively near the surface of the ground.

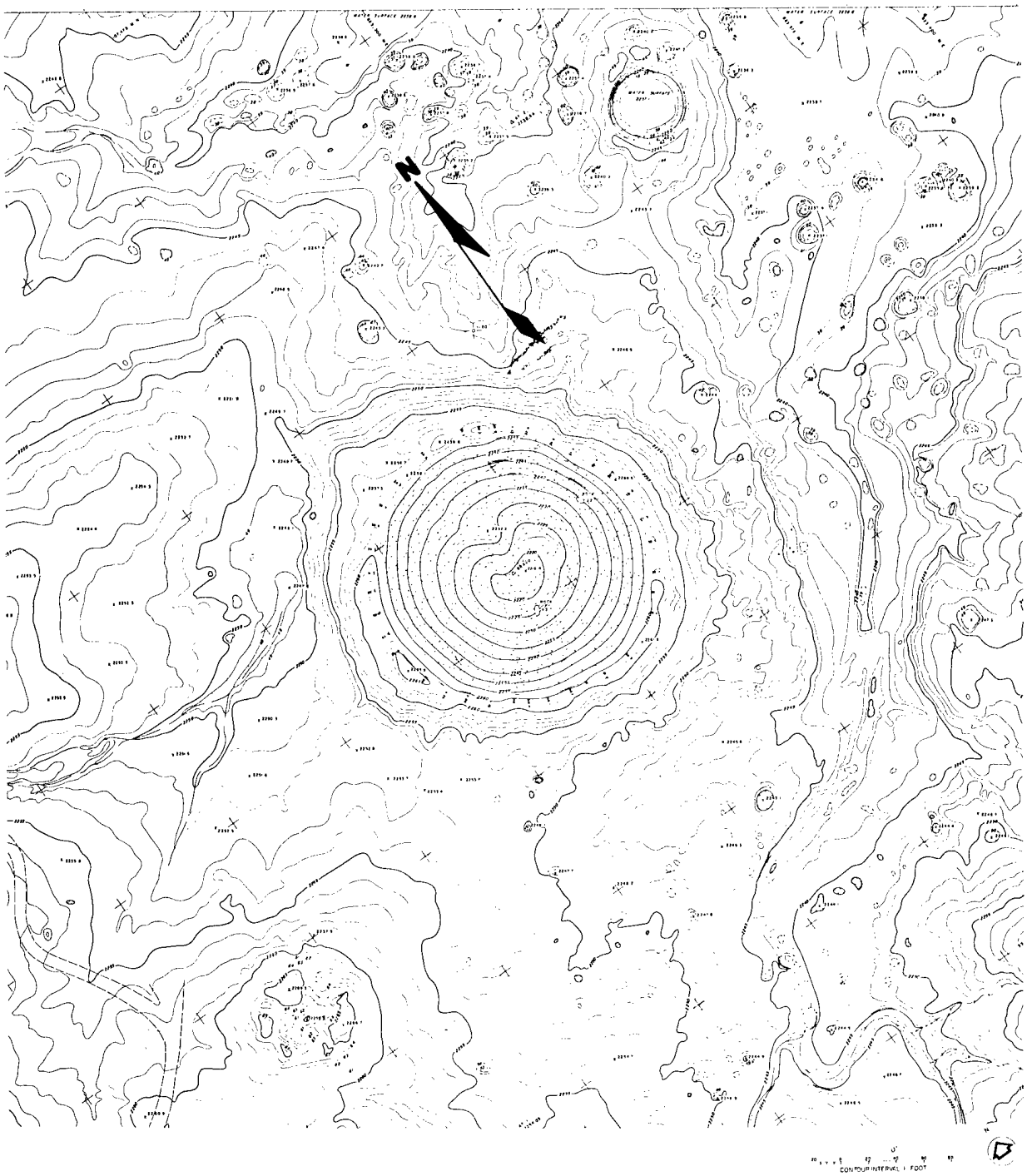

Figure 5.10 Postshot topography, Bravo crater.

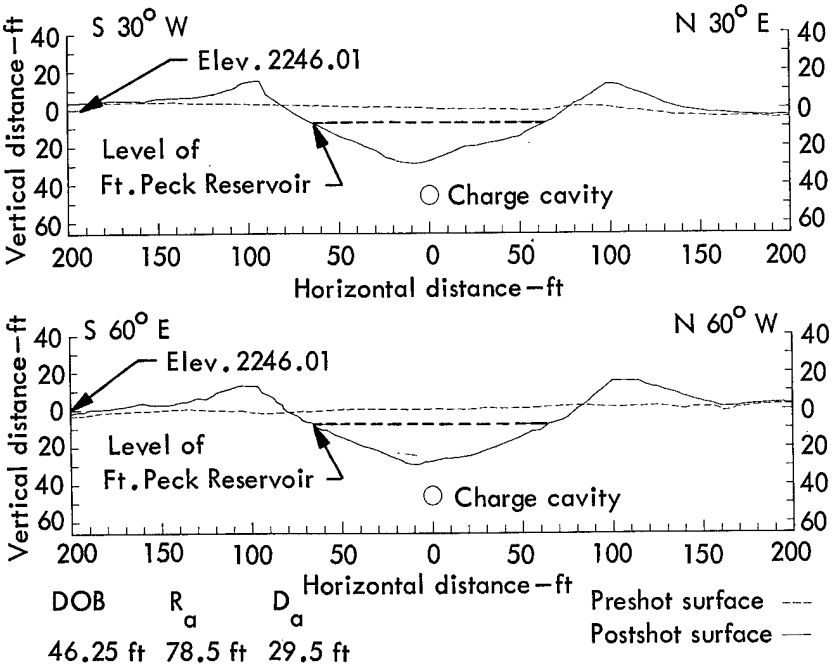

Figure 5.11 Bravo crater profiles.

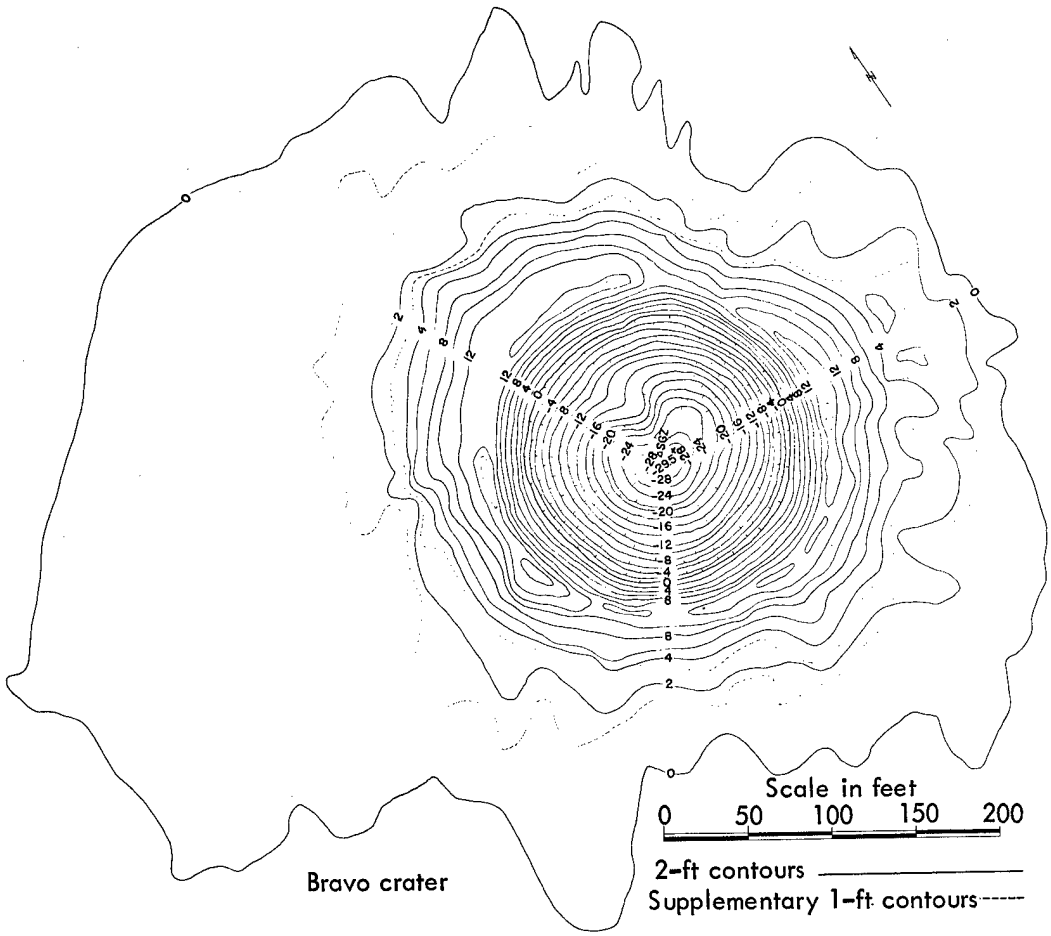

Figure 5.12 Contour map of interval between preshot and postshot ground surfaces, Bravo crater.

Figure 5.13 High-angle oblique photograph of Bravo crater.

Figure 5.14 Eastern part of Bravo apparent lip.

Figure 5.15 Bravo crater (from near bottom).

Two arrays of ejecta pellets were employed at the Bravo site. Eleven percent of 156 pellets were recovered from the "A" array, and 17 percent of 107 pellets were recovered from the "B" array. Both of these recovery percentages are below the average percentage of 20.4 percent. Figures 5.16 and 5.17 are plan views which show the locations of the postshot positions of the recovered ejecta pellets from the "A" and "B" arrays, respectively.

5.4 ALFA EVENT

The shape of the Alfa crater was approximately symmetrical, except for the occurrence of a small mound or shoulder on the northeast slope of the crater and the occurrence of a 5.5-foot displacement of the deepest point of the crater in a south-southwest direction from SGZ. Figure 5.18 is a topographic map of the Alfa crater, and Figure 5.19 shows orthogonal profiles of the preshot and postshot ground surfaces. Figure 5.20 is a contour map of the interval between the preshot and postshot ground surfaces.

Figure 5.21 is a high-angle oblique photograph of the Alfa crater. The mound within the crater is on the near crater slope. The impact craters in the foreground were produced by ejecta from the Alfa crater but those in the background were, for the most part, formed by ejecta from the Bravo crater. Ejecta rays are quite evident in the apparent crater lip. The V-shaped markers around the perimeter of the crater mark the maximum missile located in that area. Figure 5.22 is a photograph of the western side of the Alfa apparent crater lip. It is evident in Figure 5.21 and 5.22 that although occasional blocks 2 to 3 feet in diameter occur within the crater and along the inner or higher regions of the lip, the predominant block-size is less than 1 foot in diameter.

Only 15 percent of 107 ejecta pellets installed at the Alfa site were recovered. Figure 5.23 shows the locations of the postshot positions of the recovered pellets.

5.5 DELTA EVENT

The volume of the Delta apparent crater was the least of the four craters and its shape was somewhat elongated. Figure 5.24 is a topographic map of the Delta apparent crater, and Figure 5.25 shows two orthogonal topographic profiles of the preshot and postshot ground surface drawn through the SGZ. Figure 5.26, a contour map of the interval between the preshot and postshot ground surfaces, shows the elongated shape of the crater and the distribution of the ejected material.

The block-size of the Delta crater ejecta was not very different from that produced by the Alfa and Charlie Events, although the average block-size was probably somewhat greater. As seen in the aerial photograph of the Delta crater (Figure 5.27), impact craters are practically nonexistent. Figure 5.28, a photograph of the western segment of the Delta apparent lip, shows the block-size of the lip material. Figure 5.29 is a plan view of the locations of the postshot positions of the recovered ejecta pellets. Thirty-one percent, the highest of the five ejecta arrays, of 106 ejecta pellets installed were recovered.

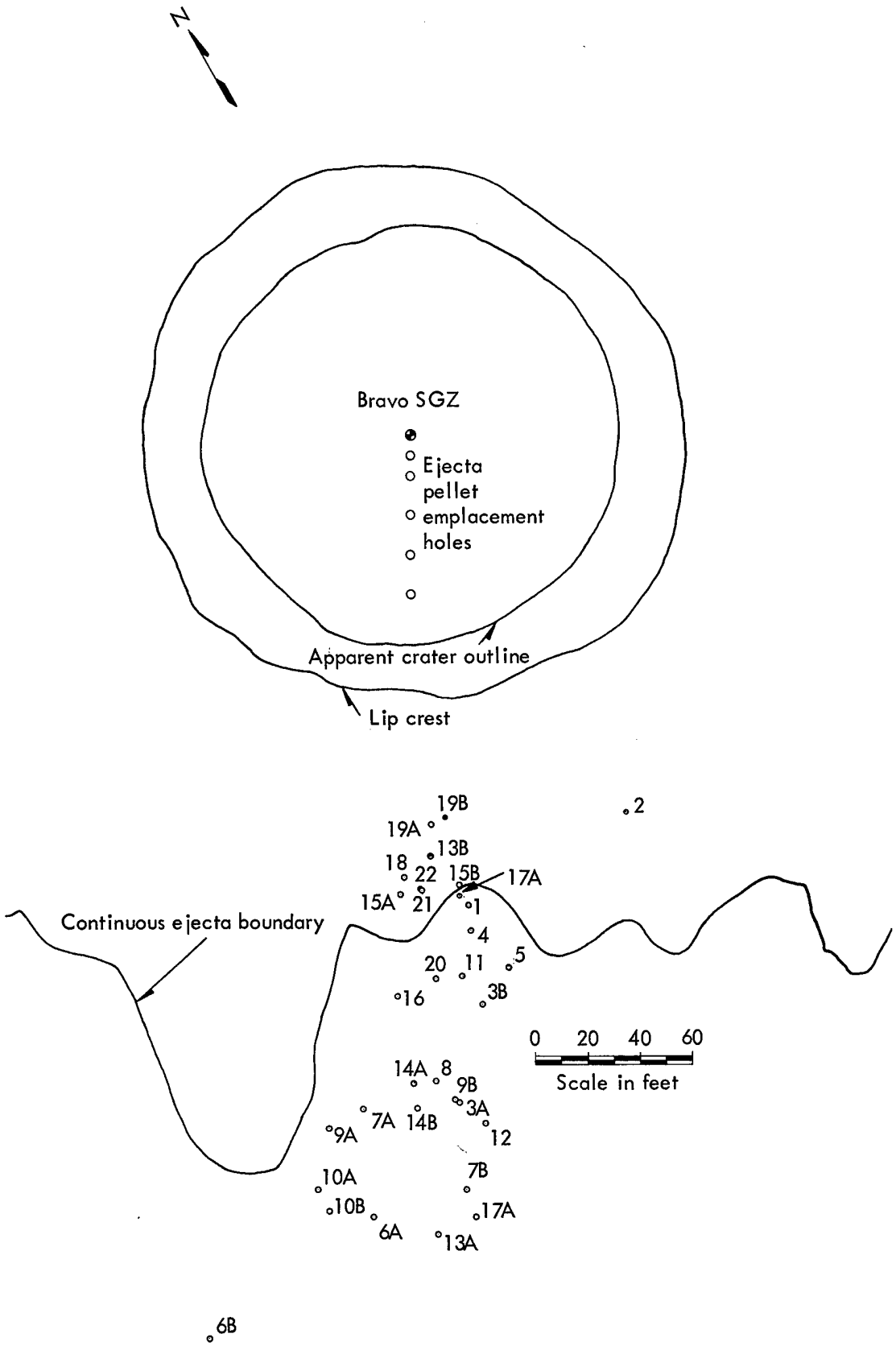

Figure 5.16 Postshot locations of Bravo "A" array ejecta pellets. Numbers adjacent to pellets correlate them with tabulated preshot and postshot ejecta data included in Appendix B.

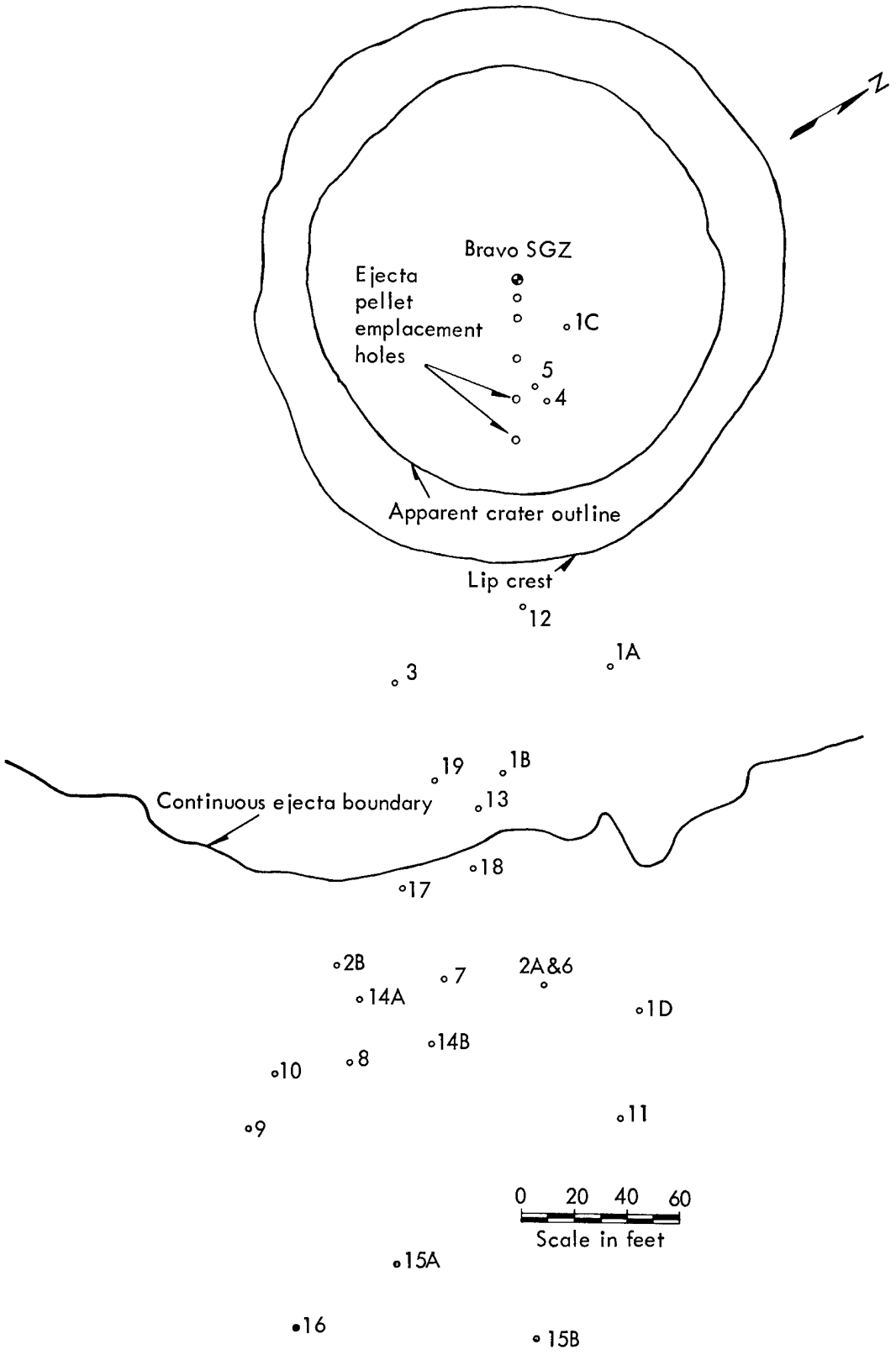

Figure 5.17 Postshot locations of Bravo "B" array ejecta pellets. Numbers adjacent to pellets correlate them with tabulated preshot and postshot ejecta data included in Appendix B.

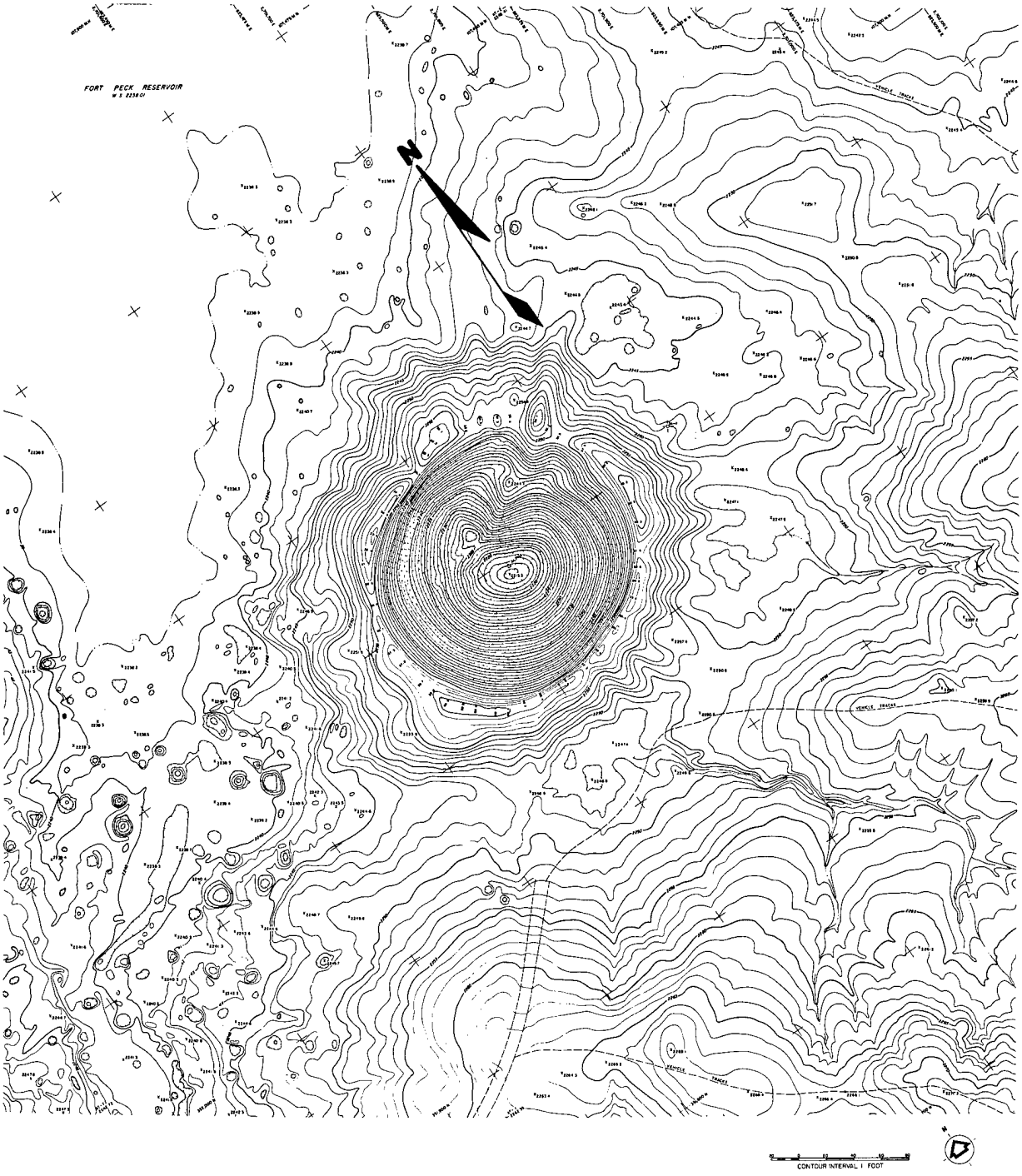

Figure 5.18 Postshot topography, Alfa crater.

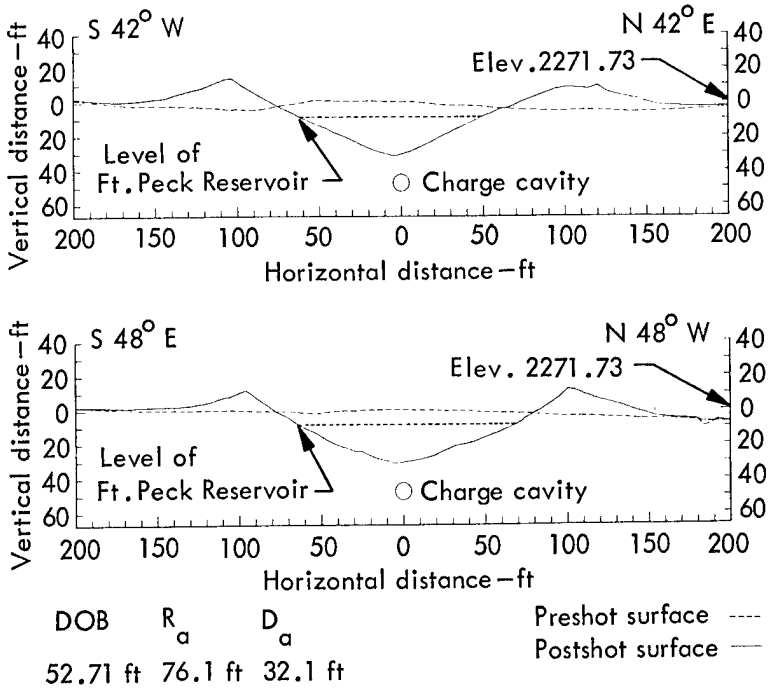

Figure 5.19 Alfa crater profiles.

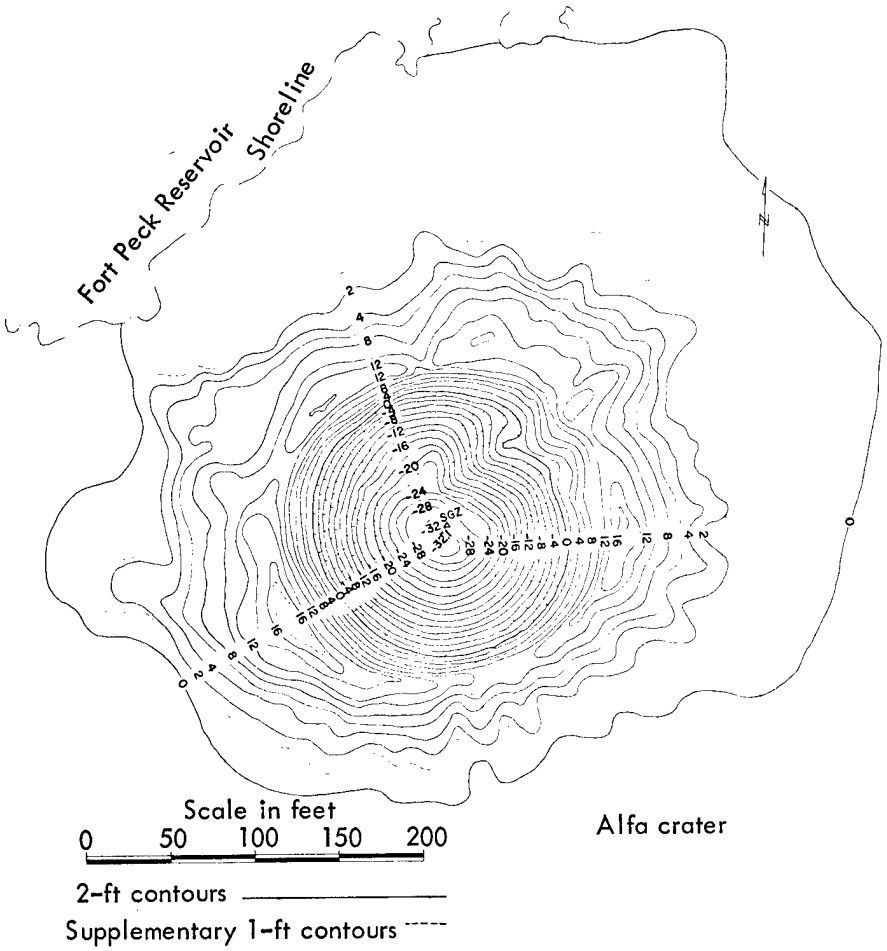

Figure 5.20 Contour map of interval between preshot and postshot ground surfaces, Alfa crater.

Figure 5.21 High-angle oblique photograph of Alfa crater.

Figure 5.22 Western part of Alfa apparent lip.

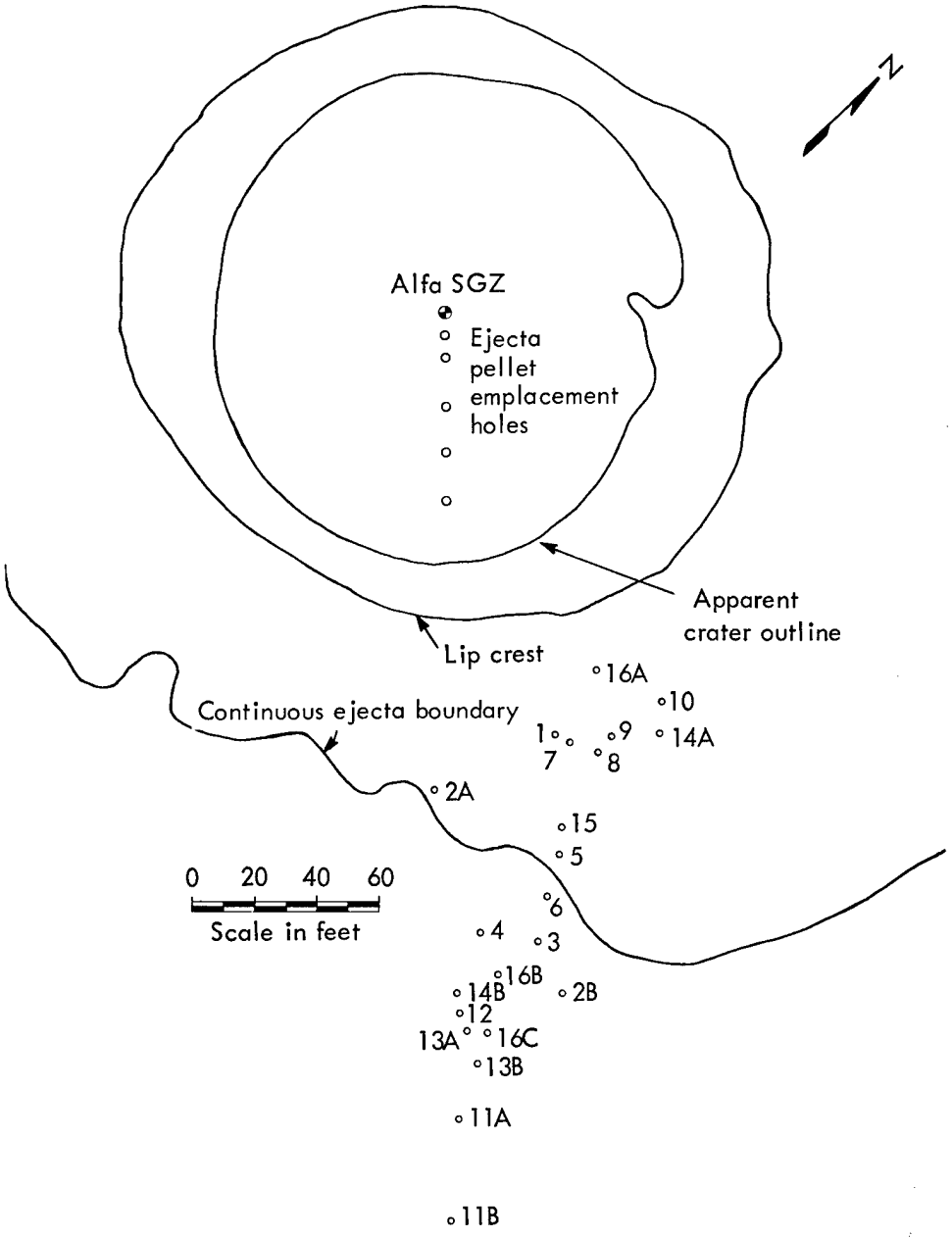

Figure 5.23 Postshot locations of Alfa ejecta pellets. Numbers adjacent to pellets correlate them with tabulated preshot and postshot ejecta data included in Appendix B.

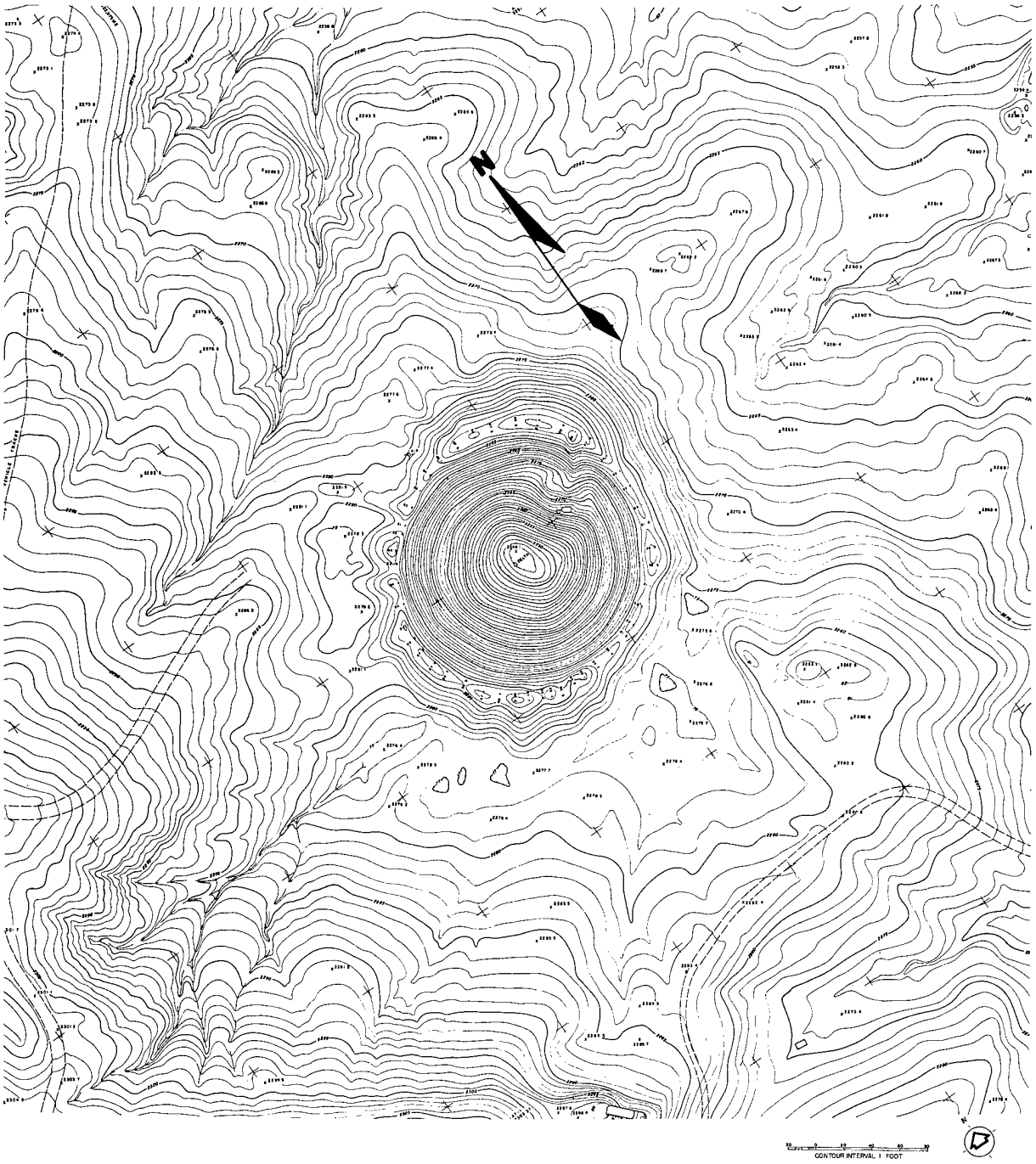

Figure 5.24 Postshot topography, Delta crater.

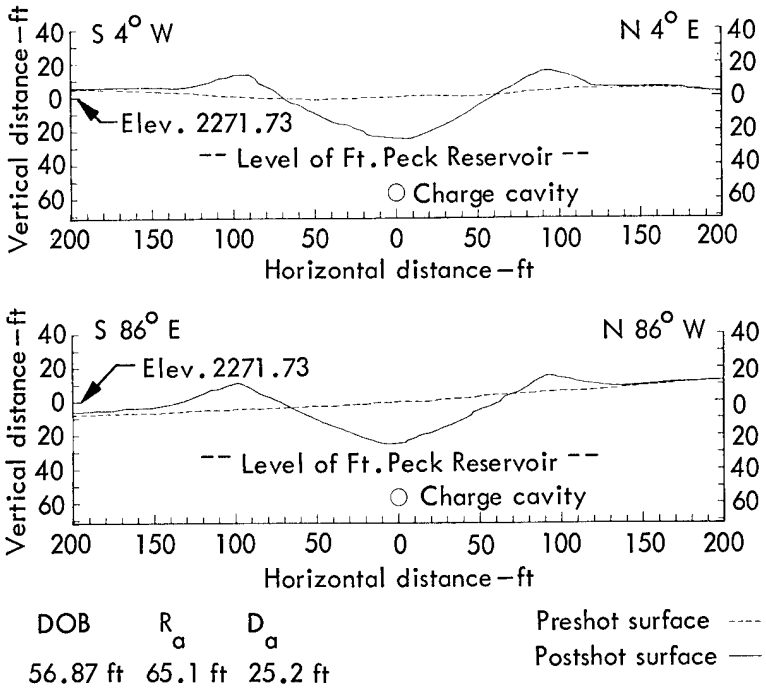

Figure 5.25 Preshot and postshot topographic profiles drawn through Delta surface ground zero.

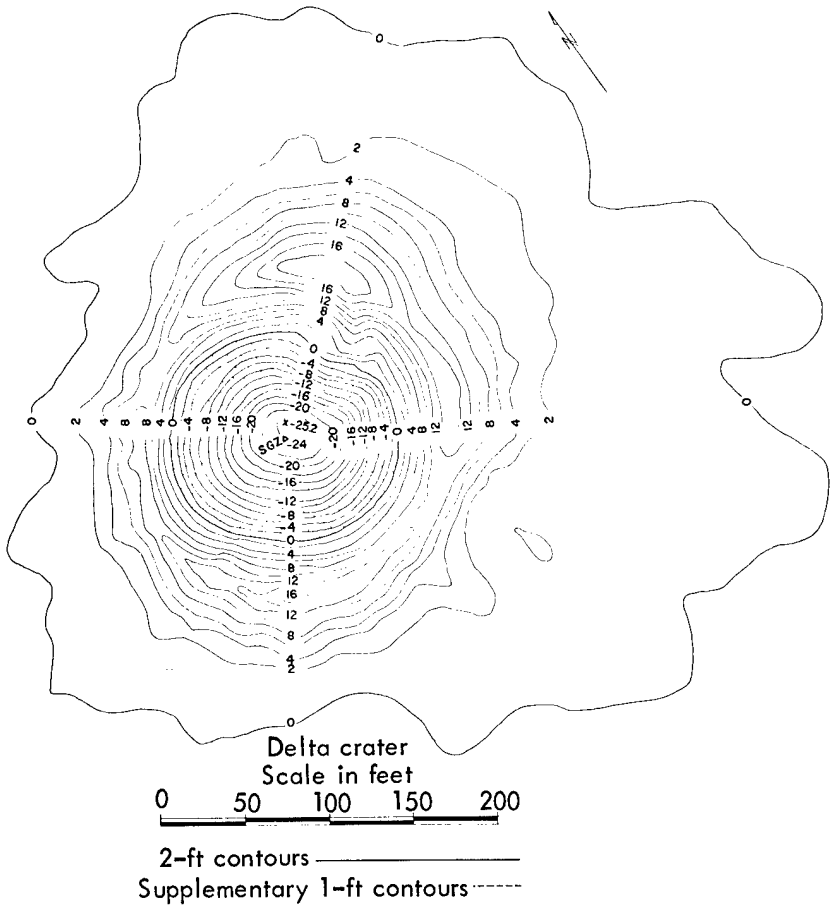

Figure 5.26 Contour map of interval between preshot and postshot ground surfaces, Delta crater.

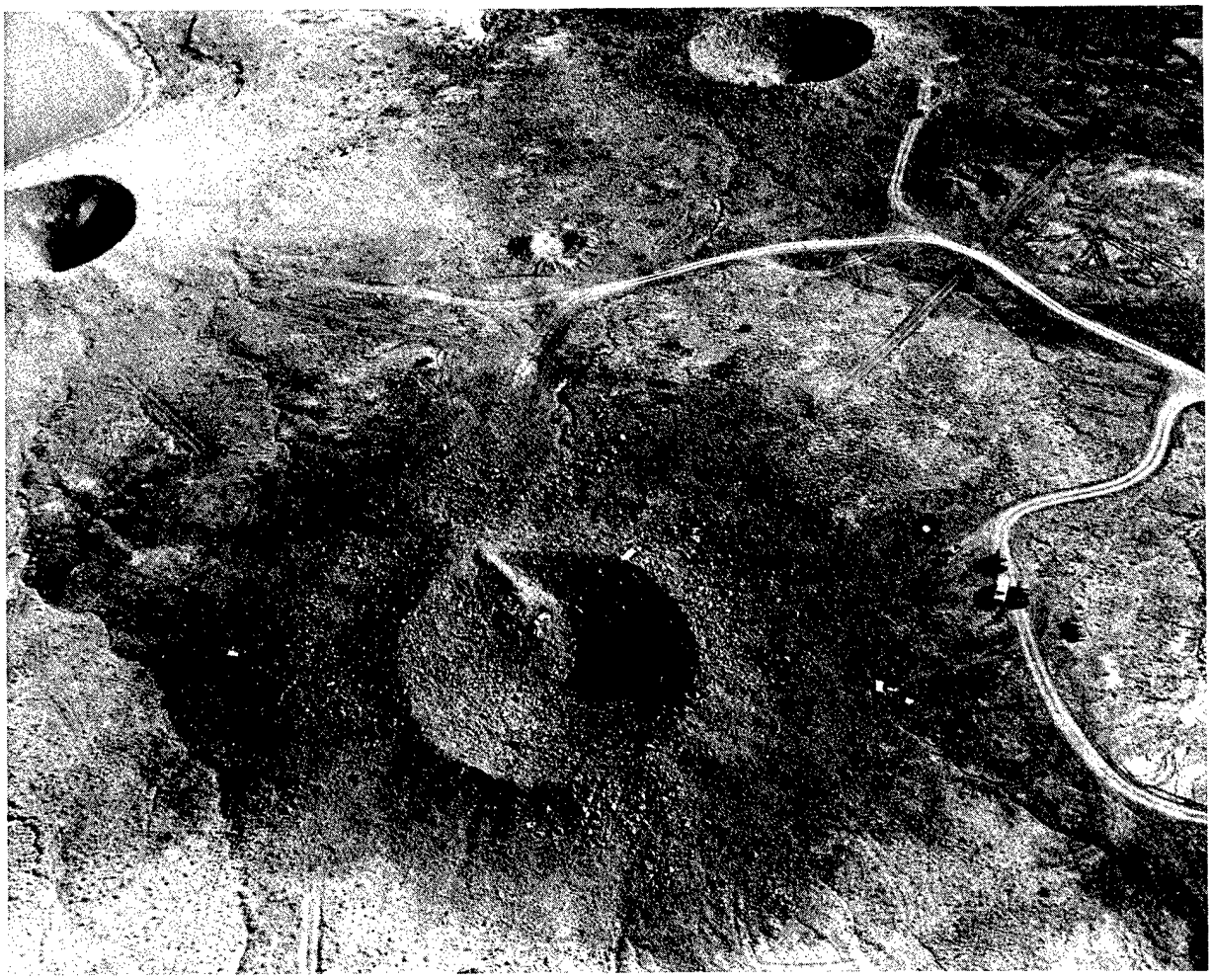

Figure 5.27 High-angle oblique photograph of Delta crater.

Figure 5.28 Western part of Delta apparent lip.

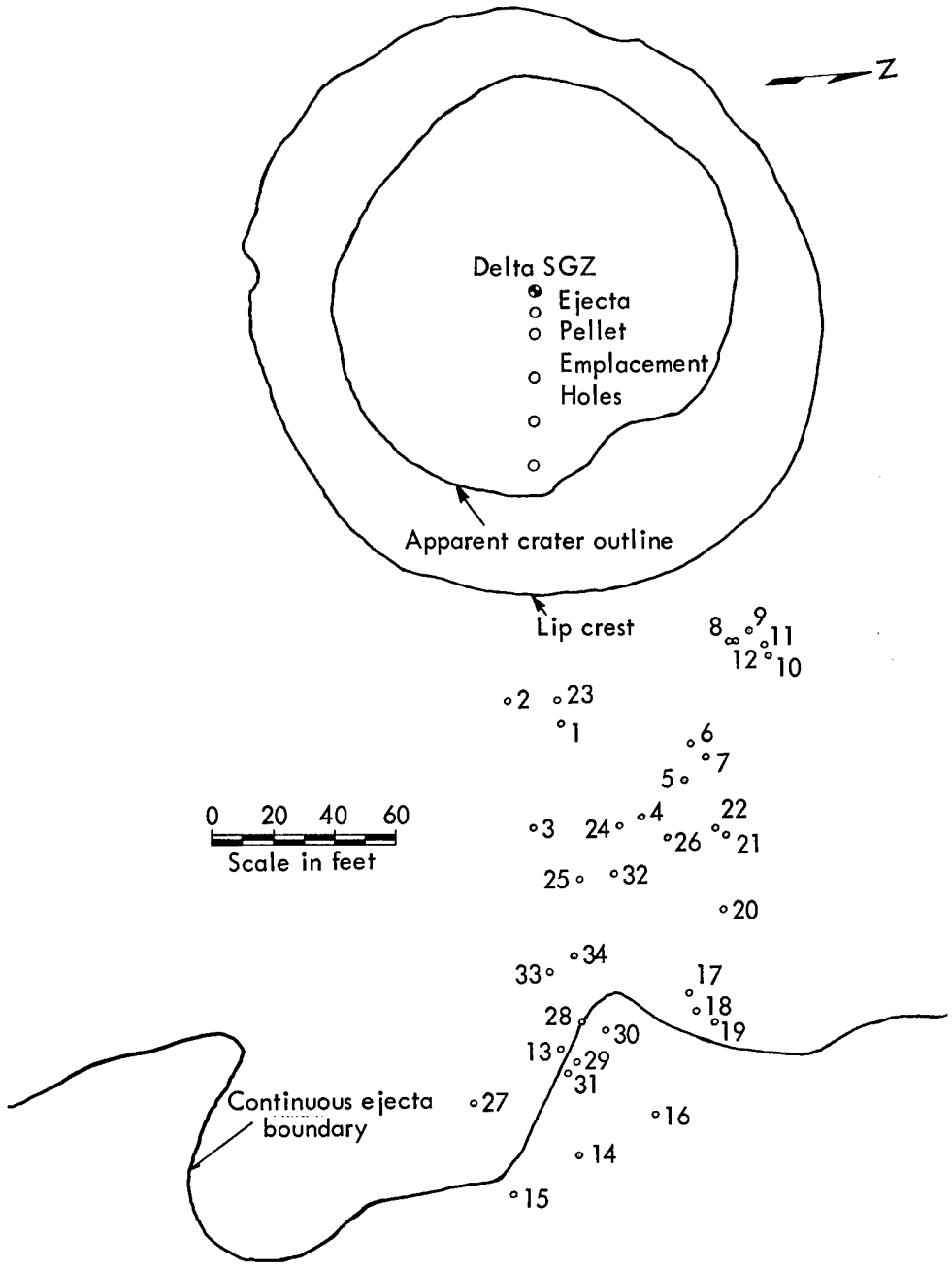

Figure 5.29 Postshot locations of Delta ejecta pellets. Numbers adjacent to pellets correlate them with tabulated preshot and postshot ejecta data included in Appendix B.

CHAPTER 6
ANALYSIS AND INTERPRETATION

6.1 APPARENT CRATER DIMENSIONS

The dimensions of the Pre-Gondola I cratering events provide the first reliable data that can be utilized to draw cratering curves for any type of shale medium. Because the physical properties of different shale media vary significantly it is only appropriate, at the present time, to use the curves for predicting depths and radii of craters made in Bearpaw shale. Later, when more data are available on the cratering characteristics of different types of shale, general cratering curves may be drawn for predicting both crater depth and crater radius.

Only very limited data on the cratering characteristics of any type of shale, except 1,000-pound Seismic Site Calibration Series data, were available prior to the Pre-Gondola I series of events. However, it is of interest to note that, on the average, the predictions of the apparent crater radii and depths were within 4 and 14 percent, respectively, of the measured values. Table 6.1 gives a comparison of the measured, predicted, and scaled crater measurements. Also included within the table is the percentage of error of each prediction.

Figures 6.1 and 6.2 are cratering curves for the prediction of apparent crater radii and depths in Bearpaw shale. The crater dimensions utilized in the curves were scaled to 1 kt by the 3.4th root of the equivalent yield of the actual charge weights. The curves were fitted by eye using a procedure of heavily weighting the 40,000-pound shots in comparison with the 1,000-pound shots. Because of the large amount of scatter, the 1,000-pound shots were used only to determine the approximate direction of the curves in the region of the greater DOB. The dashed portions of the curves are inferred from information available in Reference 3. The cratering curves indicate that the optimum DOB for the apparent crater radius and depth is about 130 $ft/kt^{1/3.4}$.

The rapid decrease in the apparent crater dimensions with increasing charge depths deeper than the optimum depth is assumed to result principally from an increase in the volume of broken rock (bulking) and a decrease in ejecta velocities. The low value of crater depth for the Bravo Event may be related to the block-size and the bulking factor of the fallback. In addition, a 2-meter overburden at the site apparently affected surface motion phenomena (see Part II, PNE-1107).

TABLE 6.1 COMPARISON OF MEASURED AND PREDICTED CRATER PARAMETERS

Dimension[a]	Units	Event			
		Charlie	Bravo	Alfa	Delta
Average Radius, R_a	(ft)	80.4	78.5	76.1	65.1
Scaled r_a	($ft/kt^{1/3.4}$)	248.0	243.4	232.5	199.3
Predicted R_a	(ft)	78.3	78.3	77.3	74.0
Scaled Predicted Radius r_a	($ft/kt^{1/3.4}$)	240.0	240.0	237.0	227.0
Error of Predicted Value	(%)	2.5	0.5	1.5	12.0
Crater Depth, D_a	(ft)	32.6	29.5	32.1	25.2
Scaled d_a	($ft/kt^{1/3.4}$)	100.7	91.5	98.1	77.1
Predicted D_a	(ft)	37.5	36.8	34.2	30.3
Scaled Predicted Depth d_a	($ft/kt^{1/3.4}$)	115.0	113.0	105.0	93.0
Error of Predicted Value	(%)	13.0	20.0	6.0	17.0
Maximum Missile Range, R_{me}	(ft)	800	905	545	453
Scaled r_{me}	($ft/kt^{1/3.4}$)	2,471	2,806	1,665	1,376
Predicted R_{me}	(ft)	1,370	1,160	900	730
Scaled Predicted Value r_{me}	($ft/kt^{1/3.4}$)	4,200	3,550	2,750	2,250
Error of Predicted Value	(%)	41.5	21.0	39.5	38.0

[a]Scaled dimensions are indicated by lower case letters.

6.2 COMPARISON OF CRATERING CHARACTERISTICS OF DIFFERENT MEDIA

Figures 6.3 through 6.6 show the cratering curves for basalt and alluvium, respectively. All of the data utilized in the preparation of these figures were scaled to a common yield of 1 kt using 1/3.4 root scaling. An examination of the alluvium cratering curves (Figures 6.5 and 6.6) shows that the DOB necessary to obtain maximum depths and radii in alluvium are significantly different. However, the DOB necessary to obtain maximum crater dimensions in Bearpaw shale (see Figures 6.1 and 6.2) and basalt (see Figures 6.3 and 6.4) are nearly the same.

A comparison of the radius versus DOB cratering curves for Bearpaw shale, basalt, and alluvium, Figures 6.1, 6.3, and 6.5, respectively, indicates that for the craters produced by identical charges placed at the medium's optimum DOB, the radius of the crater formed in Bearpaw shale will be 63 percent greater than the one produced in basalt and 33 percent greater than the one produced in alluvium. The depth of the crater produced in Bearpaw shale, however, will be only 27 percent greater than the one produced in basalt and only 7 percent greater than the one produced in alluvium.

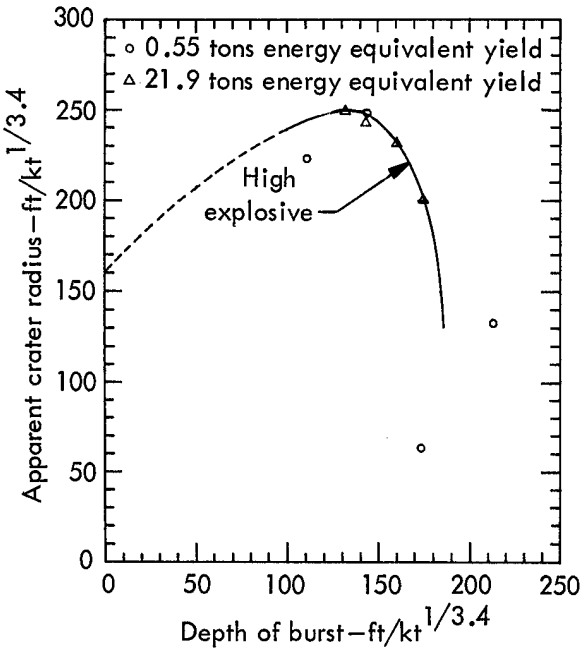

Figure 6.1 Apparent crater radius versus depth of burst for Bearpaw shale.

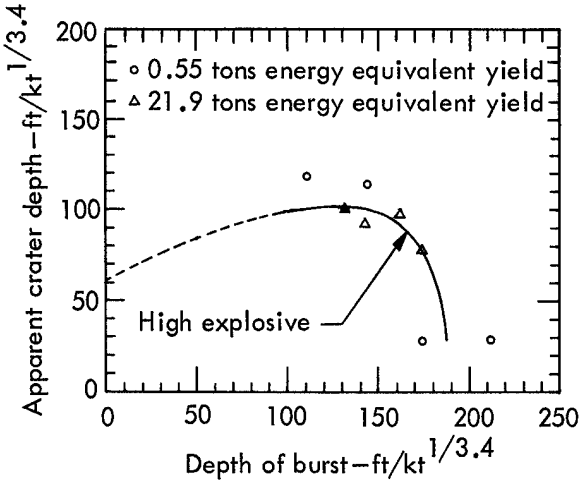

Figure 6.2 Apparent crater depth versus depth of burst for Bearpaw shale.

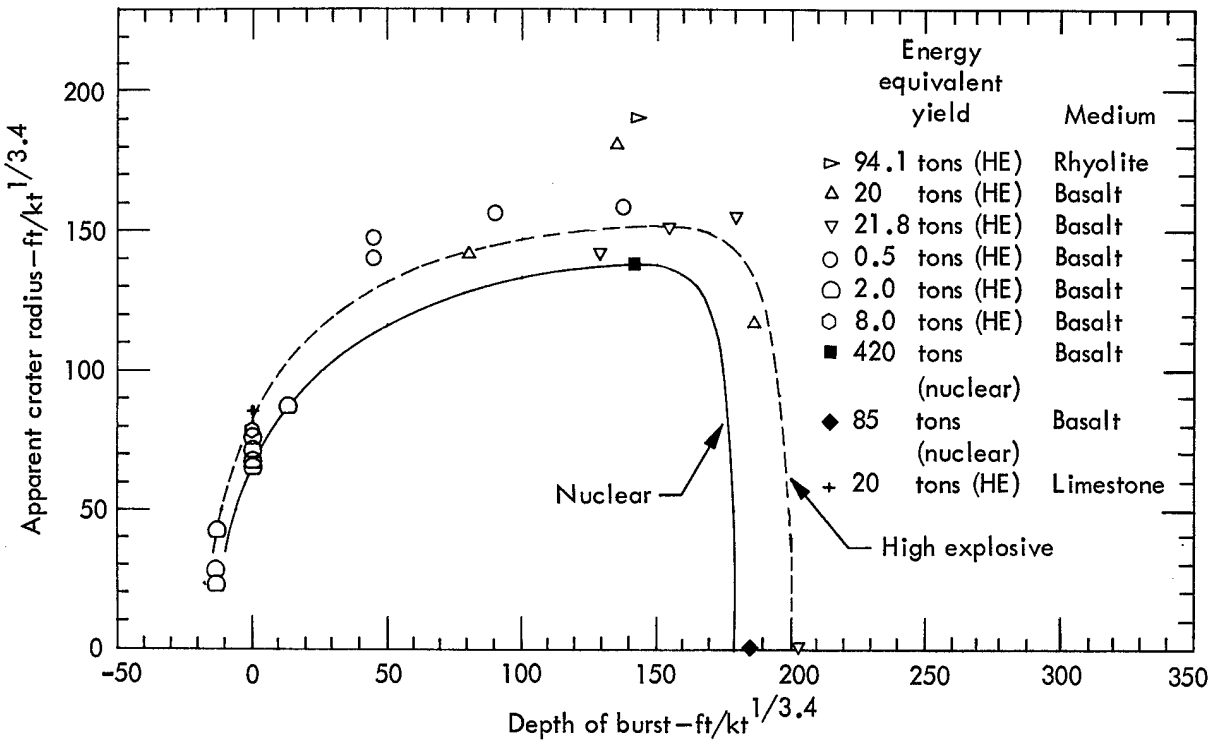

Figure 6.3 Apparent crater radius versus depth of burst for hard rock.

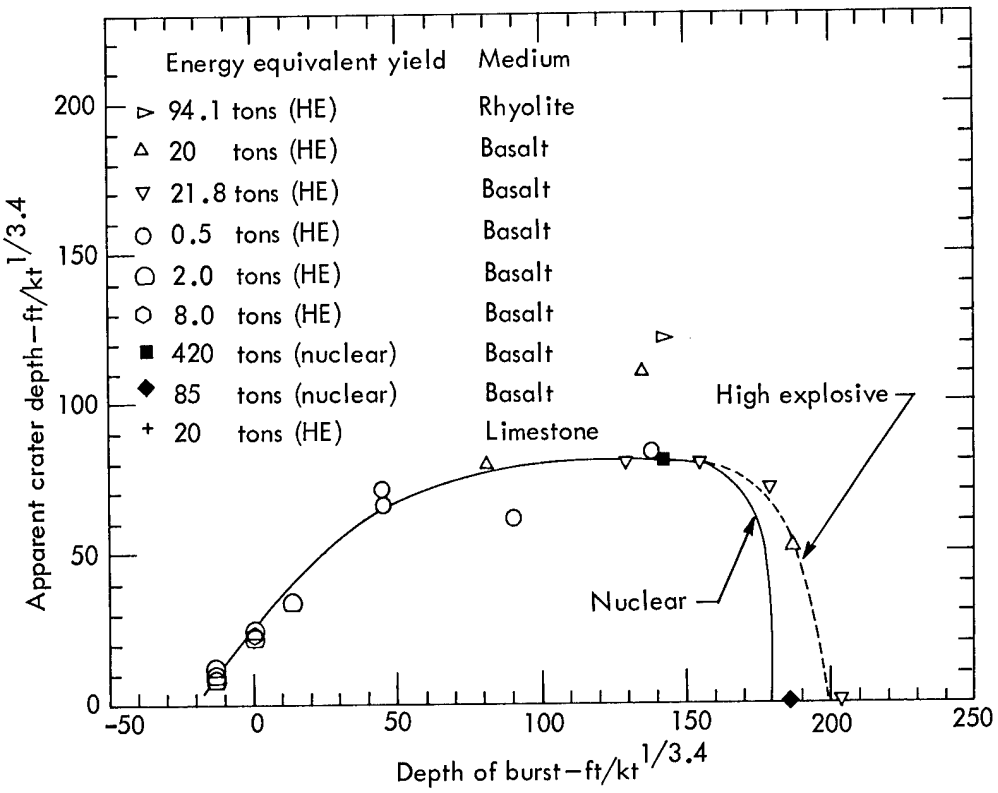

Figure 6.4 Apparent crater depth versus depth of burst for hard rock.

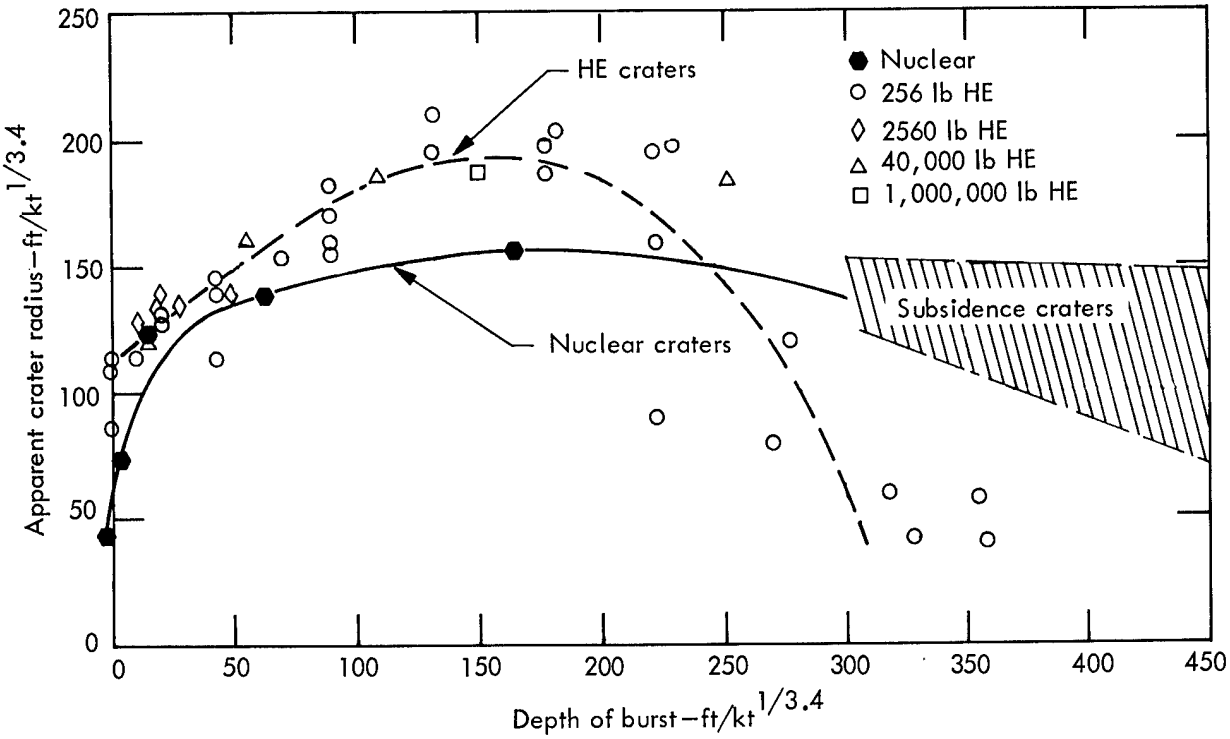

Figure 6.5 Apparent crater radius versus depth of burst for alluvium.

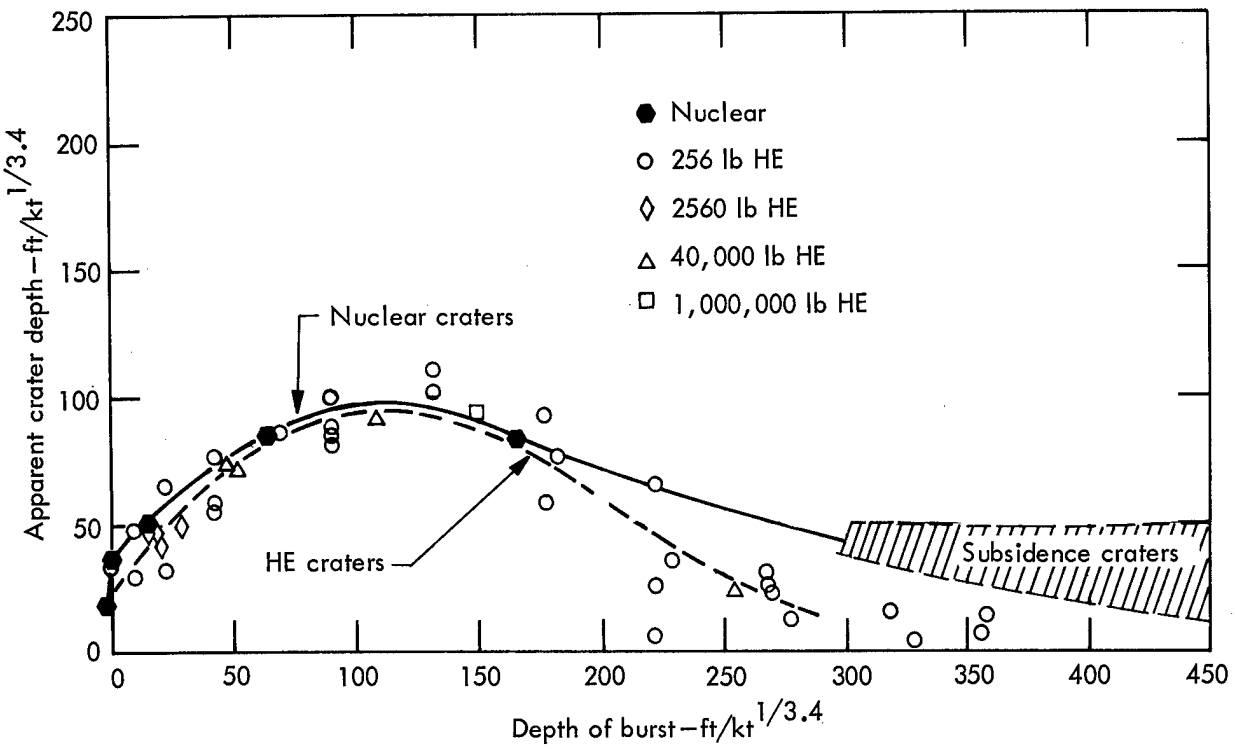

Figure 6.6 Apparent crater depth versus depth of burst for alluvium.

An analysis (Reference 5) of 13 craters showed that the average slope of the apparent crater at the preshot ground surface (θ) was 35 degrees for alluvium. The comparable value for seven basalt craters was 32.5 degrees. An analysis of the four Pre-Gondola I craters resulted in a θ value of 29 degrees. The average ratio of the apparent crater radius to depth, R_a/D_a, of the four Pre-Gondola I craters is about 2.48, while the same ratios for craters produced in alluvium and basalt are 2.12 and 1.92, respectively.

The above data are summarized in Table 6.2. Also included in the table are the maximum apparent crater radii and depths with the corresponding DOB required to obtain the particular dimension. Each of the dimensions was extracted from the appropriate cratering curve for the particular medium.

TABLE 6.2 SUMMARY OF CRATER SIZE AND SHAPE

	Optimum DOB	Maximum R_a	Optimum DOB	Maximum D_a	R_a/D_a	Average Asymptotic Slope
	$ft/kt^{1/3.4}$	$ft/kt^{1/3.4}$	$ft/kt^{1/3.4}$	$ft/kt^{1/3.4}$		degree
Bearpaw Shale	130	250	130	102	2.48	29.0
Alluvium	160	187	112	95	2.12	32.5
Basalt	150	153	130-150	80	1.92	35.0

6.3 APPARENT CRATER GEOMETRY

Profiles of each crater, drawn along orthogonal lines through the apparent crater, are shown in Figures 5.3, 5.11, 5.19, and 5.25. An average crater profile of each of the Pre-Gondola I apparent craters was determined by measuring the average radius of each contour line within the crater in a manner similar to that used for determining the average apparent crater radius (see Chapter 3), and by plotting each average radius so obtained at its respective elevation. Figure 6.7 shows each of the average crater profiles which were adjusted vertically so that their deepest points coincided.

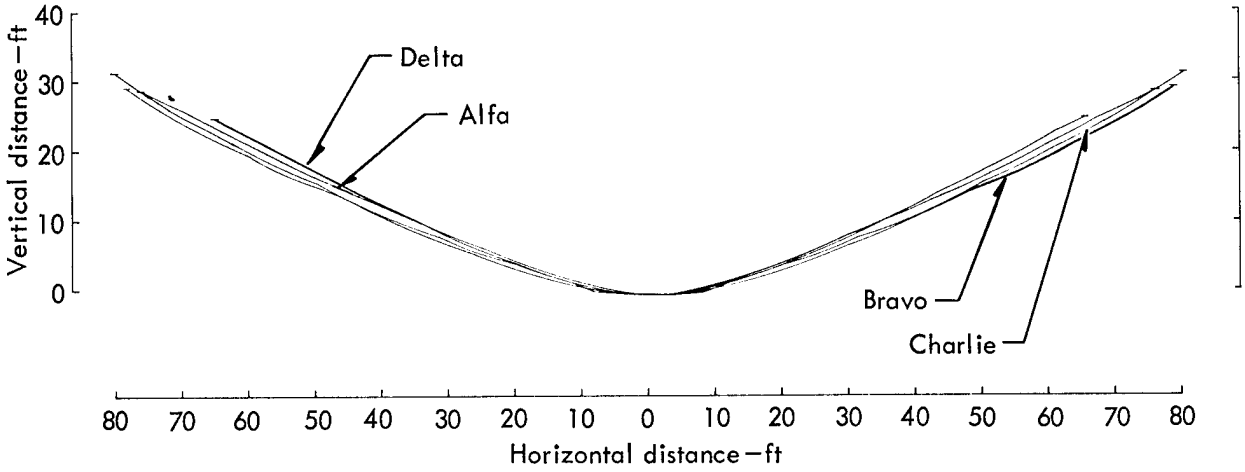

Figure 6.7 Comparison of average crater cross sections.

An examination of the orthogonal and average profiles drawn for each of the craters shows that while the average slope of the craters at the preshot ground surface (θ) is 29 degrees, the average slope of the craters along most of the crater profile is approximately 26 degrees. These slopes are significantly flatter than those observed in either alluvium or basalt.

From Figure 6.7 it is readily apparent that there was very little difference in the average shape of the four craters regardless of DOB. The slight variation of crater shape does not appear to be related to DOB, at least within the range of depths encountered, because the slopes of the Charlie crater (shallowest DOB) are somewhat steeper than those of the Bravo crater (next to shallowest DOB).

Because only slight variations in the average crater profiles exist, the Charlie average crater profile was selected as representative and thus was used for comparison with the shape of a hyperbola (Figure 6.8). From this figure it is seen that the shape of the craters produced in Bearpaw shale by detonations at near optimum depths of burial can be closely approximated by a hyperbola.

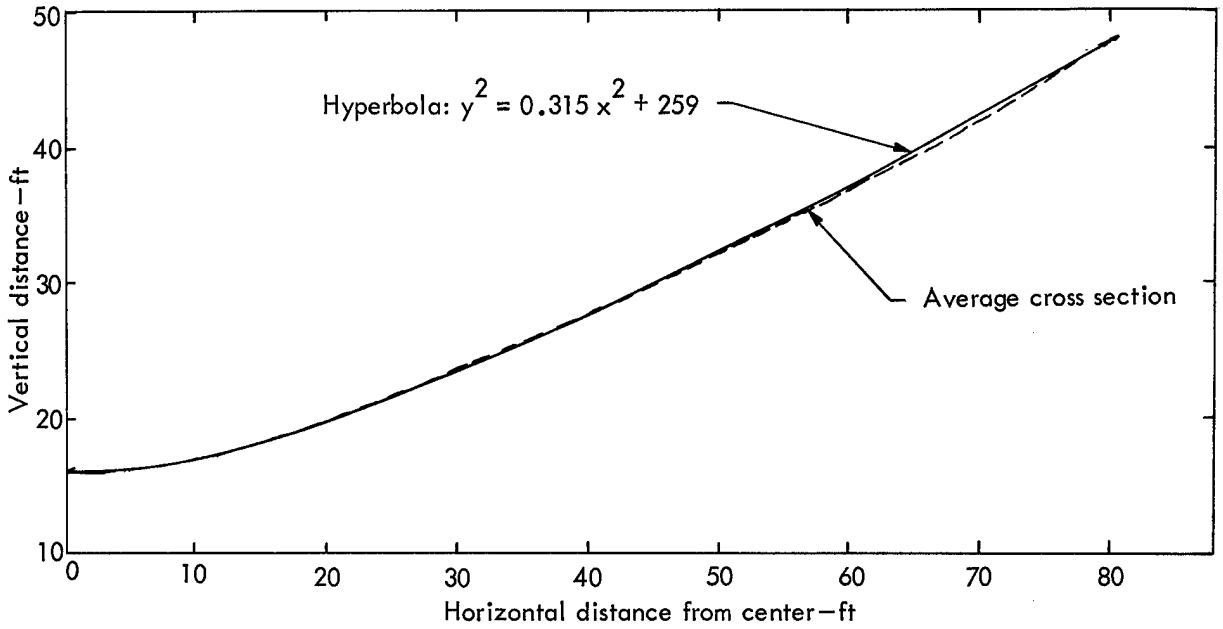

Figure 6.8 Comparison of Charlie average crater cross section with hyperbola.

6.4 CRATER LIP

Table 6.3 tabulates the maximum, minimum, and average lip height and lip crest radius measurements of each of the Pre-Gondola I apparent lips. Included in the same table are the H_{al}/R_a, H_{al}/R_{al}, and R_{al}/R_a values of each crater and their average values. Data from the Bearpaw shale indicate that in this medium $H_{al} = 0.14\ R_{al}$, or $H_{al} = 0.18\ R_a$. Similarly, $R_{al} = 1.34\ R_a$.

TABLE 6.3 APPARENT LIP DATA

	Charlie	Bravo	Alfa	Delta	Average
Lip Height (H_{al})					
Average (ft)	14.5	13.7	13.9	13.0	13.8
Maximum (ft)	17.2	16.3	17.8	19.9	17.8
Minimum (ft)	12.4	10.8	9.9	6.2	9.8
H_{al}/R_a	0.18	0.17	0.18	0.20	0.18
H_{al}/R_{al}	0.14	0.13	0.14	0.14	0.14
Lip Crest Radius (R_{al})					
Average (ft)	101.8	102.1	100.4	94.5	99.7
Maximum (ft)	106.9	107.9	107.6	99.7	105.5
Minimum (ft)	95.9	96.9	92.4	89.0	93.6
R_{al}/R_a	1.27	1.32	1.30	1.45	1.34

6.5 MAXIMUM RANGE OF MISSILES

The most distant missiles from SGZ were located beyond the R_{eb} of each of the craters. In every case these missiles consisted of approximately one-half to one-pound fragments of weathered shale or soil. The ground surface in the experimental area was sufficiently flat that the small impact crater made by the missile could usually be found within a few feet of the missile. It is improbable that any of the missiles rolled more than about 15 feet from their point of impact. Figure 6.9 is a photograph of a typical missile lying on the apex of its V-shaped marker.

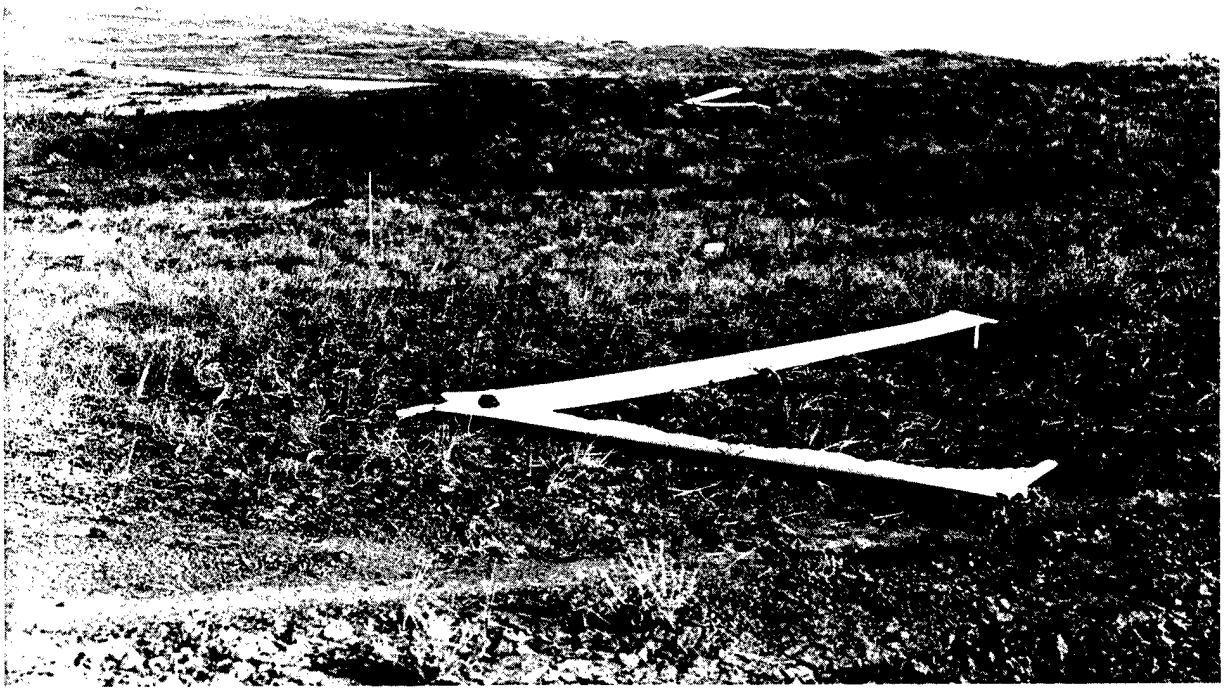

Figure 6.9 Maximum missile lying on white plastic panel marker.

As observed earlier, the predicted maximum range of missiles was in error by 35 percent on the average, using $W^{1/3.4}$ scaling, as opposed to average errors of 4 and 14 percent for the predicted values of crater radii and crater depths, respectively. The maximum missile range predictions were based on a curve drawn through the appropriately scaled maximum missile ranges of the four 1000-pound (0.5-ton) Seismic Site Calibration shots where the resulting curve approximated the maximum missile curve for alluvium that had been obtained by $W^{1/3.4}$ scaling. Each of the predictions made from the curve was significantly greater than the observed values.

An analysis of the maximum missile ranges from both the 0.5- and 20-ton events indicates that the ranges for single-charge craters are best represented by the equation:

$$\frac{R_{me}}{W^{1/3.8}} = K\left[\frac{DOB}{W^{1/3.8}}\right]^{-2} \qquad \text{where } K = 3 \times 10^{7}$$

This equation was empirically arrived at by a graphical adjustment of the maximum missile ranges for both the 0.5- and 20-ton detonations to a common straight line on a double logarithmic plot (Figure 6.10). The foregoing implies that a scaling of $W^{1/3.4}$ is not applicable to the Pre-Gondola medium. The Bravo Event as stated earlier in this report and in PNE-1107 Part II behaved anomalously when compared to the other 20-ton events. Thus, the author believes that the relatively large maximum missile range of the Bravo Event should be treated as anomalous data and that the best information available indicates that the maximum missile ranges for single-charge craters in Bearpaw shale can best be scaled by $W^{1/3.8}$.

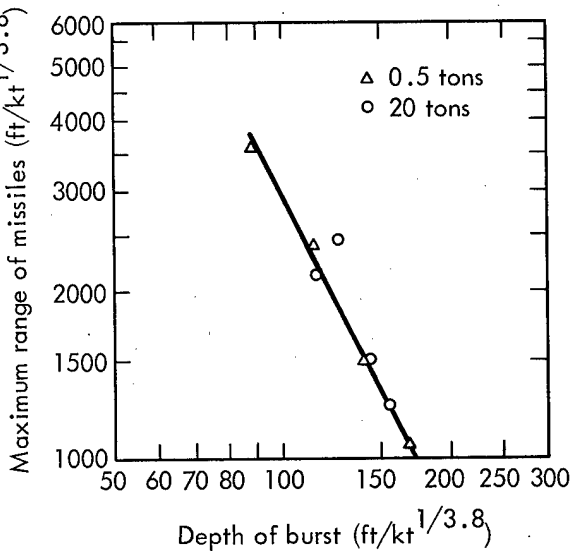

Figure 6.10 Maximum range of missiles for Bearpaw shale.

CHAPTER 7
CONCLUSIONS

As a result of the Pre-Gondola I cratering calibration series, the cratering characteristics of the Bearpaw shale have been calibrated. Apparent crater radii and depths in Bearpaw shale at optimum and deeper DOB can be predicted with a relatively good degree of accuracy. The optimum DOB for both apparent crater depth and apparent crater radius is about 130 $ft/kt^{1/3.4}$. The maximum missile range for varying yields and DOB can also be predicted relatively accurately from the Bearpaw shale maximum missile curve. These data are available for use in the design of future experiments in the Pre-Gondola medium and for evaluating data collected from detonations in other media.

The pertinent data for the Pre-Gondola I crater dimensions are summarized in Table 7.1.

TABLE 7.1 SUMMARY OF PRE-GONDOLA I CRATER DIMENSIONS

Event	Energy Equivalent Yield	Depth of Burst		Apparent Crater Radius		Apparent Crater Depth	
	tons	feet	$ft/kt^{1/3.4}$	feet	$ft/kt^{1/3.4}$	feet	$ft/kt^{1/3.4}$
Charlie	21.58	42.49	131.2	80.4	248.0	32.6	100.7
Bravo	21.30	46.25	143.4	78.5	243.4	29.5	91.5
Alfa	22.39	52.71	161.1	76.1	232.5	32.1	98.1
Delta	22.26	56.87	174.0	65.1	199.3	25.2	77.1

The craters produced were both significantly deeper and especially wider than craters produced in alluvium and basalt, and had flatter average crater slopes.

REFERENCES

1. M. K. Kurtz; "A Report of the Scope and Preliminary Results of Project Pre-Gondola I"; NCG/TM 66-20, December 1966; U. S. Army Engineer Nuclear Cratering Group, Livermore, California.

2. W. W. Dudley and H. A. Jack; "Site-Selection Investigations, Project Pre-Gondola"; PNE-1101, February 1967, U. S. Army Engineer Nuclear Cratering Group, Livermore, California.

3. D. L. Ornellas; "The Heat and Products of Detonation of Cyclotetramethylene Tetranitramine (HMX), 2, 4, 6-Trinitrotoluene (TNT, Nitromethane (NM), and Bis(2, 2-Dinitro-2-Fluoro-Ethyl)-Formal (FEFO)"; UCRL-70444 (Preprint - May 1967) Lawrence Radiation Laboratory, Livermore, California.

4. "Crater Tests in Cucaracha and Culebra Formations"; Isthmian Canal Studies Memorandum 283-P, April 1948; Panama Canal Company, Diablo Heights, Canal Zone.

5. B. C. Hughes, R. H. Benfer, F. H. Foster; "Study of the Shape and Slope of Explosion-Produced Craters"; NCG/TM 65-8, November 1965; U. S. Army Engineer Nuclear Cratering Group, Livermore, California.

APPENDIX A
RESULTS OF SEISMIC SITE CALIBRATION
CRATER STUDIES PROGRAM

SEISMIC SITE CALIBRATION CRATER MEASUREMENTS

Dimension[a]	Units	Event SC-4[b]	SC-2[c]	SC-1[d]	SC-3[e]
Charge Weight, W	(tons)	0.5	0.5	0.5	0.5
Energy Equivalent Scaling Factor	($ft/kt^{1/3.4}$)	0.11	0.11	0.11	0.11
Depth of Burst, DOB	(ft)	12.2	15.8	19.1	23.3
Scaled dob	($ft/kt^{1/3.4}$)	111	144	179	212
Average Radius, R_a	(ft)	24.5	27.3	7.1[f]	14.6[f]
Scaled r_a	($ft/kt^{1/3.4}$)	223	248	64.5[f]	133[f]
Average Depth, D_a	(ft)	13.0	12.5	2.8[f]	3.4[f]
Scaled d_a	($ft/kt^{1/3.4}$)	118	114	25[f]	31[f]
Lip Radius, R_{al}	(ft)	30	32	29	26
Lip Height, H_{al}	(ft)	3.8	3.1	3.7	4.3
Average Radius of Lip Boundary, R_{eb}	(ft)	111	86	103	69
Maximum Missile Range, R_{me}	(ft)	500	333	206	147
Ejecta Pellet Recovery	(%)	52.5	62.4	54.3	48.6
Ejecta Pellet Shot Point Angle	(deg)	45	34	25	22
Maximum Ejecta Pellet Range	(ft)	233	196	121	64

[a]Scaled dimensions are designated by lower case letters.

[b]SC-4 - Weathered shale, above water table; very small block size.

[c]SC-2 - Saturated unweathered shale, below water table; medium block size.

[d]SC-1 - Weathered shale, above water table, slightly sloping ground; small block size.

[d]SC-3 - Saturated, slightly weathered shale, at or above water table, slightly sloping ground; medium block size.

[f]Poorly defined and very asymmetrical.

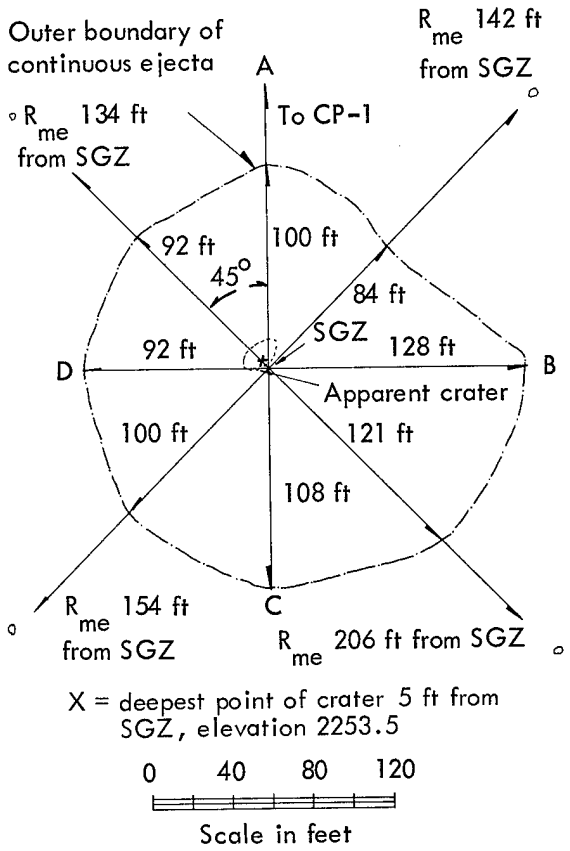

Figure A1 Shot SC-1 crater outlines.

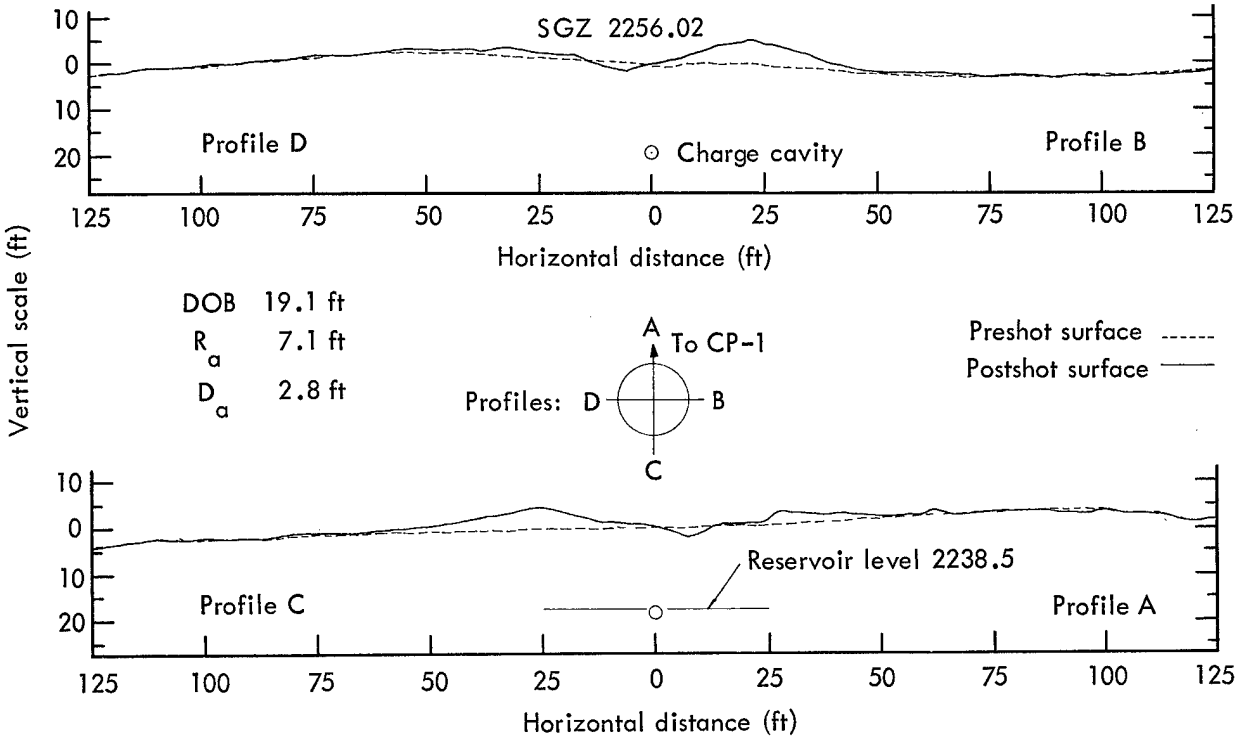

Figure A2 Shot SC-1 crater profiles.

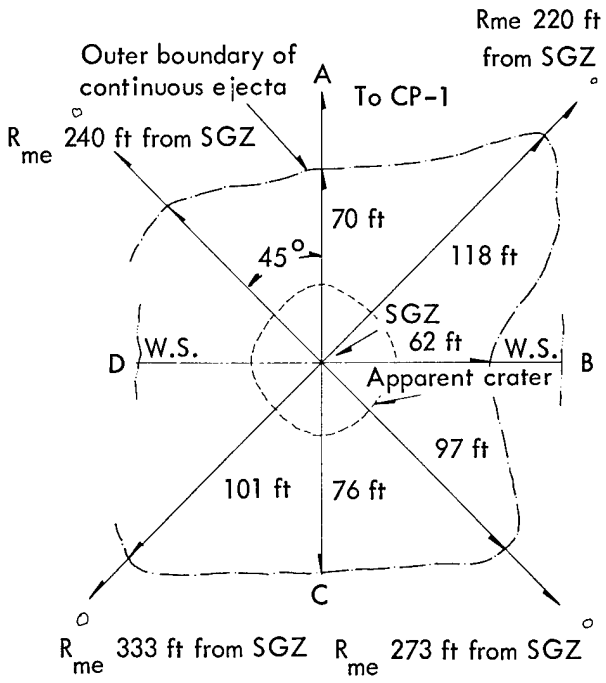

Figure A3 Shot SC-2 crater outlines.

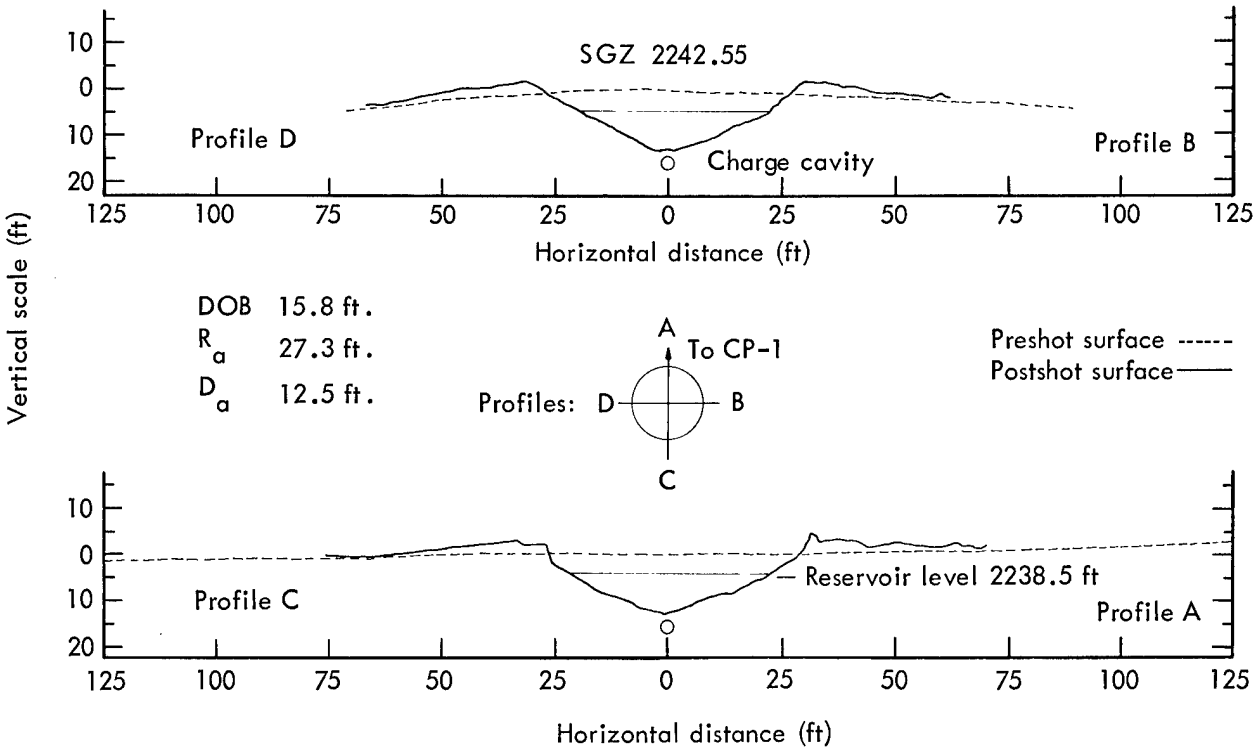

Figure A4 Shot SC-2 crater profiles.

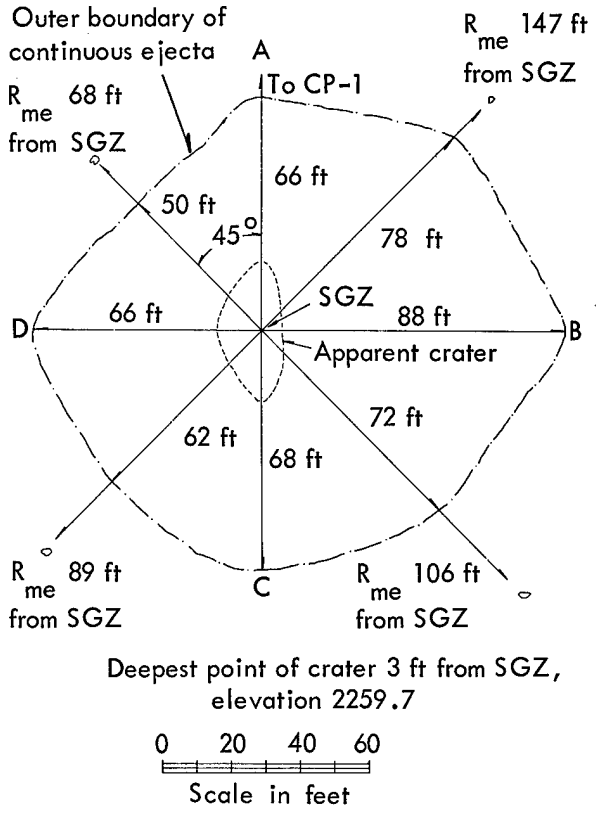

Figure A5 Shot SC-3 crater outlines.

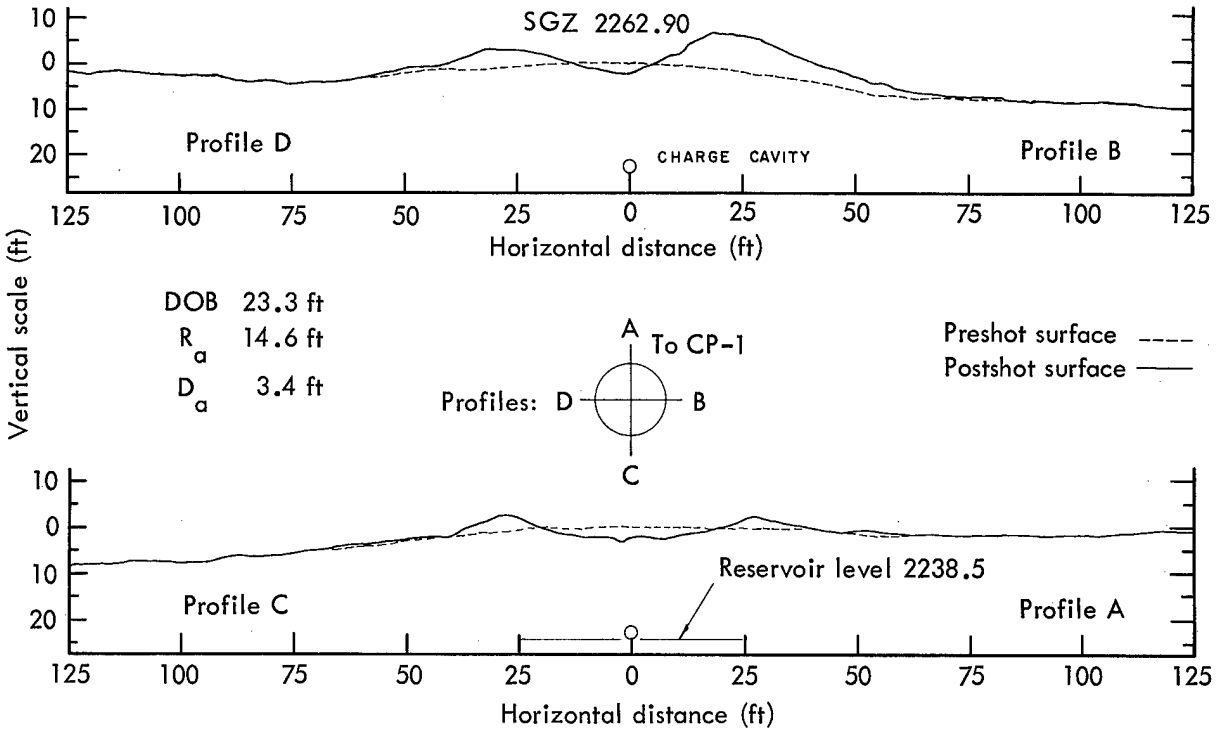

Figure A6 Shot SC-3 crater profiles.

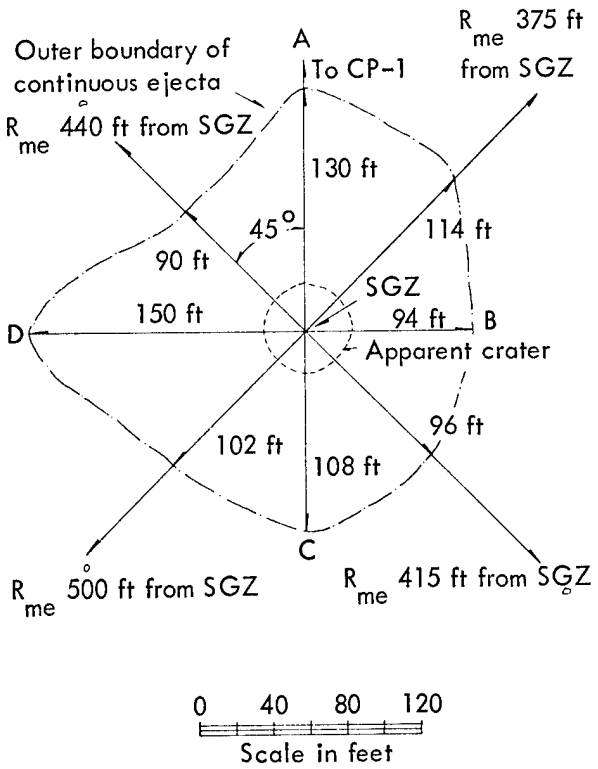

Figure A7 Shot SC-4 crater outlines.

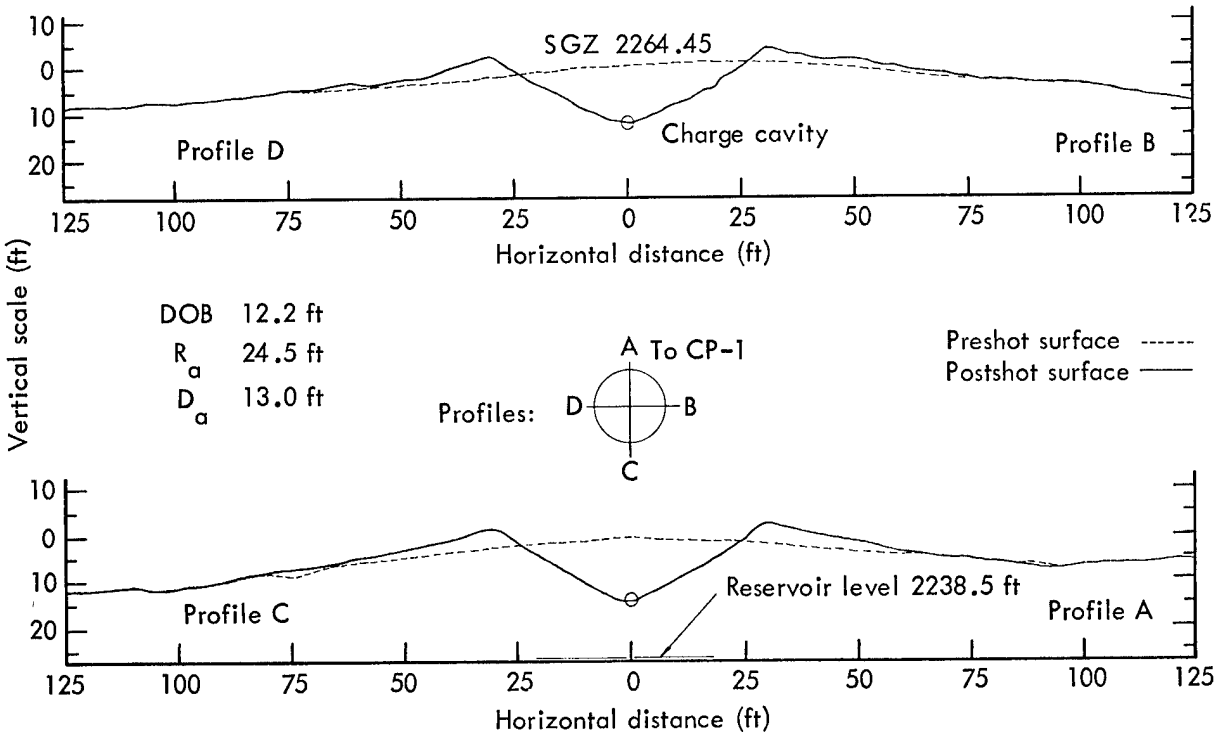

Figure A8 Shot SC-4 crater profiles.

APPENDIX B
EJECTA STUDY DATA

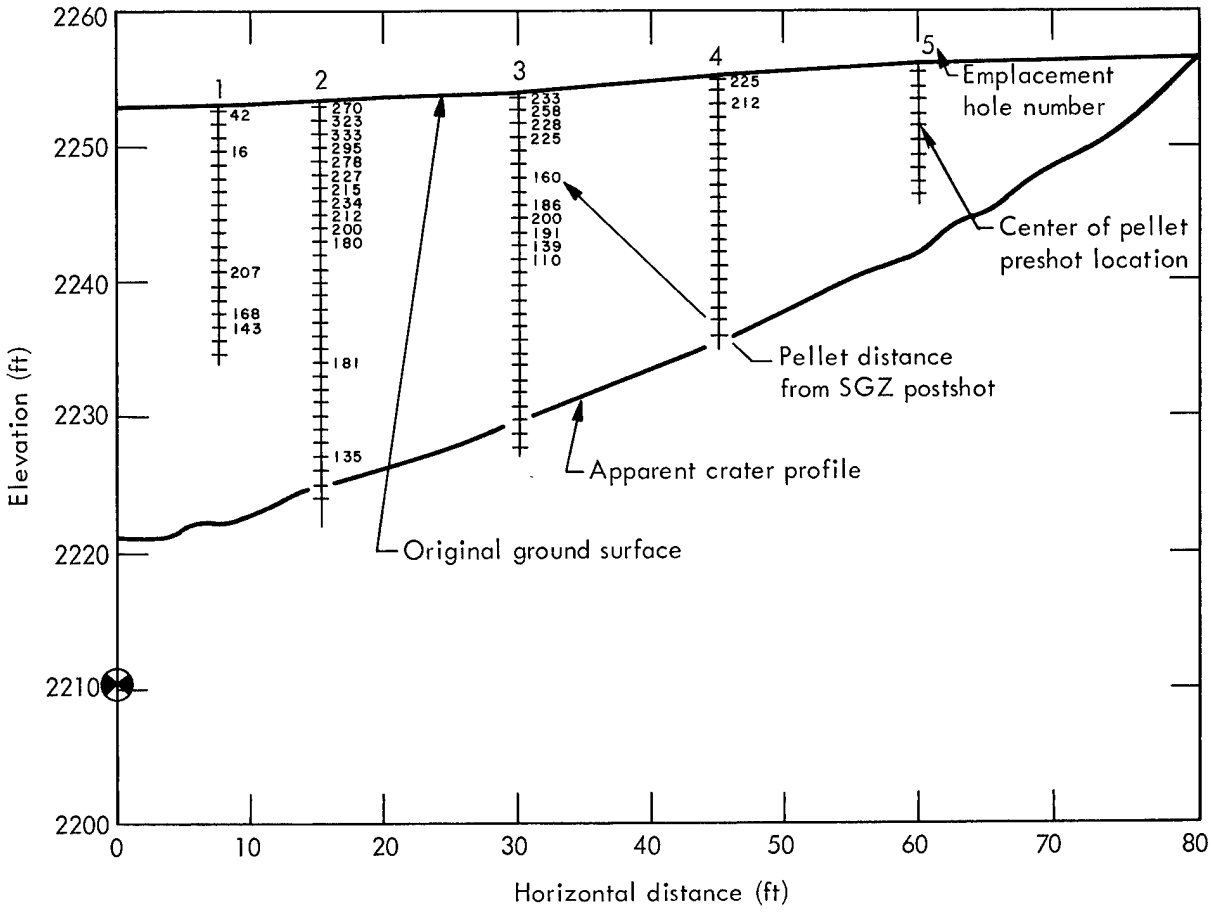

Figure B1 Pre-Gondola I Charlie Event.

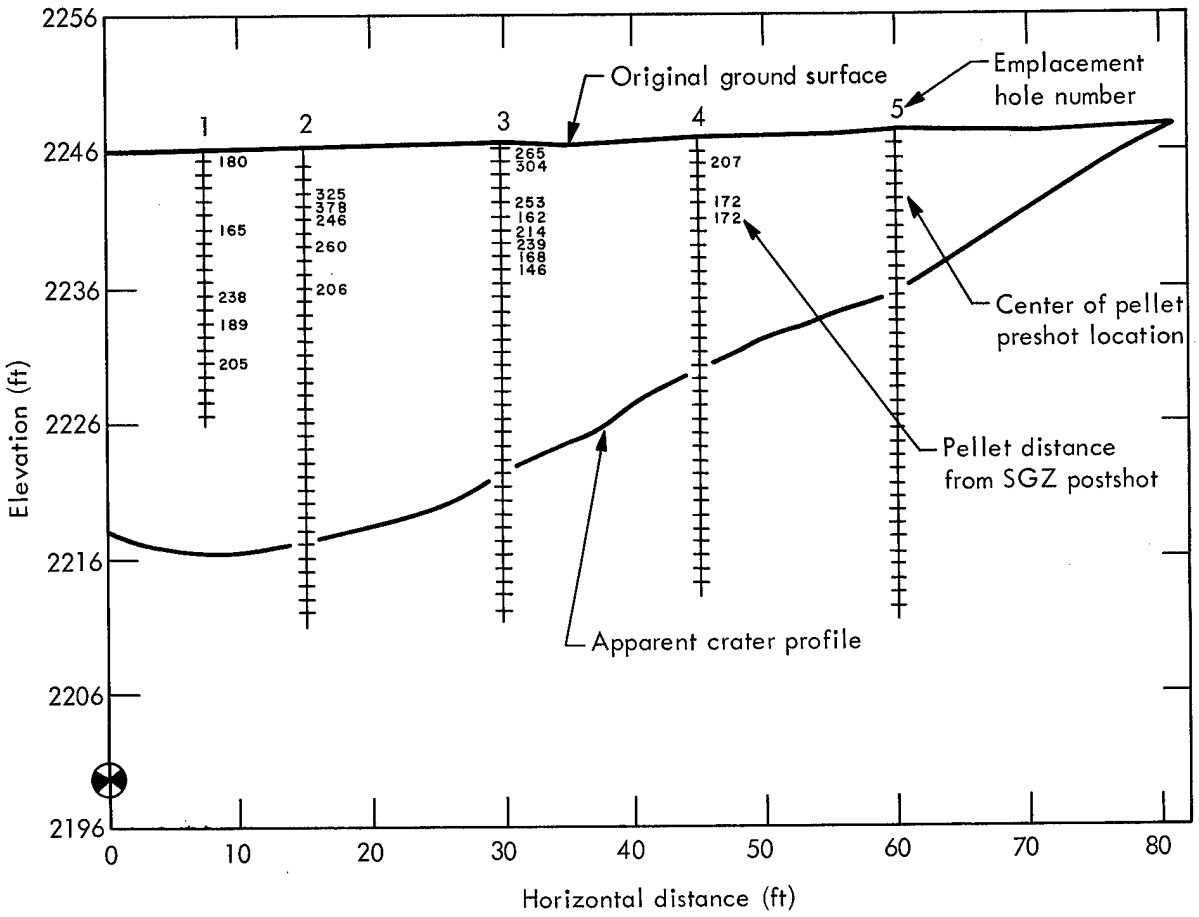

Figure B2 Pre-Gondola I Bravo Event "A" Array.

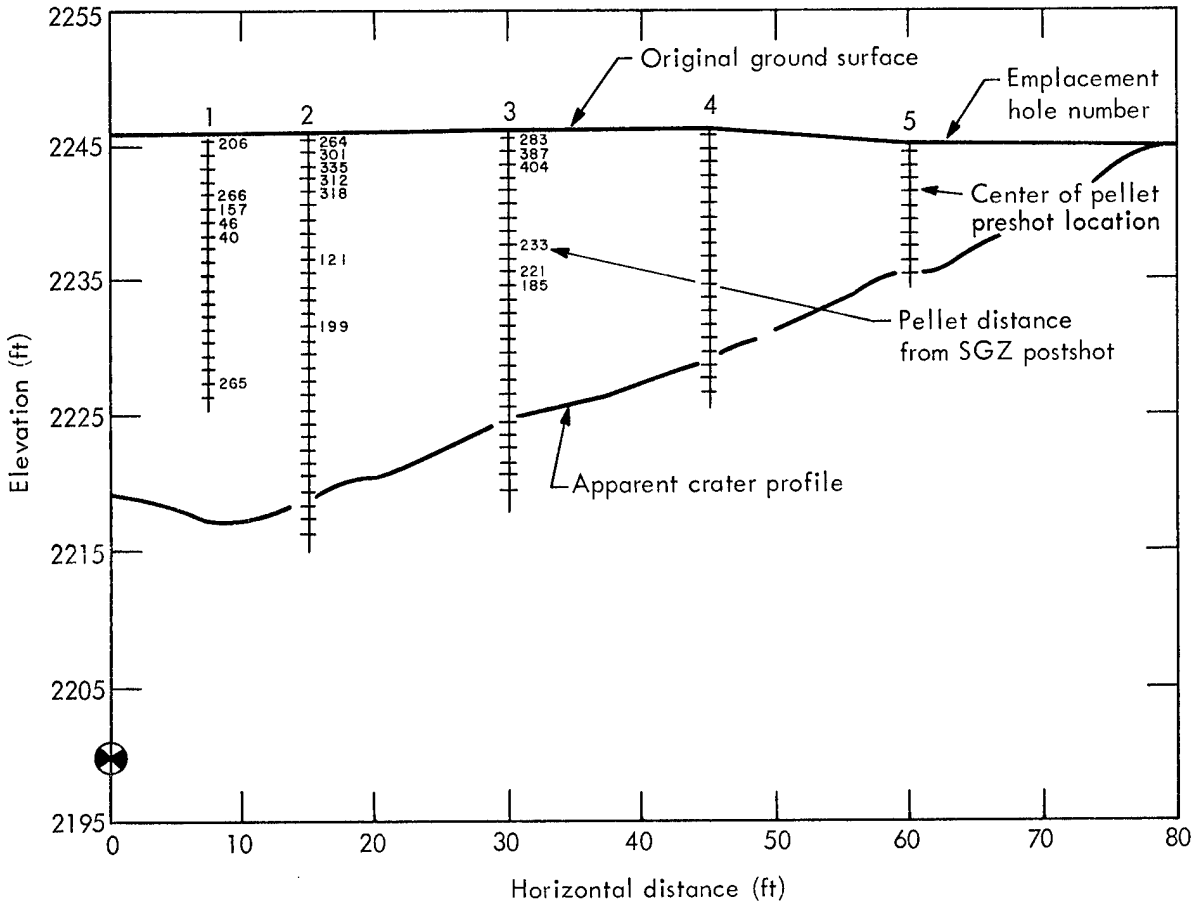

Figure B3 Pre-Gondola I Bravo Event "B" Array.

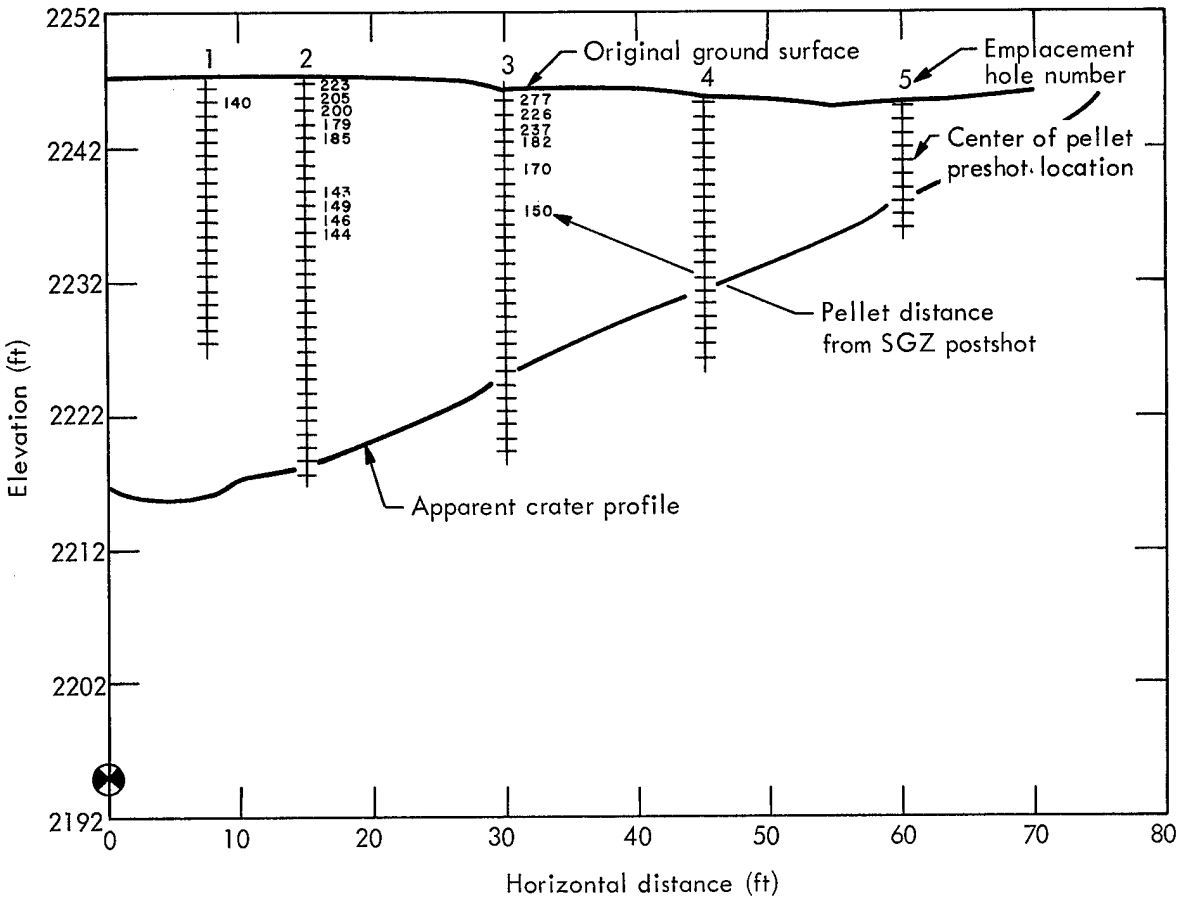

Figure B4 Pre-Gondola I Alfa Event.

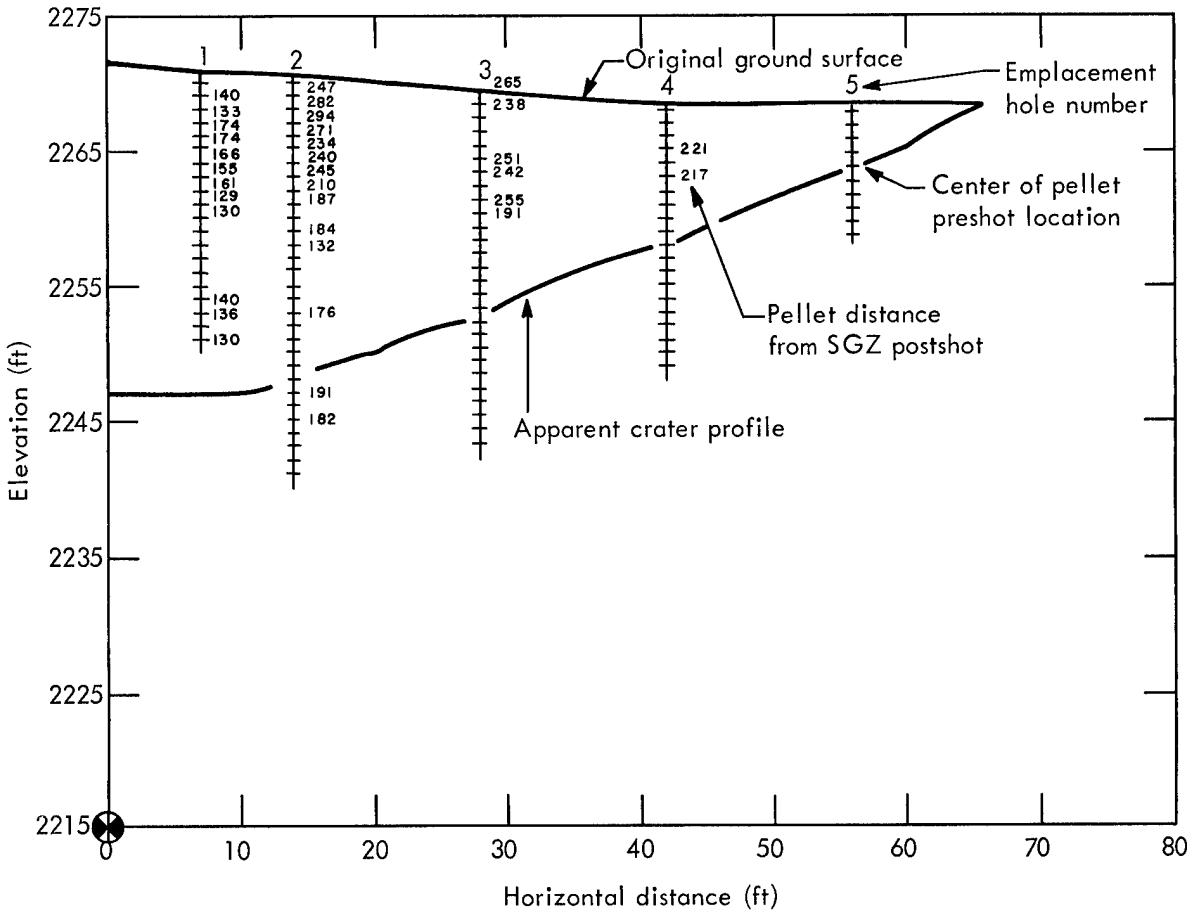

Figure B5 Pre-Gondola I Delta Event.

TABLE B1 TABULATED PRESHOT AND POSTSHOT EJECTA STUDY DATA, CHARLIE EVENT

Preshot		Postshot	
Emplacement Hole Distance from SGZ	Depth to Top of Pellet	Fragment Number[a]	Horizontal Distance From SGZ
feet	feet		feet
7.5	+0.2	1	42
7.5	-2.8	2	16
7.5	-11.8	3a	192
7.5	-11.8	3b	197
7.5	-11.8	3c	231
7.5	-14.8	4	168
7.5	-15.8	5	143
15	+0.1	6a	294
15	+0.1	6b	247
15	-0.9	7	323
15	-1.9	8a	323
15	-1.9	8b	333
15	-1.9	8c	334
15	-2.9	9	295
15	-3.9	10	278
15	-4.9	11	227
15	-5.9	12	215
15	-6.9	13	234
15	-7.9	14a	264
15	-7.9	14b	255
15	-7.9	14c	116
15	-8.9	15	200
15	-9.9	16	180
15	-18.9	17	181
15	-25.9	18	135
30	+0.3	19	233
30	-0.7	20a	241
30	-0.7	20b	274
30	-1.7	21a	216
30	-1.7	21b	240
30	-2.7	22a	202
30	-2.7	22b	247
30	-5.7	23a	136
30	-5.7	23b	197
30	-5.7	23c	146
30	-7.7	24a	148
30	-7.7	24b	223
30	-8.7	25a	192
30	-8.7	25b	206
30	-8.7	25c	200
30	-9.7	26	191
30	-10.7	27	139
30	-11.7	28	110
45	+0.4	29a	187
45	+0.4	29b	262
45	-1.6	30	212

[a]These numbers correlate these data with the corresponding pellet locations in Figure 5.9.

TABLE B2 TABULATED PRESHOT AND POSTSHOT EJECTA STUDY DATA, BRAVO EVENT "A" ARRAY

Preshot		Postshot	
Emplacement Hole Distance from SGZ	Depth to Top of Pellet	Fragment Number[a]	Horizontal Distance From SGZ
feet	feet		feet
7.5	0.0	1	180
7.5	-5.0	2	165
7.5	-10.0	3a	255
7.5	-10.0	3b	221
7.5	-12.0	4	189
7.5	-15.0	5	205
15	-2.4	6a	298
15	-2.4	6b	352
15	-3.4	7a	257
15	-3.4	7b	288
15	-4.4	8	246
15	-6.4	9a	266
15	-6.4	9b	254
15	-8.4	10a	289
15	-8.4	10b	296
15	-11.4	11	206
30	-0.0	12	265
30	-1.0	13a	304
30	-1.0	13b	160
30	-4.0	14a	247
30	-4.0	14b	257
30	-5.0	15a	156
30	-5.0	15b	168
30	-6.0	16	214
30	-7.0	17a	298
30	-7.0	17b	179
30	-8.0	18	168
30	-9.0	19a	147
30	-9.0	19b	146
45	-1.4	20	207
45	-4.4	21	172
45	-5.4	22	172

[a]These numbers correlate these data with the corresponding pellet locations in Figure 5.17.

TABLE B3 TABULATED PRESHOT AND POSTSHOT EJECTA STUDY DATA, BRAVO EVENT "B" ARRAY

Preshot		Postshot	
Emplacement Hole Distance from SGZ	Depth to Top of Pellet	Fragment Number[a]	Horizontal Distance From SGZ
feet	feet		feet
7.5	-0.1	1a	149
7.5	-0.1	1b	184
7.5	-0.1	1c	20
7.5	-0.1	1d	279
7.5	-4.1	2a	265
7.5	-4.1	2b	266
7.5	-5.1	3	157
7.5	-6.1	4	46
7.5	-7.1	5	40
7.5	-18.1	6	265
15	+0.2	7	264
15	-0.8	8	301
15	-1.8	9	335
15	-2.8	10	312
15	-3.8	11	318
15	-8.8	12	121
15	-13.8	13	199
30	-0.0	14a	277
30	-0	14b	289
30	-1.0	15a	374
30	-1.0	15b	400
30	-2.0	16	404
30	-8.0	17	233
30	-10.0	18	221
30	-11.0	19	185

[a]These numbers correlate these data with the corresponding pellet locations in Figure 5.18.

TABLE B4 TABULATED PRESHOT AND POSTSHOT EJECTA STUDY DATA, ALFA EVENT

Preshot		Postshot	
Emplacement Hole Distance from SGZ	Depth to Top of Pellet	Fragment Number[a]	Horizontal Distance From SGZ
feet	feet		feet
7.5	-1.2	1	140
15	+0.3	2a	148
15	+0.3	2b	223
15	-0.7	3	205
15	-1.7	4	200
15	-2.7	5	179
15	-3.7	6	185
15	-7.7	7	143
15	-8.7	8	149
15	-9.7	9	146
15	-10.7	10	144
30	+0.1	11a	260
30	+0.1	11b	293
30	-0.9	12	226
30	-1.9	13a	231
30	-1.9	13b	243
30	-2.9	14a	172
30	-2.9	14b	219
30	-4.9	15	170
30	-7.9	16a	125
30	-7.9	16b	214
30	-7.9	16c	233

[a]These numbers correlate these data with the corresponding pellet locations in Figure 5.26.

TABLE B5 TABULATED PRESHOT AND POSTSHOT EJECTA STUDY DATA, DELTA EVENT

Preshot		Postshot	
Emplacement Hole Distance from SGZ	Depth to Top of Pellet	Fragment Number[a]	Horizontal Distance From SGZ
feet	feet		feet
7	-0.4	1	140
7	-1.4	2	133
7	-2.4	3	174
7	-3.4	4	174
7	-4.4	5	166
7	-5.4	6	155
7	-6.4	7	161
7	-7.4	8	129
7	-8.4	9	130
7	-15.4	10	140
7	-16.4	11	136
7	-18.4	12	130
14	-0.1	13	247
14	-1.1	14	282
14	-2.1	15	294
14	-3.1	16	271
14	-4.1	17	234
14	-5.1	18	240
14	-6.1	19	245
14	-7.1	20	210
14	-8.1	21	187
14	-10.1	22	184
14	-11.1	23	132
14	-17.1	24	176
14	-23.1	25	191
14	-25.1	26	182
28	+0.6	27	265
28	-0.4	28	238
28	-4.4	29	251
28	-5.4	30	242
28	-7.4	31	255
28	-8.4	32	191
42	-2.9	33	221
42	-4.9	34	217

[a]These numbers correlate these data with the corresponding pellet locations in Figure 5.33.

APPENDIX C
PRE-GONDOLA I TECHNICAL REPORTS

APPENDIX C
PRE-GONDOLA TECHNICAL REPORTS

Title of Report	Agency	Author and/or Technical Program Officer	Report Number
Pre-Gondola -			
Seismic Site Calibration	NCG	M. K. Kurtz B. B. Redpath	PNE-1100
Site-Selection Investigations	NCG/Omaha	H. A. Jack W. W. Dudley	PNE-1101
Pre-Gondola I -			
Technical Director's Summary Report	NCG	M. K. Kurtz et al.	PNE-1102
Geologic and Engineering Properties Investigations	NCG/Omaha	P. R. Fisher et al.	PNE-1103
Close-in Ground Motion, Earth Stress, and Pore Pressure Measurements	WES	J. D. Day et al.	PNE-1104
Intermediate Range Ground Motion	LRL	D. V. Power	PNE-1105
Structures Instrumentation	WES	R. F. Ballard	PNE-1106
Crater Studies: Crater Measurements	NCG	R. W. Harlan	PNE-1107 Part I
Surface Motion	NCG	W. G. Christopher	PNE-1107 Part II
Cloud Development Studies	NCG/LRL	W. C. Day R. F. Rohrer	PNE-1108
Close-in Displacement Studies	AFWL	C. J. Lemont	PNE-1109
Lidar Observations of Pre-Gondola I Clouds	SRI	J. W. Oblanas R. T. H. Collis	PNE-1110
Preshot Geophysical Measurements	LRL-N	R. T. Stearns J. T. Rambo	PNE-1111

DISTRIBUTION

LRL Internal Distribution

Michael M. May
R. Batzel
J. Gofman
H. L. Reynolds
C. Haussmann
J. Rosengren
D. Sewell
C. Van Atta
P. Moulthrop
F. Eby
E. Goldberg
G. Higgins
J. Carothers
S. Fernbach
J. Hadley
J. Kane
B. Rubin
J. Kury
P. Stevenson
J. Bell
E. Hulse
W. Decker
W. Harford
G. Werth
M. Nordyke
F. Holzer
H. Tewes
J. Toman 2
J. Knox
E. Teller, Berkeley
D. M. Wilkes, Berkeley
L. Crooks, Mercury
TID Berkeley
TID File 30

External Distribution

D. J. Convey
Department of Mines and Technical Surveys
Ottawa, Ontario, Canada

G. W. Govier
Oil and Gas Conservation Board
Calgary, Alberta, Canada

U. S. Army Engineer Division
Lower Mississippi Valley
Vicksburg, Mississippi

U. S. Army Engineer District
Memphis, Tennessee

U. S. Army Engineer District
New Orleans, Louisiana

U. S. Army Engineer District
St. Louis, Missouri

U. S. Army Engineer District
Vicksburg, Mississippi

U. S. Army Engineer Division, Mediterranean
Leghorn, Italy

U. S. Army Liaison Detachment
New York, N. Y.

U. S. Army Engineer District, GULF
Teheran, Iran

U. S. Army Engineer Division, Missouri River 2
Omaha, Nebraska

U. S. Army Engineer District
Kansas City, Missouri

U. S. Army Engineer District 2
Omaha, Nebraska

U. S. Army Engineer Division, New England
Waltham, Massachusetts

U. S. Army Engineer Division, North Atlantic
New York, N. Y.

U. S. Army Engineer District
Baltimore, Maryland

U. S. Army Engineer District
New York, N. Y.

U. S. Army Engineer District
Norfolk, Virginia

External Distribution (Continued)

U. S. Army Engineer District
Philadelphia, Pennsylvania

U. S. Army Engineer Division, North Central,
Chicago, Illinois

U. S. Army Engineer District
Buffalo, New York

U. S. Army Engineer District
Chicago, Illinois

U. S. Army Engineer District
Detroit, Michigan

U. S. Army Engineer District,
Rock Island, Illinois

U. S. Army Engineer District
St. Paul, Minnesota

U. S. Army Engineer District, Lake Survey
Detroit, Michigan

U. S. Army Engineer Division, North Pacific
Portland, Oregon

U. S. Army Engineer District
Portland, Oregon

U. S. Army Engineer District, Alaska
Anchorage, Alaska

U. S. Army Engineer District
Seattle, Washington

U. S. Army Engineer District
Walla Walla, Washington

U. S. Army Engineer Division, Ohio River
Cincinnati, Ohio

U. S. Army Engineer District
Huntington, West Virginia

U. S. Army Engineer District
Louisville, Kentucky

U. S. Army Engineer District
Nashville, Tennessee

U. S. Army Engineer District
Pittsburgh, Pennsylvania

U. S. Army Engineer Division, Pacific Ocean
Honolulu, Hawaii

U. S. Army Engineer District, Far East
San Francisco, California

External Distribution (Continued)

U. S. Army Engineer District
Honolulu, Hawaii

U. S. Army Engineer District, Okinawa
San Francisco, California

U. S. Army Engineer District, South Atlantic
Atlanta, Georgia

U. S. Army Engineer Division, Canaveral
Merritt Island, Florida

U. S. Army Engineer District
Charleston, South Carolina

U. S. Army Engineer District
Jacksonville, Florida

U. S. Army Engineer District
Mobile, Alabama

U. S. Army Engineer District
Savannah, Georgia

U. S. Army Engineer District
Wilmington, North Carolina

U. S. Army Engineer Division, South Pacific
San Francisco, California

U. S. Army Engineer District
Los Angeles, California

U. S. Army Engineer District
Sacramento, California

U. S. Army Engineer District
San Francisco, California

U. S. Army Engineer Division, Southwestern
Dallas, Texas

U. S. Army Engineer District
Albuquerque, New Mexico

U. S. Army Engineer District
Forth Worth, Texas

U. S. Army Engineer District
Galveston, Texas

U. S. Army Engineer District
Little Rock, Arkansas

U. S. Army Engineer District
Tulsa, Oklahoma

Mississippi River Commission
Vicksburg, Mississippi

External Distribution (Continued)

Rivers and Harbors
Board of Engineers,
Washington, D. C.

Corps of Engineer Ballistic Missile Construction Office
Norton Air Force Base, California

U. S. Army Engineer Center
Ft. Belvoir, Virginia

U. S. Army Engineering School
Ft. Belvoir, Virginia

U. S. Army Engineer Reactors Group
Ft. Belvoir, Virginia

U. S. Army Engineer Training Center
Ft. Leonard Wood, Missouri

U. S. Coastal Engineering Research Board
Washington, D. C.

U. S. Army Engineer Nuclear Cratering Group 75
Livermore, California

TID-4500, UC-35, Nuclear Explosions-Peaceful Applications 292

WF:rd